FUNDAMENTAL INVESTIGATION OF PORE PRESSURE PREDICTION

DURING DRILLING FROM THE MECHANICAL BEHAVIOR OF ROCK

A Dissertation

by

JUAN ALBERTO RIVAS CARDONA

Submitted to the Office of Graduate Studies of
Texas A&M University
in partial fulfillment of the requirements for the degree of

DOCTOR OF PHILOSOPHY

August 2011

Major Subject: Mechanical Engineering

Fundamental Investigation of Pore Pressure Prediction

During Drilling from the Mechanical Behavior of Rock

FUNDAMENTAL INVESTIGATION OF PORE PRESSURE PREDICTION

DURING DRILLING FROM THE MECHANICAL BEHAVIOR OF ROCK

A Dissertation

by

JUAN ALBERTO RIVAS CARDONA

Submitted to the Office of Graduate Studies of
Texas A&M University
in partial fulfillment of the requirements for the degree of

DOCTOR OF PHILOSOPHY

Approved by:

Co-Chairs of Committee,	Thomas Lalk
	Egidio Marotta
Committee Members,	Frederick Chester
	Judith Chester
Head of Department,	Jerald Caton

August 2011

Major Subject: Mechanical Engineering

ABSTRACT

Fundamental Investigation of Pore Pressure Prediction

During Drilling from the Mechanical Behavior of Rock. (August 2011)

Juan Alberto Rivas Cardona, B.S., Universidad de Guanajuato, Mexico;

M.S., Texas A&M University

Co-Chairs of Advisory Committee: Dr. Thomas Lalk
Dr. Egidio Marotta

An investigation was conducted as a preliminary effort to develop a methodology to predict pore pressure in a rock formation during drilling, for all types of rocks and situations. Specifically, it was investigated whether or not the virgin pore pressure (the pore pressure of the undisturbed rock) can be determined at the drill bit from drilling and environmental parameters, as well as solid and pore fluid properties.

Several drilling situations were analyzed to develop models relating pore pressure to drilling and environmental parameters, as well as solid and pore fluid properties. Three approaches to the modeling of such drilling situations were considered, which were used to predict pore pressure and compare the predictions to actual drilling data. The first approach used the concept of the effective stress in conjunction to the Mohr-Coulomb failure criterion. The second approach used the concept of the mechanical specific energy. The third approach made use of basic principles to relating virgin pore pressure to drilling and environmental parameters, as well as solid and pore fluid properties. This third approach resulted in the proposal of a more fundamental way of viewing mechanical specific energy (MSE) and the use of Biot's poroelasticity theory to describe the cutting process of rock.

The first approach did not provide an adequate prediction of virgin pore pressure for all types of rocks and situations. The second approach showed promising results with

limited actual drilling data. A sensitivity analysis of the model resulting from the third approach indicated that pore pressure, type of rock, and back rake angle of the cutter are the most significant factors affecting the energy required to break the rock. Moreover, rate of cutting stress, depth of cut, and type of pore fluid become significant factors of the cutting process only when a low-porosity, low-permeability rock is considered.

It was concluded that there exists a relationship among pore pressure, drilling and environmental parameters, as well as solid and pore fluid properties. Therefore, it is possible in principle to determine the virgin pore pressure at the drill bit from drilling parameters, environmental parameters, and material properties. However, further work is required to establish a quantitative relationship among the significant parameters before a methodology to predict virgin pore pressure for all types of rocks and situations can be developed.

DEDICATION

This work is dedicated to Wendy, who encouraged and supported me throughout this endeavor; to my sister, Alejandra, for those great discussions that made us enjoy being Ph.D. students; and to my parents Juan Jose and Ma. del Pilar✚, because they instilled in me the joy of learning.

ACKNOWLEDGEMENTS

I would like to thank my two advisors: Dr. Tom Lalk, for those long hours of discussions, thoughtful insights, and laughs; and Dr. Ed Marotta, for his trust and the opportunity to work in his group. They focused on providing a quality education rather than training, and that surely helped me in my professional development. Their support, encouragement, and help to achieve the completion of this dissertation are greatly appreciated.

I would also like to thank Dr. Fred Chester and Dr. Judith Chester for being part of my committee, and for providing useful information, insights, and feedback related to this work. Similarly, I like to thank Buddy Bollfrass for his assistance and insights provided.

Finally, I would like to express my deep appreciation for all those, close or far away, who have supported me in either way during my time in College Station, especially my family and my very good friends.

NOMENCLATURE

A	surface area, in^2
A_{chip}	surface area of the lateral face of the rock chip, in^2
AEP^3	Acoustical Emission for Pore Pressure Prediction
CCS	Confined Compressive Strength, psi
C_f	compressibility of the fluid, psi^{-1}
C_m	compressibility of the solid matrix, psi^{-1}
D	depth measured from the seawater floor, ft
D_b	diameter of the borehole, in
d_{cut}	depth of cut, in
D_{cut}	depth of cut, ft
D_{sw}	depth of seawater, ft
E	Young's modulus, psi
ECD	Equivalent Circulation Density, ppg
EFF$_{M}$	mechanical efficiency
$\boldsymbol{F}$	force vector, lbf
F_{cutter}	cutting force of the drill bit tooth, lbf
g	gravitational acceleration, 32.2 ft/s^2
$\boldsymbol{g}$	gravitational acceleration vector, 32.2 ft/s^2
G	shear modulus, psi
K_f	bulk modulus of the fluid, psi
K_m	bulk modulus of the solid matrix, psi
LWD	Logging While Drilling (LWD)
m	coefficient of internal friction
M	Biot modulus, psi
MSE	Mechanical Specific Energy, psi
MSE$_{BR}$	mechanical specific energy required solely to break the rock, psi

$M\hat{S}E_{BR}$	estimated value of MSE_{BR} from the regression model
$MSE_{downhole}$	mechanical specific energy from drilling parameters that are measured downhole, psi
$MSE_{environment}$	mechanical specific energy required to overcome the environmental conditions to which the rock is subjected, psi
$MSE_{intrinsic_{rock\,grains}}$	intrinsic property of the material that constitutes the grains of the rock, psi
MSE_N	normal trend of mechanical specific energy, psi
MSE_o	observed mechanical specific energy in abnormally pressured zones, psi
$MSE_{rock\,matrix}$	mechanical specific energy required to break the rock skeleton of a rock element, psi
$MSE_{rock\,structure}$	mechanical specific energy required to counteract the structural characteristics of the rock skeleton in order to break it, psi
$MSE_{surface}$	mechanical specific energy calculated from drilling parameters that are measured at the surface of the rig, psi
MWD	Measurement While Drilling
OB	overburden stress, psi
$\boldsymbol{p}$	traction vector, psi
PDC	Polycrystalline Diamond Compact
P_h	hydrostatic mud pressure or confining pressure due to the drilling mud, psi
P_p	pore pressure, psi
Pp_N	normal pore pressure, psi
PSP[3]	Principal Stress Pore Pressure Prediction
$\mathbf{q}$	fluid flux vector, ft/s
q_z	fluid flux in the z-direction, ft/s
r	moment arm from cylindrical center of bit, in
R	radius of the drill bit, in

R_n	resistivity of normal trend at same depth as R_o, ohm·m
R_o	observed resistivity at a given depth, ohm·m
ROP	Rate of Penetration, ft/h
RPM	Revolutions per Minute
S_c	cutting stress, psi
$\dot{S}_c$	rate of cutting stress, psi/s
S_0	cohesion of rock, psi
T	torque, lb·ft
T_f	temperature of the pore fluid, °F
TVD	True Vertical Depth, ft
T_s	temperature of the rock, °F
v	velocity of cutter, in/s
V_b	bulk volume, ft^3
V_p	pore volume, ft^3
WOB	Weight on Bit, lbf
x_m	main factors of regression model (for $m = 1,2,3,\dots$)
x_{mn}	interactions between the factors m and n (for $m = 1,2,3,\dots$ and $n = 1,2,3,\dots$)

Greek Symbols

α	Biot-Willis coefficient
$\hat{\beta}_{mn}$	coefficient estimates of the regression model (for $m = 1,2,3,\dots$ and $n = 1,2,3,\dots$)
δ_{ij}	Kronecker delta
ϵ	random error of regression model
ε_b	volumetric bulk strain
ε_{ij}	strain tensor
ε_m	volumetric strain of the solid matrix
ζ	volumetric pore fluid content

η_{cutter}	efficiency of the energy transferred from the drill bit to the rock.
$\eta_{overall}$	overall efficiency of the drilling process
η_{string}	efficiency of the energy transferred along the drill string from the surface to the bottomhole
θ	back rake angle of cutter, degrees (°)
κ	permeability (constant), Darcies
$\overline{\overline{k}}$	permeability second-order tensor, Darcies
μ	bit-specific coefficient of sliding friction
μ_f	dynamic viscosity of the fluid, centipoise
ν	Poisson's ratio
ρ_b	bulk density of the rock, g/cc
ρ_f	density of the pore fluid, g/cc
ρ_s	density of the rock matrix, g/cc
ρ_{sw}	density of seawater, g/cc
σ	normal stress at the failure plane, psi
σ'	effective stress, psi
σ_c	confining stress, psi
σ_i	intermediate stress, psi
σ_{ij}	stress tensor, psi
σ_{max}	maximum principal normal stress, psi
σ'_{max}	maximum principal effective stress, psi
σ_{min}	minimum principal normal stress , psi
σ'_{min}	minimum principal effective stress, psi
σ_s	normal stress at the failure plane, psi
σ_T	total stress, psi
τ_s	shear stress at the failure plane, psi
ϕ	angle of internal friction of rock, degrees (°)
ϕ_s	porosity of the rock

TABLE OF CONTENTS

LIST OF FIGURES

LIST OF TABLES

CHAPTER I
INTRODUCTION

Rocks can be described as solid aggregates composed of crystals and amorphous mineral particles that are joined by cementitious materials [1]. In general, there are three main types of rocks: igneous, metamorphic, and sedimentary. Igneous rocks consist of a completely crystalline assemblage of minerals. Metamorphic rocks are formed from igneous and sedimentary rocks that were chemically and/or physically modified as a result of excessive temperature and pressure. Sedimentary rocks consist of an assemblage of mineral grains and particles from other rocks in a matrix of materials such as clay minerals, calcite, quartz, etc. Since sedimentary rocks are formed from loose material that is then compacted, they can contain voids or empty spaces, some of which may form an interconnected system of pores [1]. Sedimentary rocks constitute the majority of the oil producing formations since they generally contain fluids within their pores. The present work is relevant only to sedimentary rocks. Igneous and metamorphic rocks are not included in the scope of this work.

Unlike other materials, the mechanical behavior of sedimentary rocks depends to a large extent on the *non-solid* part (pores or void space) of the material [2] and the fluids inside the pores. The pressure exerted by the fluids trapped inside the pores of a rock is termed pore pressure. Pore pressure is an important parameter in the mechanical behavior of the rock because it corresponds to the portion of the total stresses applied to the rock that is supported by the pore fluid.

Terzaghi [3] used the term *effective stress* to define the portion of the load supported solely by the rock matrix, that is, the total stress minus the pore pressure. Knowledge of the pore pressure in the formation is of great importance in the oil and gas industry,

_____

This dissertation follows the style of the International Journal of Rock Mechanics and Mining Sciences.

because a high pore pressure makes a well more prolific, but it also represents a potential hazard during drilling.

Drilling fluid is usually circulated when a borehole is being drilled into the Earth. The drilling fluid is commonly termed *drilling mud* or *mud.* In the oil and gas industry, the drilling mud is characterized by its density and the term *mud weight* is commonly used to refer to the density of the mud. Therefore, the adjustments in hydrostatic pressure in the borehole are then made by varying the density of the mud (that is, varying the mud weight). The circulating mud has several purposes: (1) it carries the crushed rock from the bottom hole to the surface; (2) it serves as a cooling fluid for the drilling process; but perhaps even more important, (3) the hydrostatic column of mud in the borehole maintains equilibrium with the formation pore pressure.

It is desirable that the hydrostatic (mud) pressure be equal to the formation pore pressure to maintain a perfect equilibrium during drilling. This requires a means to determine the pore pressure ahead of the bit in the formation before drilling into it. A distinction has to be made between the formation pore pressure in the undisturbed rock (before drilling), which is termed *virgin pore pressure* in this dissertation, and the *modified pore pressure* at the bit caused by the drilling process. Ideally, it is desirable that the drilling operator would have means to determine and monitor formation virgin pore pressure ahead of the drill bit during drilling. With this information, the drilling mud weight (density) could subtly, and by choice, be changed to prevent the flow of formation fluids into the drill bore and/or minimize mud flow into the oil producing formation. With this capability, petroleum engineers could minimize formation damage, whether due to drilling mud invasion or to later formation outflow, which would result in maximum formation production life. Additionally, an ability to alter drilling fluid density by choice behind the bit would support remote and real-time intervention from the surface.

Any improvement in the drilling process that reduces formation degradation caused by an over-balanced situation will ultimately increase formation production volume and producing life. An increase in the production provides the opportunity to receive billions of dollars of additional revenue per well. Problems associated with controlling abnormally pressurized formations and wellbore instability were estimated to cost the oil and gas industry $7 – $8 billion annually [4]. Current efforts at minimizing drilling mud weight increase the risk of gas kicks or blowouts, reservoir flow damage, wellbore instability, and subsequent sticking of tools or pipe. In 2004, a study in the Gulf of Mexico revealed that non-productive time associated with formation-fluid influx, drilling fluid loss, and wellbore instability was responsible for more than 40% of all non-productive time during well construction [4]. Such expenses at BP America generate average losses of $180 million per annum. For these reasons, **there is a need to develop a method that could be used to determine the virgin pore pressure ahead of the bit during drilling**. BP America asked the Department of Mechanical Engineering at Texas A&M University to investigate the possibility of developing such methods. Because of the significance of any such methodologies and subsequent technologies that could reduce this loss, BP America asked that the investigation begin with a thorough evaluation of existing technologies, as well as existing or potential theories.

A functional decomposition allowed identifying two main top-level functions for the design of a methodology that could be used to determine virgin pore pressure ahead of the bit during drilling. The two functions of such methodology are: (1) to provide means to determine the virgin pore pressure at the bit, and (2) to provide means to relate the virgin pore pressure at the bit to the virgin pore pressure at the far-field. The far-field is defined as the location away from the drill bit where the pore pressure has not been altered by the drilling process.

In early stages of the project with BP America, a literature search for methods to measure pressure or formation properties was conducted. The literature database was

then used to aid in the generation of the concepts that could satisfy the need. Two selected concepts (Acoustical Emission for Pore Pressure Prediction, AEP[3], and Principal Stress Pore Pressure Prediction, PSP[3]) were chosen for further investigation and evaluation. Both concepts were proposed as possible means to determine the virgin pore pressure at the bit. However, the need remains for a concept that can be used to relate the pore pressure at the bit to the pore pressure at the far-field. Detailed descriptions of these processes and results have been given previously in Interim Reports to BP America [5-7] and are not described in this dissertation. Additionally, early stages of the development of the PSP[3] concept have been described by Richardson [8]. The work presented in this dissertation is a continuation of the investigation on the PSP[3] concept conducted for BP America from a fundamental perspective rather than an empirical approach. Work done on the AEP[3] concept is not part of the scope of this dissertation.

The PSP[3] concept was originally thought to be a method that could relate drilling measurements already available to virgin pore pressure, making it relatively inexpensive to implement. The hypothesis was that the virgin pore pressure at the bit could be determined during drilling by identifying the effective stresses of the rock being drilled, in combination with a Mohr-Coulomb failure criterion. Empirical previous work on the PSP[3] concept indicated that, besides the effective stress, a relationship between the amount of energy required to fragment the rock and virgin pore pressure might exist. Teale [9] used the term Mechanical Specific Energy (MSE) to designate that amount of energy per unit volume required to fragment the face of a solid wall of rock. A mathematical expression that could describe such a relationship was also developed, and it conveniently expressed the virgin pore pressure as a function of mechanical specific energy, hydrostatic (mud) pressure, and rock properties. However, the virgin pore pressure determined with this PSP[3] equation could not be validated against the actual virgin pore pressure (at the bit) provided.

The lack of validation of the PSP^3 equation has led us to reconsider the basis of the PSP^3 concept from a different perspective. For instance, material properties such as cohesion and friction angle of the rock formation have already been considered in the development of the PSP^3 equation. However, other properties such as porosity and permeability have not been considered and they might have a significant influence on the virgin pore pressure encountered in the formation. Ultimately, it is desirable to develop a methodology that can be used to determine virgin pore pressure from drilling parameters that would be reliable for all types of rocks and situations. The different situations encountered in a formation during drilling will depend on the environmental conditions, which can be described by several parameters. Environmental parameters can be divided in two groups: the external parameters describing the *surrounding* conditions to which a rock element is subjected during drilling, for example, confining stresses from Earth, and hydrostatic (mud) pressure; and (2) the internal parameters describing the conditions at the interior of the solid matrix such as type of fluid inside the pores, pore pressure, and temperature.

Therefore, the objective of this work is to determine whether or not it is possible to determine the virgin pore pressure at the drill bit from drilling parameters, environmental parameters, and material properties.

In order to satisfy this objective, three approaches have been considered in an effort to establish a relationship among virgin pore pressure, drilling parameters, environmental parameters, and rock properties. The first and second approaches considered were developed empirically. Results from the first and second approach indicated that a fundamental understanding of the relationship among virgin pore pressure, drilling parameters, environmental parameters, and rock properties is required. Therefore, a fundamental approach (third approach) considering fluid mechanics, porous media, heat transfer, thermodynamics, and rock mechanics, is proposed to explain the role of virgin pore pressure in the mechanical behavior of rock during drilling. This fundamental

approach could eventually evolve into a methodology for virgin pore pressure determination that would be reliable for all types of rocks, and situations.

This dissertation begins with a background of the work conducted to provide means to predict virgin pore pressure at the drill bit from drilling parameters, environmental parameters, and material properties (Chapter II). Then, the development of the PSP^3 concept is presented in Chapter III, which includes the results of the attempts to validate this concept. The second approach that proposes to use the fundamental parameter MSE in Eaton's equation [10] (instead of electrical resistivity or sonic log data) is described in Chapter IV. Subsequently, a fundamental approach to relating pore pressure to drilling parameters, environmental parameters, and material properties is presented in Chapter V. As part of this fundamental approach, a numerical analysis based on Biot's poroelasticity theory was conducted, which considers fluid mechanics, rock mechanics, and porous media interactions. Results from the numerical analysis are presented in Chapter VI which allow determining the significant parameters of the drilling process. Numerical experiments were also run to determine whether the PSP^3 concept and the concept of using the fundamental parameter MSE in Eaton's equation comply with basic principles of fluid mechanics, rock mechanics, and porous media. A summary of this work is presented in Chapter VII, along with the conclusion of the investigation. Finally, recommendations for future work are presented in Chapter VIII.

CHAPTER II
BACKGROUND

In this chapter, the background and motivation of the current investigation is presented. A definition of basic terms used in this dissertation is presented first, followed by a description of the current methods used to predict pore pressure in industry. Then, a need analysis is presented where the functions needed to satisfy the objective of this dissertation are identified. A historical background of the approaches considered in the course of this investigation in order to address the functions identified in the need analysis is also presented. The ideas presented in this chapter are accompanied with a literature review of relevant investigations that have addressed or attempted to address some of the functions that have been identified in the present work as needed to satisfy the objective.

2.1 Definition of terms

Underground formations are the result of multiple layers of sediment that were sequentially deposited over previous layers. This process is conducted over geological time. The underground formation has to carry the weight of the overlying formations. The vertical stress at the bottom of a column of rock sediments is known as *overburden*, and it can be expressed mathematically as

$$OB = \rho_{sw} g D_{sw} + \int_0^D \rho_b(z) g \, dz \qquad (2.1)$$

where ρ_{sw} is the density of seawater, D_{sw} is the depth of seawater, $\rho_b(z) = (1 - \phi_s)\rho_s(z) + \phi_s \rho_f(z)$ is the bulk density of the rock [11], ρ_s is the density of the rock matrix, ρ_f is the density of the pore fluid, ϕ_s is the porosity of the rock, g is the acceleration of gravity, D is the depth measured from the seawater floor (*mudline*), and the z-direction is pointing vertically downwards and has its origin at mudline. Equation

(2.1) implies that the overburden stress is the pressure exerted by all overlying material, both solid and fluid (and both, fluid above the rock and fluid within the rock). The typical gradient of overburden stress is ~1 psi/ft [2].

As the rock sediments are deposited, the formation is compacted, the pore size decreases, and the fluids are expelled from the pores. In formations with high permeability (which accounts for the connectivity of the pores), the pore fluid can escape and migrate to the surface at about the same rate as the rate of compaction. In this case, the fluid in the pores will only support the weight of the fluid column above, and a *normal trend of pore pressure* is maintained. The *normal pore pressure* at a given depth D from the mudline can be expressed as

$$Pp_N = \int_0^D \rho_f(z)g\,dz \tag{2.2}$$

where $\rho_f(z)$ is the density of the pore fluid, g is the acceleration of gravity, D is the depth from the mudline, and the z-direction is pointing vertically downwards and has its origin at the mudline. The typical gradient of normal pore pressure is 0.45 psi/ft [2]. It can be observed from Equation (2.2) that the normal pore pressure trend can be readily known if the density of the pore fluid is known. In real drilling situations, however, it is common to encounter formation zones where the pore pressure is significantly different from the normal pore pressure. These zones are termed *abnormally-pressured*, and it is said that they exhibit an *abnormal pore pressure*. Usually, abnormally-pressured zones exhibit pore pressure that is above the normal pore pressure. In this case, it is said to be an *over-pressured zone*. It is extremely important to detect over-pressured zones before drilling into them since they represent a potential hazard during drilling. Figure 2.1 illustrates the typical situation of overburden stress, normal trend of pore pressure, and over-pressured zones encountered in offshore drilling. Figure 2.1 also shows the *fracture*

pressure which is the pressure required to induce fractures in the rock formation at a given depth.
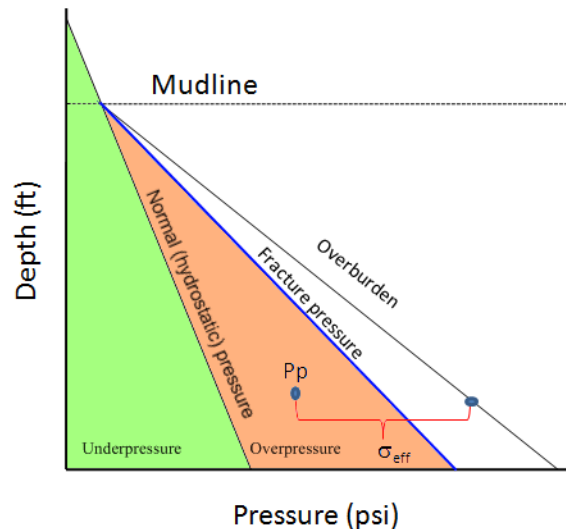
Figure 2.1 Typical overburden, fracture pressure, and normal pore pressure trends in offshore drilling.

There are several mechanisms that can cause a zone to be over-pressured. Fjaer et al. [2] groups the causes of over-pressure from investigations done by other researchers [12-14] in three main mechanisms: "(1) the rate of sedimentation and compaction is higher than the rate of fluid expulsion and migration, (2) tectonic loading that leads to undrained shear stress with associated pore pressure development, and (3) pore fluid generation or expansion by thermal or chemical processes."

It is important to note that the definitions of pore pressure (either normal or abnormal pressure) described above refer to the *virgin pore* pressure of the formation. That is, the pore pressure on the undisturbed rock that has been in equilibrium for a long period of time, and before any external process (such as drilling) has perturbed the formation. Furthermore, the drilling process causes a local change in the formation pressure due to the large stresses imposed on the rock to break it and the pressures of the drilling mud.

In this dissertation, the terms pore pressure and abnormal pore pressure refer to the virgin pore pressure (either normal or abnormal), even if not specified, unless otherwise stated.

Regardless of the cause of abnormal pore pressure, the ultimate goal is to determine the (abnormal) virgin pore pressure ahead of the bit during drilling. A brief review of the current methods to predict abnormal pore pressure is presented in the following section.

2.2 Current pore pressure prediction methods

The history of pore pressure prediction dates back to the 1930s when Terzaghi [3, 15] introduced the concept of effective stress. Terzaghi used the term *effective stress* to define the portion of the load supported solely by the soil skeleton. Terzaghi related the effective stress to the total stress and to the pore pressure as

$$\sigma' = \sigma_T - P_p \qquad\qquad (2.3)$$

where σ' is the effective stress, σ_T is the total stress, and P_p is the pore pressure. Terzaghi used the adjective *effective* to remark that only a fraction of the total stress (the effective stress) is effective in causing important changes in strength, volume, or shape of the solid matrix. The concept of effective stress was developed empirically for soils, but it was theoretically proved correct several years later with Biot's general theory of consolidation [16], and its application was extended to rocks.

Although Terzaghi's work on soil mechanics was presented in the 1930s, it was until the 1960s that pore pressure prediction became a serious pursuit in the oil industry [17]. In 1965, Hottmann and Johnson [18] presented probably the first formal method for predicting abnormal pore pressure using resistivity and sonic log data. The method of Hottmann and Johnson was based on the effective stress concept of Terzaghi and the observations of Hubbert and Rubey [19] of the effective stress changes in clay. Hubbert

and Rubey observed that the effective stress in porous clay depended solely upon the degree of compaction of clay. Since the porosity of clay is a useful indicator of the degree of compaction, it was inferred that for each value of porosity there exists a maximum value of effective stress which the clay can support. Therefore, Hottmann and Johnson proposed that the fluid pressure could be related to the degree of compaction of the rock, and the porosity of the rock could be used as a measure of the degree of compaction. Moreover, the porosity of the rock could be estimated from acoustic or resistivity methods. Therefore, Hottmann and Johnson proposed a method for determining abnormal pore pressure from resistivity and sonic logs. Hottmann and Johnson observed from acoustic and sonic logs that the porosity decreases as a function of depth in formation zones that exhibit a hydrostatic (normal) pore pressure. Hottmann and Johnson found that the porosity as function of depth in zones with a normal pore pressure trend exhibits a *normal compaction trend* (NCT). In abnormally-pressured zones, the data from sonic or resistivity logs deviated from the NCT. In order to determine the abnormal pore pressure, Hottmann and Johnson proposed to measure the amount of divergence (at a given depth) from the NCT and relate it to the observed pressure in adjacent reservoir formations.

In 1975, Eaton [10] extended the work of Hottmann and Johnson by incorporating the effects of the overburden stress to the method of determining pore pressure. He presented in equation form a method to determine abnormal pore pressure from the electrical resistivity. The equation proposed by Eaton was

$$\frac{P_p}{D} = \frac{OB}{D} - \left[\frac{OB}{D} - \left(\frac{P_p}{D}\right)_N\right]\left(\frac{R_o}{R_n}\right)^n \qquad (2.4)$$

$\frac{P_p}{D}$ = virgin pore pressure gradient (psi/ft)

$\frac{OB}{D}$ = overburden stress gradient (psi/ft)

$\left(\frac{P_p}{D}\right)_n$ = normal virgin pore pressure gradient (psi/ft)

R_o = observed resistivity at a given depth (ohm.m)

R_n = resistivity of normal trend at same depth as R_o (ohm.m)

In Equation (2.4), the expression $\left[\frac{OB}{D} - \left(\frac{P_p}{D}\right)_N\right]$ represents the effective stress of the formation in normal compaction; whereas the n-power of the ratio $\left(\frac{R_o}{R_n}\right)$ represents the ratio of the effective stress in the abnormally-pressured zone to the effective stress in the hypothetical normal-pressured zone at the same depth. It is important to mention that Equation (2.4) was developed from trial-and-error fitting of data. After evaluation of Equation (2.4) with available data, Eaton found that the n coefficient with a value of 1.2 better fit the resistivity data that was used. Eaton also recognized that the ratio of other measurements could be utilized in Equation (2.4) instead of electrical resistivity. He proposed the use of electrical conductivity (which is the inverse of resistivity), the corrected d-exponent, and sonic-log data (with a value of 3 for the exponent).

In principle, Eaton's reasoning to develop Equation (2.4) seems to be logical. By using the ratio of actual resistivity to the resistivity in a normal compaction situation, Eaton attempted to determine the portion of overburden load supported by the fluid. The question remains of whether or not electrical resistivity (or any of the other parameters used by Eaton) is the best parameter to track a change in the normal virgin pore pressure trend.

It was reasoned originally that electrical resistivity would be a good indicator of the water content in the rock [18]. Moreover, it was assumed that the more water content the higher (virgin) pore pressure and the lower the resistivity would be. However, this theory, which is the basis for the Eaton's equation, remains questionable [20]. Electrical resistivity is affected by other factors such as porosity of the rock, permeability, moisture content, concentration of dissolved electrolytes, temperature, phase of the pore fluid,

clay content, among others. Thus, there might be other parameters that affect the resistivity value of a rock but have negligible effect on the virgin pore pressure. In other words, a change in the value of resistivity from its normal trend might have, in certain occasions, nothing to do with abnormal virgin pore pressure. Nevertheless, Eaton's equation is until today one of the most commonly used relationships to determine virgin pore pressure [21].

Since Eaton presented his famous equation, there has been an enormous amount of publications and proprietary work on pore pressure predictions. According to Standifird et al. [4], investment to better understand abnormal pore pressure can be categorized into three areas: data acquisition, modeling, and software. Currently, the main sources of data acquisition to understand rock and fluid properties are surface logging, electric logging (wireline or logging while drilling [22]), and seismic reflection. A big effort has been focused on developing deterministic and stochastic models [23, 24] to better translate the measurements into the desired properties [4]. Advancements in software improve the efficiency of using the available models. However, the pore pressure prediction methods are still based on the concept of effective stress and Eaton's equation. That is, current pore pressure prediction is primarily based on the divergence of the petrophysical measurements from the normal compaction trend [25-27]. This implies that well planning to estimate the pore pressures is based on neighboring well information and usually seismic data of the well being planned (since seismic data can be gathered before the well is drilled).

Neighboring wells provide the most accurate information for pore pressure prediction. This is valid because formation layout can span several hundred miles. After a well is drilled, wireline operations can be used to measure other properties of formations adjacent to the wellbore. This data can then be applied to the new well site within close proximity. However, these formations may be separated by faulting, and the new well site will exhibit different properties.

Seismic modeling can also provide valuable pre-drill data. However, the most advanced seismic methods, seismic tomography, have a resolution on a readable scale of half a kilometer [28] when used from the surface. These methods may allow for ballpark estimates, but abnormal pressures variations may occur within a few hundred feet. These methods can be improved by applying down-hole seismic measurement data, cuttings data, leak-off test data, and other drilling information to improve the model. Pore pressure can also be estimated using inference methods, but these methods estimate pressures in shale, not sand. The pressures in nearby regions of sand and shale are not necessarily the same; therefore, there is no way to predict pressure changes at their boundaries until they have been crossed.

An advanced method of monitoring downhole pressure is measurement while drilling (MWD). MWD data can be taken by several tools. These tools are able to measure direct formation pressure by inserting a probe or drawing down on the formation. The instruments measure the formation pressure after allowing the pressure to equilibrate. Though helpful, this technique cannot be applied to shales that have a very low permeability since the time for pressure equilibration is extremely long. Furthermore, these measurements must be taken behind the bit, and the pore pressure of neighboring sand/shale formations cannot be assumed to have the same formation pressure. Therefore, the pore pressure will be previously encountered before the formation pressure can be measured. Even though pore pressure problems can be prepared for in advance, the drilling operator will not know at what exact depth they will occur. Thus, the need is sill for a method that can be used to predict pore pressure ahead of the bit during drilling. Next section describes a need analysis conducted in an effort to identify the functions that are necessary for a methodology that can be used to determine pore pressure ahead of the bit.

2.3 Need analysis

In a perfect drilling situation, the hydrostatic (mud) pressure would always equal the virgin pore pressure. This perfect drilling situation would be easily accomplished if the virgin pore pressure could be exactly determined at each depth. In real drilling situations, however, the hydrostatic (mud) pressure is kept above the pore pressure to equilibrate small or unexpected variances in virgin (abnormal) pore pressure, but below the fracture pressure to prevent damage to the formation. Thus, the pressure of the hydrostatic column of mud must be controlled between two boundaries: the formation pore pressure and the formation fracture pressure (see Figure 2.1). If the hydrostatic pressure of the mud column decreases to a value lower than the pore pressure (under-balanced situation), the fluids in the formation will flow into the wellbore and drilling must be stopped to prevent kicks, blowouts, or collapses. In an over-balanced situation, the mud pressure is higher than the formation pore pressure. However, if the mud pressure is increased above the fracture pressure of the exposed formation, the mud will flow into the formation and mud circulation within the wellbore will be lost, increasing the risk of collapses and damage of the reservoir formation.

The difference between the hydrostatic (mud) pressure and the pore pressure in the formation is termed *differential pressure.* The margin of safety provided by a positive *differential pressure* must be increased as the uncertainty in virgin pore pressure at the bit increases. Due to the pressure difference, drilling rates of penetration in an over-balanced situation are decreased and a portion of the mud flows into the formation. Mud flow into the formation is undesirable because it damages the future reservoir's production volume and life. If the formation virgin pore pressure ahead of the bit is known, that gives time to the drilling operator at the surface to properly adjust the mud density in order to match the hydrostatic pressure to the virgin pore pressure at the drill bit when that formation is reached. Drilling with a small margin of safety could be effective in formations with high permeability that maintain a constant virgin pore pressure gradient (~ 0.45 psi/ft), until an unexpected zone with *abnormal pressure* is

encountered in the formation. If an unexpected zone of abnormal pore pressure is reached during drilling, and the hydrostatic mud pressure is significantly less than the abnormal pore pressure, the risk of gas kicks or blowouts, reservoir flow damage, wellbore instability, and sticking of tools or pipe increases dramatically. Thus, there is a need to provide means to determine the virgin pore pressure ahead of the bit during drilling.

In order to satisfy the need, it would be desirable to develop a method that could be used to determine virgin pore pressure from parameters that can be easily determined and/or measured during drilling. Furthermore, it would be desirable that such a method would be generally applicable for all types of rock and situations.

Parameters that are currently measured during drilling (using drilling monitoring systems) are torque, rate of penetration (ROP), weight on bit (WOB), bit revolutions per minute (RPM), equivalent circulation density (ECD), among others. These parameters are termed *drilling parameters* throughout this dissertation. The type of rock can be characterized with the *material properties* of both the solid matrix and the pore fluid. Tools such as *logging while drilling* (LWD) and *measurement while drilling* (MWD) provide measurements of natural gamma ray, neutron porosity, electrical resistivity, density and photoelectric index, etc., which can be used to infer the material properties of rock. However, rock properties can also be estimated using sonic or seismic techniques before drilling. Different situations can be described with *environmental parameters* which can be subdivided in two groups: (1) the *external parameters* defining the surrounding conditions to which a rock element is subjected during drilling, for example, confining stresses from Earth, the hydrostatic (mud) pressure, the load imposed by the drill bit, the overburden; and (2) the physical internal conditions of rock, such as pore pressure and temperature.

Following this reasoning, the ultimate goal would be to develop a method that could be used to determine virgin pore pressure ahead of the bit during drilling from drilling parameters, environmental parameters, and material properties.

A functional decomposition allowed identifying two main top-level functions for the design of a methodology that could be used to determine virgin pore pressure ahead of the bit during drilling from drilling parameters, environmental parameters, and material properties. The drilling process affects the original (virgin) state of the rock, both the stress state and pore pressure, due to the large stresses that the drill bit imposes on the rock. Since the drilling parameters are measured at the bit, it was hypothesized that the virgin pore pressure at the bit could be determined first, and then it could be related to the pore pressure ahead of the bit. Thus, the two functions for the design of this methodology are: (1) to provide means to determine the virgin pore pressure at the bit from drilling parameters, environmental parameters, and material properties; and (2) to provide means to relate the virgin pore pressure at the bit to the virgin pore pressure at the far-field. The far-field is defined as the location ahead of the drill bit where the pore pressure has not been altered by the drilling process.

The first top-level function has been identified from the hypothesis that the drilling parameters should be affected by the initial state of the virgin formation (including the pore pressure). However, there is a possibility that the virgin pore pressure has a negligible effect on the drilling parameters for a given set of environmental parameters. That is, the virgin pore pressure could be determined at the bit if at least one drilling parameter were significantly affected by the pore pressure. Therefore, it is necessary to determine if such drilling parameter(s) exists. For this reason, the objective of this dissertation is to determine whether or not it is possible to determine the virgin pore pressure at the bit from drilling parameters, environmental parameters, and material properties. The second top-level function is not addressed in detail in this dissertation. However, a recommended approach to satisfy this function is proposed in Chapter VIII.

Three functions have been identify to be needed in order to be able to predict virgin pore pressure at the bit from drilling and environmental parameters, and material properties: (1) provide means to identify the drilling and environmental parameters that are affected by the virgin pore pressure, (2) provide means to identify the material properties that play a role in the physics of the drilling process, (3) provide means to relate the virgin pore pressure, drilling parameters, environmental parameters, and material properties. A function structure of the methodology to determine pore pressure is presented in Figure 2.2. The function structure is an aid to visualize all the functions that are needed in order to satisfy the objective.
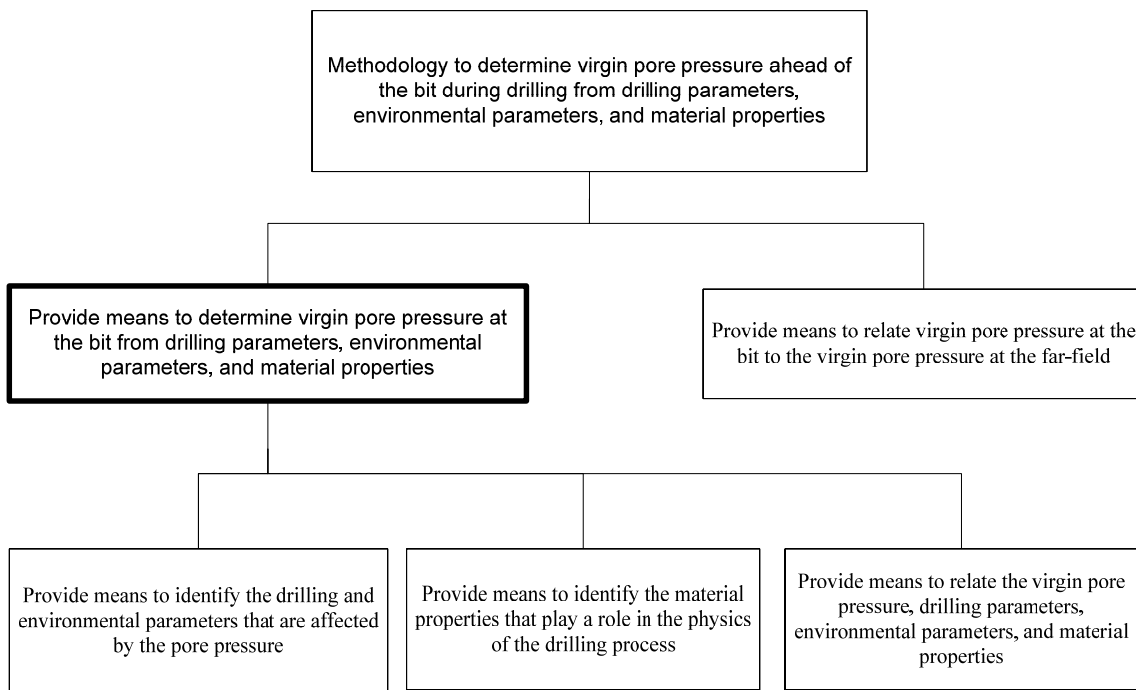
Figure 2.2 Function structure of the methodology to predict pore pressure ahead of the bit from drilling parameters, environmental parameters, and material properties.

The darker box in Figure 2.2 corresponds to the function that is the objective of this dissertation. A description of the approaches considered in order to address the functions

that are needed to satisfy the objective of this dissertation is presented in the next section.

2.4 Approaches considered to address the functions from the need analysis

Three approaches have been considered in an attempt to address all the functions described in the previous section for a methodology to determine virgin pore pressure ahead of the bit from drilling parameters, environmental parameters, and material properties. A historical background of the reasoning pursued on each approach is presented in this section. Technical details and developments from each approach are presented in Chapters III, IV, and V, respectively. The approaches considered are presented in the chronological order in which they were conceived. The work done in all three approaches considered attempts to address the three bottom-level functions in the function structure (see Figure 2.2): (1) provide means to identify the drilling and environmental parameters that are affected by the virgin pore pressure, (2) provide means to identify the material properties that play a role in the physics of the drilling process, (3) provide means to relate the virgin pore pressure, drilling parameters, environmental parameters, and material properties.

2.4.1 First approach considered

The first approach considered is the Principal Stress Pore Pressure Prediction (PSP^3) concept, which initially developments were reported to BP America [5-7]. Early work on the PSP^3 concept has also been presented in [8]. The Principal Stress Pore Pressure Prediction (PSP^3) concept has been developed under the hypothesis that the virgin pore pressure at the bit could be determined during drilling by identifying the effective stresses (from drilling parameters) of the rock being drilled, in combination with a Mohr-Coulomb failure criterion. The concept of effective stress implies that it is the effective stress, rather than the total stress, that determines whether the rock fails or not due to an external load. Furthermore, it has been recognized that the drilling parameters are not independent from each other, but they could be grouped into a fundamental

parameter: the *mechanical specific energy* (MSE). Teale [9] used for the first time the term Mechanical Specific Energy (MSE) to designate that amount of energy per unit volume required to fragment the face of a solid wall of rock, even though previous investigations on the energy requirements for rock fracture had been conducted by Simon [29]. The concept of mechanical specific energy has been used in the oil and gas industry as a quantifier of common drilling problems [30], as an indicator used to maximize the rate of penetration [31], and in general, as an index to evaluate the drilling performance [32]. However, there is no information available in current open literature that suggests the use of MSE to predict virgin pore pressure. The PSP[3] concept has been developed under the premise that the MSE should be a function of the effective stress rather than the total stress of the rock, and from this relationship the virgin pore pressure could be predicted.

If effective stresses in the drilling process and the Mohr-Coulomb failure envelope of the rock being drilled are identified, it is possible to solve for the virgin pore pressure. An expression to determine virgin pore pressure was derived in terms of drilling parameters, the hydrostatic mud pressure (environmental parameter), and the failure envelope parameters (material properties). Thus, empirical work on the PSP[3] concept indicates that, besides the effective stress, a relationship between the amount of energy required to fragment the rock and virgin pore pressure might exist. However, results show that the calculated virgin pore pressure is not always in agreement with the virgin pore pressure from a post-drill analysis (considered as the true value of virgin pore pressure) of three wells for which data is available. Details of the development of the PSP[3] concept and its results are presented in Chapter III.

The lack of validation of the PSP[3] concept led to believe that the parameters used in the PSP[3] concept are not enough to correctly describe the drilling process. It was recognized that there are other parameters and material properties that are not accounted for in the PSP[3] concept, for example, porosity, permeability of the rock, type of fluid in the pores,

and temperature, which might have an important effect in the formation virgin pore pressure. These shortcomings suggest that a fundamental understanding of the parameters that affect or are affected by virgin pore pressure is required in order to achieve a successful virgin pore pressure prediction methodology.

In order to gain a better understanding of the PSP[3] concept (first approach considered) and use it to proposed a second approach to address the functions presented in the function structure (see Figure 2.2), a literature review was conducted to identify if there were any prior fundamental investigations of virgin pore pressure prediction from drilling and environmental parameters. Besides Eaton's equation, Equation (2.4), two perspectives were identified from the literature to be important in the fundamental understanding of the role of virgin pore pressure in the mechanical behavior of rock.

The first perspective is the work developed by Detournay and Atkinson [33]. By using the effective stress concept and the Mohr-Coulomb failure criterion, Detournay and Atkinson developed a relationship between mechanical specific energy and pore pressure by analyzing the forces applied to the rock by a cutting tool during the cutting process. Detournay and Atkinson had previously investigated the decomposition of forces acting on rock by the cutting tools [34, 35] during the cutting process. They based their analysis of forces on previous analyses conducted by Merchant for metal cutting [36, 37]. By using the effective stress concept and the Mohr-Coulomb failure criterion, Detournay and Atkinson were able to derive a relationship for the MSE (drilling parameters) as a function of differential pressure (environmental parameters), geometrical parameters of the drill bit (drilling parameters), and failure parameters (material properties). The relationship derived by Detournay and Atkinson [33] expresses MSE as the dependent variable. Physically this is true, since the specific energy required to fracture a rock must be a function of the initial state of that rock (including the pore pressure), but the virgin pore pressure is by no means affected by the energy applied to break the rock. Nevertheless, if the MSE is known (or calculated from

drilling parameters), as well as the geometrical parameters of the bit, the pore pressure can be back-calculated.

Detournay and Atkinson [33] reasoned that the pore volume increases at the shear zone during rock cutting since the rock expands. As the volume of the pores increases, the pore pressure in low-permeability rock decreases if enough fluid is not supplied into the expanded pores. Because of the low permeability, the rapid decrease in pore pressure can be so large that cavitation in the shear zone might occur (the pore pressure would be effectively zero). Therefore, Detournay and Atkinson [33] concluded that, in the cutting process of low-permeability rocks, MSE is independent of the virgin pore pressure and depends only on the hydrostatic (mud) pressure. They supported their conclusion with experimental work conducted by Zijsling [38]. However, Zijsling's findings are only consistent with Detournay and Atkinson's theory for one set of data run for a medium-hard illitic Mancos shale that was initially under-saturated. Furthermore, the earlier work of Zijsling showed that for a fully saturated soft montmorillonitic Pierre shale, the cutting process was affected by both, the pore pressure and the hydrostatic pressure, which is in disagreement with Detournay and Atkinson's conclusion.

The work presented by Detournay and Atkinson [33] is probably the only one that attempts to describe the relationship between pore pressure at the shear zone and pore pressure in the far-field from basic principles. However, the relationship presented by Detournay and Atkinson between mechanical specific energy and pore pressure does not seem to be derived from basic principles. Detournay and Atkinson expresses that the MSE is a function of differential pressure, material properties, and geometric properties of the drill bit. A relationship based on a fundamental approach should not be a function of geometric parameters of the cutting tool, because it should not matter how the energy is applied to break the material, but how much energy is applied and absorbed by the material.

The second perspective, the US Patent 7,412,331-B2 by Calhoun, et al., claims a method to predict rate of penetration (ROP) of a drill bit drilling a wellbore, that uses an equation based upon specific energy principles [39]. The method uses several relationships among the confined compressive strength (CCS), the bit-specific coefficient of sliding friction (μ), mechanical efficiency (EFF_M), weight on bit (WOB), bit RPM. Even though the claim of the patent is to predict the rate of penetration of a drill bit in a drilling process by using specific energy principles, special emphasis was placed on the calculation of the in-situ (virgin) pore pressure. It is noteworthy to point out that this work attempts to determine the change in virgin pore pressure at the shear zone rather than assuming that the pore pressure at the shear zone in low-permeability rock is effectively zero as concluded by Detournay and Atkinson [33]. That change in pore pressure at the shearing zone was determined by the so-called Skempton [40] pore pressure coefficients. The concepts and relationships described in the patent could be utilized to calculate virgin pore pressure, assuming that the ROP is known. Thus, the relationships on this patent also attempt to relate pore pressure to MSE (drilling parameters), material properties, and environmental conditions [39].

Attempts to validate the relationships from these two perspectives with drilling log data failed. Details of the attempted validation are presented in [7]. The lack of validation led to explore ideas for a more fundamental approach to the problem of pore pressure prediction, which prompted the proposal of the second approach presented in this dissertation.

2.4.2 Second approach considered

The second approach considered in the course of this investigation is the proposal of a fundamental parameter that can be used in Eaton's equation [Equation (2.4)] to replace the parameters originally proposed by Eaton [10]. After reviewing the ideas presented by Eaton [10] and analyzing drilling data (torque, ROP, resistivity, RPMs, WOB) of logs from three wells available to the author, it was reasoned that a fundamental parameter,

such as MSE, could be used as the variable in the ratio in Eaton's equation. This reasoning is explained in Chapter IV, and attempts of validation of this concept are presented as well. Validation of this new equation against post-drill pore pressure, using drilling log data from three different wells, shows promising results. However, it is also recognized that further work is needed in order to understand why this relationship correctly predicts the pore pressure for the data used in the validation. Therefore, a fundamental approach based on basic principles is proposed to understand the solid-fluid interactions of rock during drilling. This fundamental approach is the third approach considered in this dissertation.

2.4.3 Third approach considered

The third approach considered is a fundamental approach to relating pore pressure, drilling parameters, environmental parameters, and material properties. The background of this fundamental approach is presented in this section and technical details are presented in Chapter V.

It has been recognized that a fundamental understanding of the rock-fluid interactions during drilling could provide an insight of the relationships among pore pressure, drilling parameters, environmental parameters, and material properties. In order to understand the possible relationship between pore pressure and mechanical specific energy, a more fundamental way of viewing MSE is proposed (see Chapter V). It has also been recognized that a fundamental approach based on basic principles such fluid mechanics, porous media, thermodynamics, and rock mechanics, could be used to explain the role of virgin pore pressure in the mechanical behavior of rock and eventually evolve into a methodology for virgin pore pressure prediction that would be reliable for all types of rocks, and situations.

In order to identify the basic principles that describe the rock-fluid interactions during the drilling process, the cutting process of rock during drilling must be analyzed. The

failure of rock during drilling is caused by the large stresses imposed on the rock by the drill bit. These stresses cause the rock to deform until failure is reached. The process of deformation of rock results in a change in pore volume. Depending on the permeability of the rock (which dictates how fast the pore fluid can be expelled from or filled in the pores), the local pore pressure at the cutting zone can either increase or decrease. It was mentioned above that the pore pressure plays an important role in the mechanical behavior of rock, since part of the stress applied to the rock are supported by the pore fluid. Thus, a change in pore pressure during drilling will result in a change in the mechanical behavior of rock, but a change in the mechanical deformation results in a change in pore pressure too. That is, there is a two-way coupling between the mechanical deformation and the pore pressure of rock. The general theory that accounts for this coupled hydro-mechanical behavior is *poroelasticity* [1]. This theory was first proposed by Biot [16] in 1941, and developed further by Rice and Cleary [41], and Detournay and Cheng [42], among others. This theory accounts for deviatoric stresses, as well as hydrostatic stresses, and pore fluid pressures.

For many years, Biot's poroelasticity theory [16] was used only to solve problems involving consolidation of soils. However, a few decades later the equations of poroelasticity were successfully applied to solve problems in tectonophysics [43], petroleum-related rock mechanics [1], and even in the medical field to study the behavior of bones [44]. In petroleum-related rock mechanics, the effort has been concentrated on borehole stability, hydraulic fracturing, and compaction near pumping wells [45, 46]. However, to the best knowledge of the author, there are no investigations available in open literature that attempt to describe the drilling process (rock cutting) using poroelasticity equations.

Nevertheless, there are no indications that suggest that the equations of poroelasticity should not be used to describe the process of cutting rock. This is one of the main contributions of the present work: the use of the poroelasticity equations to describe the

cutting of rock. The equations of poroelasticity are solved numerically using the commercial software COMSOL Multiphysics. The proposed model is presented in Chapter V along with details of the poroelasticity equations. The model is validated with experimental data available in open literature. Once the model is validated it can be used to identify the drilling parameters, environmental parameters, and material properties that significantly affect (or are affected) by the drilling process (functions 1 and 2 in bottom level of function structure in Figure 2.2). In order to identify the significant parameters, a sensitivity analysis is conducted. The poroelastic model of the cutting process is also used to investigate if the PSP[3] concept (first approach considered) and the concept of using MSE as a new parameter in Eaton's equation (second approach considered) comply with basic principles of fluid mechanics, rock mechanics, and porous media. With this information, the question (and objective of this dissertation) of whether or not it is possible to determine the virgin pore pressure at the drill bit from drilling parameters, environmental parameters, and material properties may be answered.

In summary, the first and second approaches are empirical approaches for addressing the functions needed to satisfy the objective of this dissertation; whereas, the third approach is a fundamental approach based on basic principles including rock mechanics, porous media, and fluid mechanics.

In this chapter, the background of the investigation presented in this dissertation has been described. Next chapter of this dissertation presents technical details of the development of the PSP[3] concept.

CHAPTER III

PRINCIPAL STRESS

PORE PRESSURE PREDICTION (PSP^3)

The work done on the first approach considered in this dissertation in order to determine whether or not it is possible to determine pore pressure at the bit from drilling parameters, environmental parameters, and material properties is presented in this chapter. The first approach considered is the Principal Stress Pore Pressure Prediction (PSP^3) concept. The PSP^3 concept has been developed under the hypothesis that the virgin pore pressure at the bit could be determined during drilling by identifying the effective stresses (from drilling and environmental parameters) of the rock being drilled, in combination with the Mohr-Coulomb failure criterion (material properties). This chapter describes the theoretical background used as a basis for the development of the PSP^3 concept. Subsequently, the development of the PSP^3 concept is presented, which includes the identification of the stress state of the rock during drilling, and geometric relations used to determine the PSP^3 equation (which expresses pore pressure as a function of drilling parameters, environmental parameters, and material properties). Finally, attempts to validate the PSP^3 concept with post-drill pore pressure data available from three oil wells are presented.

3.1 Theoretical background of the PSP^3 concept

The theoretical background used as a basis for the development of the PSP^3 concept is presented in this section. The graphical representation of the stress state of a rock, which is based on the analysis of stress in two dimensions, is presented first. Subsequently, the Mohr-Coulomb failure criterion is described.

3.1.1 Graphical representation of stress

In rock mechanics, the forces acting at any point in the interior of a rock body are best described with the concept of stress, since the force applied usually varies from point to

point. Stress is defined as the force acting on a surface area. The analysis of stress is a matter of pure statics and does not depend on the material properties [47]. The discussion of representation of stresses is presented in two dimensions since it is simpler than in three dimensions, without lost of generality.

The forces acting at a point in the interior of a body may be described by considering the ratio of the force to an area in a plane that passes through the same point. The limiting value of such a ratio when the area tends to zero is the *stress vector* or *traction vector*, and it is mathematically expressed as

$$\boldsymbol{p} = \lim_{\delta A \to 0} \frac{\delta \boldsymbol{F}}{\delta A} \tag{3.1}$$

where $\boldsymbol{p}$ is the traction vector, $\delta \boldsymbol{F}$ is the force acting on a plane of area δA.

In the above definition, there is no restriction on the orientation of δA. This implies that the traction vector can be different at any given point on different planes that pass through that point. This complication is eliminated by the introducing the concept of stress (by Cauchy in 1823 [1]). If a rectangular coordinate system in two dimensions (x, y) is considered, in which δA is perpendicular to the x-direction, the traction vector $\boldsymbol{p}$ has components σ_x, τ_{xy} on the x- and y-directions, respectively. The component σ_x is the *normal stress*, since this component of the traction vector acts perpendicular to δA, while the component τ_{xy} is the *shear stress,* since it acts parallel to δA. Similarly, if δA is oriented perpendicular to the y-direction, the traction vector $\boldsymbol{p}$ has components τ_{yx}, σ_y. These quantities form the stress tensor, which in two dimensions is expressed as

$$\begin{bmatrix} \sigma_x & \tau_{xy} \\ \tau_{yx} & \sigma_y \end{bmatrix} \tag{3.2}$$

The physical significance of the stress tensor is illustrated in Figure 3.1, which shows a two-dimensional rock element whose faces are each perpendicular to one of the coordinate axes. Each of the components of the stress tensor, Equation (3.2), can be considered a vector. In rock mechanics, compressive stresses are considered as positive since they are much more common than tensile stresses.
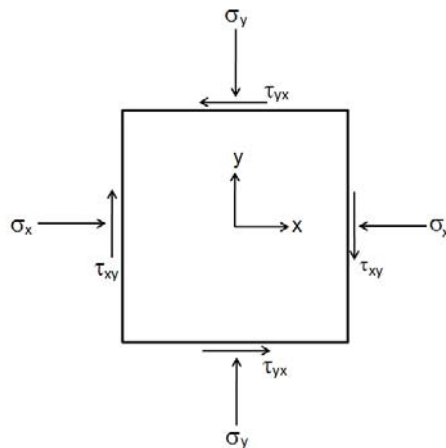
Figure 3.1 Stress components acting on a rock element.

It is important to recall that the interest is to determine the forces that act on a rock body at any point. Since the stress is the ratio of force to differential area, then the interest becomes to determine the stresses of a rock element at any plane. In order to determine the transformation of stress components at any plane, a triangular element of rock subjected to compression can be considered, see Figure 3.2. The triangular element shown in Figure 3.2 results from a plane (whose outward normal vector is rotated counterclockwise from the x-direction by an angle β) that crosses the rock element in Figure 3.1.
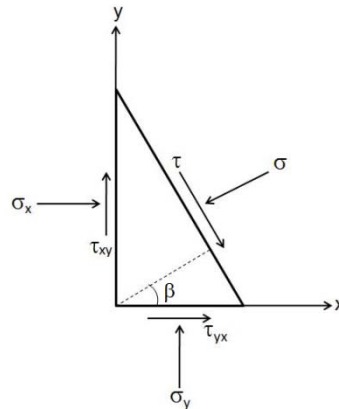
Figure 3.2 Triangular rock element used for stress transformation equations, after Jaeger et al. [1].

The normal and shearing stresses acting on a plane whose outward unit normal vector is rotated counterclockwise from the x-direction by an angle β can then be determined from

$$\sigma = \frac{1}{2}(\sigma_x + \sigma_y) + \frac{1}{2}(\sigma_x - \sigma_y)cos2\beta + \tau_{xy}sin2\beta \qquad (3.3)$$

$$\tau = \frac{1}{2}(\sigma_y - \sigma_x)\sin 2\beta + \tau_{xy}\cos 2\beta \qquad (3.4)$$

Details of the derivation of Equations (3.3) - (3.4) are explained in [1].

Mohr [48] proposed a simple graphical construction to represent the state stress of a material at any point. It can be established from Equations (3.3) and (3.4) that there are planes on which the shear stress vanishes. The normal stresses at planes where the shear stress is zero are known as *principal normal stresses.* Besides acting on planes on which there is no shear, the normal stresses are also a maximum and a minimum normal stresses that act on any plane. If the coordinate system is chosen so that the principal stresses act on the direction of the coordinate system (and in which the shear stresses are zero), Equations (3.3), and (3.4), take the form

$$\sigma = \frac{(\sigma_{max} + \sigma_{min})}{2} + \frac{(\sigma_{max} - \sigma_{min})}{2}\cos2\beta \tag{3.5}$$

$$\tau = -\frac{(\sigma_{max} - \sigma_{min})}{2}\sin2\beta \tag{3.6}$$

where σ_{max} is the maximum principal stress, σ_{min} is the minimum principal stress, and σ and τ are the normal and shear stresses, respectively, at any plane whose normal vector is rotated counterclockwise by the angle β.

In can be observed that Equations (3.5) and (3.6) are the equations of a circle in the (σ, τ) plane, with center at $\left[\sigma = \frac{\sigma_{max} + \sigma_{min}}{2}, \tau = 0\right]$, and with radius $\frac{(\sigma_{max} - \sigma_{min})}{2}$, see Figure 3.3. Many of the important properties of the two-dimensional stress tensor can be read directly from the Mohr's circle.
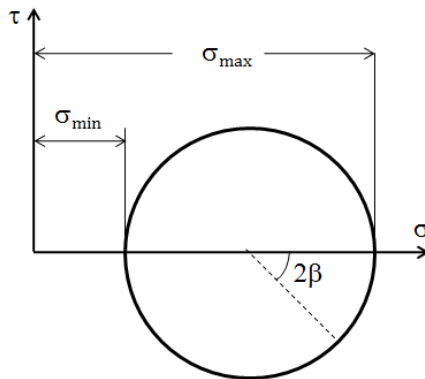
Figure 3.3 Mohr's circle representation of stresses.

The maximum principal stress (σ_{max}) is at the intersection between the normal stress axis (σ) and the farthest point of the Mohr's circle from the origin. At this state, shear stress is not being applied to the element and the largest normal stress is equal to the principal stress. The other intersection of the normal stress axis with the Mohr's circle is the minimum principal stress (σ_{min}). At this state, shear stress is also not being applied to the element and the smallest normal stress is equal to the principal stress.

Mohr's representation of stresses can also be applied to a three dimensional element as the one shown in Figure 3.4. If only principal stresses are applied to the external faces of the element, the stress state of that element can be represented with Mohr's circles as shown in Figure 3.5.
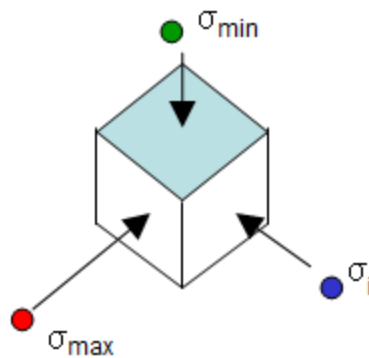
Figure 3.4 Three-dimensional stress element.
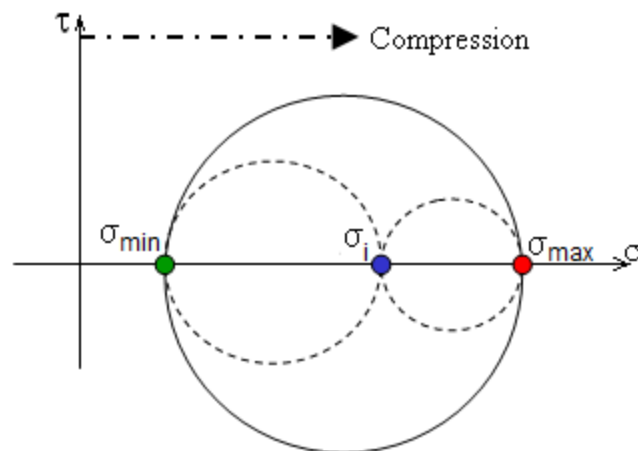
Figure 3.5 Mohr's circle representation of a three-dimensional stress element.

It can be seen from Figure 3.5 that to draw the outer Mohr's circle only the maximum and minimum principal stresses need to be defined. That is, the maximum shear stress in the three-dimensional element is found in the plane $[\sigma_{min}, \sigma_{max}]$. The intermediate stress (σ_i), which lies on the range $\sigma_{min} \leq \sigma_i \leq \sigma_{max}$, does not need to be defined in order to determine the maximum shear stress within the rock element. This has an important implication in the failure of rock under shearing, as it is explained in the next section. If the stresses on the rock are increased, the rock will be deformed until failure occurs. In order to determine the stress state of the rock when failure occurs, a failure criterion must be defined. One of the more common failure criteria used in rock mechanics is the Mohr-Coulomb failure criterion. This failure criterion is used in the development of the PSP[3] concept. Therefore, a brief description of the Mohr-Coulomb failure criterion is presented in the next section.

3.1.2 Mohr-Coulomb failure criterion

The Mohr-Coulomb failure criterion is probably the simplest and most important failure criterion used in rock mechanics. Although it is known as the Mohr-Coulomb criterion, it is important to notice that Mohr and Coulomb theories of rock failure have a different physical background.

Coulomb [49] introduced his failure criterion in 1773, after having conducted an extensive experimental investigation of friction in rock. From the findings of his investigation, Coulomb suggested that failure in rock and soil occurs along a plane due to shear stress acting on that plane. He also observed that motion of sliding surfaces along the failure plane appear to be resisted by a frictional-type force which was proportional to the normal stress acting along that plane. However, in contrast to sliding along non-welded surfaces, motion along the initially intact failure plane appeared to be resisted by an internal cohesive force of the material. That is, in the absence of a normal stress, a finite shear stress, S_0, is still needed to initiate failure. Thus, Coulomb proposed that failure will occur along a plane where

$$|\tau| = S_0 + m\sigma \tag{3.7}$$

where τ is the shear stress, S_0 is the *cohesion* of rock, m is the *coefficient of internal friction*, and σ is the normal stress. The sign of the shear stress affects only the direction of sliding after failure. Coulomb failure criterion states that failure occurs on any plane for which $|\tau| \geq S_0 + m\sigma$. In the plane $[\sigma, |\tau|]$, Equation (3.7) is a straight line with slope $m = \tan\phi$, where ϕ is the angle of internal friction of rock. The Mohr's circle corresponding to any stress state that leads to failure will be tangent to this line. It is important to point out that, despite the historical its importance, the Coulomb failure criterion is unrealistic in two aspects: (1) it over-predicts the unconfined tensile strength of rock, and (2) experimental data shows that the compressive stress required to cause failure does not increase linearly with the confining stress. Mohr [50] suggested that Coulomb's Equation (3.7) be corrected by a more general relation of the form

$$|\tau| = f(\sigma) \tag{3.8}$$

Mohr suggested that the shear stress that causes failure could be a non-linear function of the normal stress. The function in Equation (3.8) is usually determined experimentally by inserting a cylindrical rock specimen in a press and loading the specimen until it fractures. The stress required to break the rock specimen is defined as the rock compressive strength. Stress can also be applied to the sides of the specimen during testing, which is defined as the confining stress. When the specimen is loaded on three different axes, the test is termed a *tri-axial test*. Figure 3.6 shows a rock specimen under tri-axial stress conditions and the stresses being applied to it.
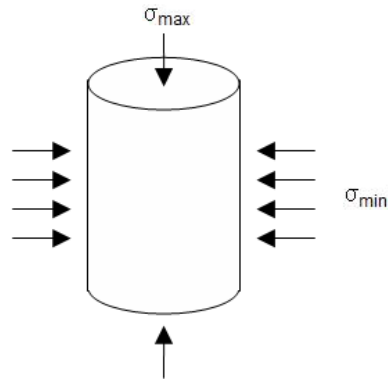
Figure 3.6 Tri-axial test.

As the confining stress (σ_{min}) is increased, the compressive stress (σ_{max}) required to fracture the rock also increases. If the tri-axial tests of increasing confining stress, and the resulting σ_{max} required to break the specimen are plotted as Mohr's circles, Figure 3.7 can be developed.
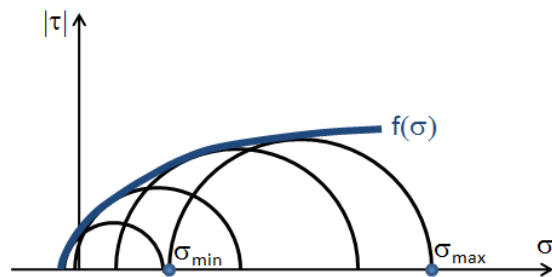
Figure 3.7 Mohr's envelope for a series of tri-axial tests.

Each circle is the graphical representation of the stress state of a rock sample at fracture. The function $|\tau| = f(\sigma)$ is the envelope that tangentially intersects all the Mohr's circles, and is termed as *Mohr's envelope*. The envelope encompasses all the Mohr's circles. A property of the Mohr's envelope is that it is unique for different rocks. That is, the function $|\tau| = f(\sigma)$ will be different for each type of rock. Even though the function is not linear, the basic ideas originally proposed by Coulomb's model are still valid.

Specifically, failure occurs if one of the Mohr's circles intersects the Mohr's envelope (also known as *failure envelope*). The value of the intermediate stress, for a situation such as the one shown in Figure 3.4 and Figure 3.5, does not affect the onset of failure. Furthermore, the Mohr-Coulomb theory predicts that the failure plane passes through the direction of the intermediate stress, and its normal vector makes an angle β with the direction of the maximum principal stress. It can also be recognized that the function $|\tau| = f(\sigma)$ may be replaced by a spline function characterized by several linear functions valid for a small range of normal stresses.

Another important consideration is the fact that rocks are porous materials that are usually saturated with a fluid. It has been mentioned before that the mechanical behavior of rock is affected by the presence of the pore fluid. Thus, it is plausible to expect that the effect of the pore fluid must be considered in rock failure. The pore pressure (internal pressure exerted by the pore fluid) can be regarded to act outward from the pore space. Moreover, pore pressure acts in some sense like a tensile stress. This reasoning leads to the Terzaghi's effective stress concept [3]. There were two arguments that led Terzaghi to the concept of effective stress: (1) increasing the external confining pressure results in the same volume change of the material as reducing the pore pressure by the same amount, (2) the shear strength depends only on the difference between the normal stress and the pore pressure. From these arguments, Terzaghi concluded that the effective stress is the portion of the load supported solely by the solid matrix and it is equal to the total stress minus the pore pressure, Equation (2.3).

The second statement above implies that it is the effective stress, rather than the total stress, that determines whether the rock fails or not due to an external load. It is reasonable to assume that the concept of effective stress is applicable to soils. However, some discrepancies may occur if the concept is applied to rocks. The Mohr-Coulomb criteria for failure of rock in terms of effective stress holds reasonably well provided that the permeability is sufficient to allow movement of fluid and that connected systems of

pores exist. Also, it is required that the pore-fluid is inert, so that the effects are purely mechanical. If these conditions are met, Equations (3.7) and (3.8) may be rewritten in terms of the effective stresses, and the failure criteria becomes

$$|\tau| = S_0 + m\sigma' \tag{3.9}$$
$$|\tau| = f(\sigma') \tag{3.10}$$

where σ' is the effective stress expressed as $\sigma - P_p$. Although the concept was proposed on an empirical basis, it has subsequently proved correct using Biot's poroelasticity theory [16]. Moreover, most experiments on rocks support the conclusion that the effective stress concept is valid [1]. In the context of Mohr's circles, replacing the total stresses σ with the effective stresses σ' has the effect of translating the Mohr's circle to the left by the magnitude of P_p, while maintaining the same diameter. This behavior is illustrated in Figure 3.8. It can be observed from Figure 3.8 that the increase of pore pressure brings a rock element closer to the failure envelope.
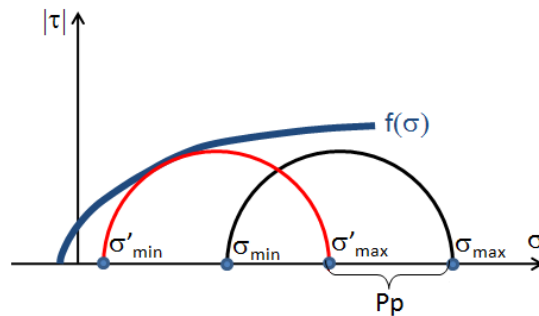
Figure 3.8 Effect of pore pressure on mechanical behavior of rock.

In this section, the theoretical background used as a basis for the development of the PSP^3 concept has been described. The development of the PSP^3 concept that led to an equation for pore pressure determination is presented in the next section.

3.2 Development of the PSP³ concept

The purpose of the development of the PSP³ concept is to determine a relationship among drilling parameters, environmental parameters, and material properties. It is desirable to determine such a relationship only among the parameters and material properties that play a significant role in the physics of the drilling process. In the development of the PSP³ concept, it was reasoned that the significant drilling and environmental parameters could be determined if the stress state of rock during drilling is determined. Furthermore, the stress state of the rock during drilling corresponds to the stress state at failure. Since the failure enveloped is unique for each type of rock, a relationship among drilling parameters, environmental parameters (including pore pressure), and material properties can be determined from the relationship between the stress state at failure and the failure envelope.

In this section, the development of the PSP³ concept is presented. The stresses acting on the rock during drilling are identified first. Then, the equation to determine pore pressure at the drill bit is presented, which is developed from geometric relations between the failure envelope and the Mohr's circle that represents the stress state of the rock during drilling.

3.2.1 Determination of the stress state of rock during drilling

In order to determine the stress state of rock at drill bit during drilling, a simplified two-dimensional model of the cutting process during drilling is considered. A schematic of a single cutter cutting on rock is illustrated in Figure 3.9.
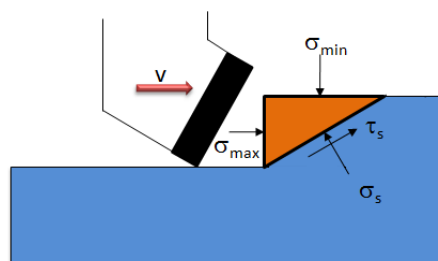
Figure 3.9 Two-dimensional sketch of a single cutter cutting a rock chip.

The two-dimensional model of the rock chip in Figure 3.9 resembles a tri-axial test. The maximum principal stress (σ_{max}) is defined by the horizontal stress applied to the chip since this is the stress that breaks the rock chip away from the rock formation. The minimum principal stress (σ_{min}) is then defined as the vertical stress acting on top of the rock chip. The shear stress (τ_s) and the normal stress (σ_s) act along the failure plane. These two stresses correspond to the intersection of the Mohr's envelope and the Mohr's circle as shown in Figure 3.10.
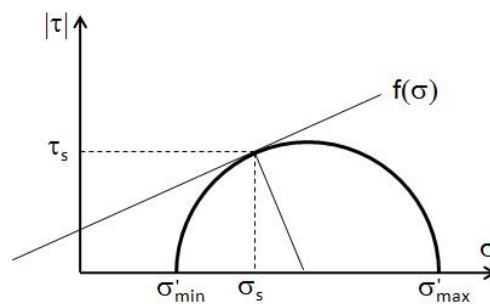
Figure 3.10 Mohr's circle representation of the stress state of the rock chip.

It has been mentioned in Chapter II that a mud fluid is used during drilling of a borehole. The hydrostatic pressure of the mud column acts, in addition to the cutting stress, in all directions around the rock chip in Figure 3.9. Therefore, the maximum and minimum principal stresses shown in the two-dimensional simplification of the drilling process (Figure 3.9) can be defined as:

- σ_{max}: Maximum Stress - Stress applied by the cutting force that acts over the lateral face of the rock chip plus the mud pressure acting on the bit.

- σ_{min}: Minimum Stress – Stress that results from the hydrostatic pressure (P_h) of the drilling mud acting on top of the rock chip.

This is represented schematically in Figure 3.11.
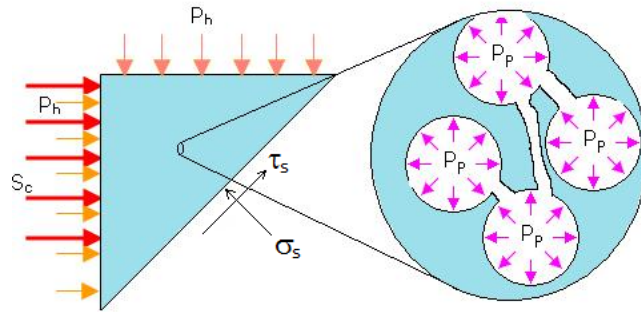
Figure 3.11 Two-dimensional stress element of rock chip with pore pressure.

It can be observed, by comparing Figure 3.9 and Figure 3.11 that the maximum principal stress (σ_{max}) in Figure 3.9 is defined as the summation of the cutting stress (S_c) applied horizontally and the hydrostatic mud pressure. It is important to recall that, for a saturated porous material such as rock, the failure criterion must be defined in terms of the effective stresses. Therefore, the maximum effective stress (σ'_{max}) for the two-dimensional model in Figure 3.9 is defined as the sum of the cutting stress (S_c) and the hydrostatic mud pressure, minus the pore pressure. Similarly, the minimum effective stress applied vertically (σ'_{min}) to the chip is defined as the differential pressure ($P_h - P_p$).

If a three-dimensional stress element is considered, then the third stress (σ'_i) is the confining stress on the element. This stress is a function of the load applied to the element by the overburden. Since this stress does not break the rock, it is assumed to be lower than the maximum stress (σ'_{max}), but higher than the vertical stress (σ'_{min}). Therefore, since the confining stress is bounded by $\sigma'_{min} \leq \sigma'_i \leq \sigma'_{max}$, then the confining stress is not required to draw the largest Mohr's circle, as it is shown in Figure 3.5.

At this point, three variables have been identified to play a role in the two-dimensional simplification of the drilling process: (1) pore pressure, (2) the hydrostatic mud pressure,

(3) the cutting stress. Since the objective is to determine the pore pressure, a relationship among the pore pressure, the hydrostatic mud pressure (environmental parameter), and the cutting stress must be determined. In a drilling situation, the hydrostatic pressure at the bottom hole is easily determined, since the density of the drilling mud is always known. Therefore, the cutting stress must be determined from of drilling parameters to facilitate the determination of pore pressure, from drilling parameters, environmental parameters, and material properties.

The cutting stress can be defined as

$$S_c = \frac{F_{cutter}}{A_{chip}} \tag{3.11}$$

where F_{cutter} is the cutting force of the drill bit tooth, and A_{chip} is the surface area of the lateral face of the rock chip.

To determine the cutting force, it is assumed that the single cutter shown in Figure 3.9 is one of many teeth on a PCD bit (polycrystalline diamond compact) which rotates at a given angular velocity while engage to the formation. Moreover, it is assumed that all teeth of the PCD bit are applying a stress larger than the compressive strength of the rock when a bit is cutting the formation. Therefore, the rock breaks away from the formation. If the bit is cutting efficiently (in absence of bit balling, missing teeth, etc) then all of the teeth will be engaged simultaneously. If the bit is assumed to be fully engaged, then all the teeth of the bit can be combined to form an "effective tooth." The "effective tooth" will have the cross-sectional area of the distance from the center line of the drill-string to the outer diameter of the hole by the depth of cut. This is can be seen in Figure 3.12.
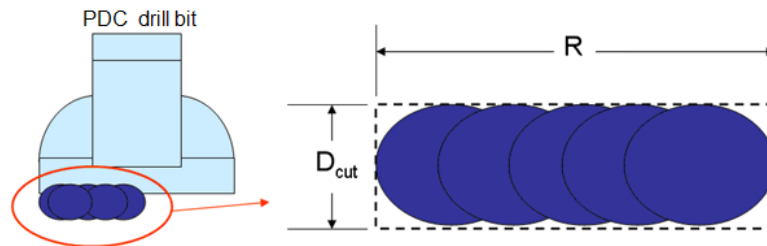
Figure 3.12 Area of effective tooth of a PDC drill bit.

From these assumptions, the integral of torque over the tooth can be defined by Equation (3.12) and rearranged to solve for the cutting stress, Equation (3.14). A schematic representation of the differential element in the torque integral is shown in Figure 3.13.

$$T = \int_0^R S_c \cdot D_{cut} \cdot r \cdot dr \tag{3.12}$$

$$T = \frac{S_c D_{cut} R^2}{2} \cdot \tag{3.13}$$

$$S_c = \frac{2T}{D_{cut} R^2} \tag{3.14}$$

where S_c is the cutting stress applied by drill bit (psi), T is the torque of the PDC bit (lb·ft), R is the radius of the drill bit (in), D_{cut} is the depth of cut (ft), r is the moment arm from cylindrical center of bit (in).
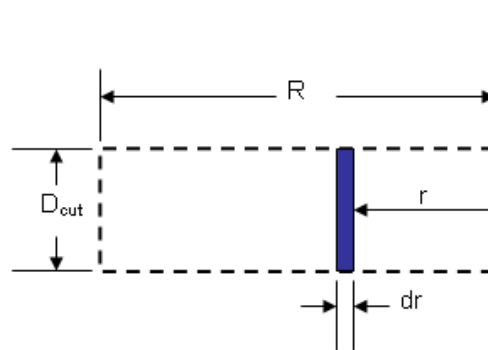
Figure 3.13 Differential element for torque integral.

The cutting stress can then be determined from Equation (3.14). Torque is a drilling parameter that is measured during drilling. Therefore, the only unknown in Equation (3.14) is the depth of cut (D_{cut}). The depth of cut must be determined to calculate the cross-sectional area to which the cutting force is applied. The penetration of the teeth can be determined as a function of volume of material removed per revolution. Therefore, the depth of cut is defined as

$$D_{cut} = \frac{ROP}{RPM} \tag{3.15}$$

where ROP is the rate of penetration (ft/h) and RPM is the angular velocity (revolutions per minute) of the drill bit. Similar to torque, both ROP and RPM are drilling parameters currently measured during drilling.

Substituting Equation (3.15) into Equation (3.14), and introducing a unit conversion factor, the following expression for the cutting stress can be determined:

$$S_c = \frac{480(RPM)(T)}{(ROP)(D_b^2)} \tag{3.16}$$

where all the variables are defined as in Equations (3.14) and (3.15) (with the same units). It can be seen that Equation (3.16) corresponds to one of the two components of the mechanical specific energy (MSE) expression originally derived by Teale [9]. MSE expression for rotary drilling accounts for the work done by both, the thrust and the torque, and is given by

$$MSE = \frac{480(RPM)(T)}{(ROP)(D_b^2)} + \frac{WOB}{A} \tag{3.17}$$

Mechanical specific energy (MSE) is defined as the amount of energy per unit volume required to fragment the face of a solid wall of rock [9]. MSE is commonly used to indirectly determine the downhole drilling environment from drilling measurements. Drilling measurements, including torque (T), rate of penetration (ROP), weight on bit (WOB), revolutions per minute (RPM), and diameter of the borehole (D_b), are combined in an equation that accounts for the input energy per unit volume required to fragment the rock formation. The units of MSE and rock strength are those of stress (typically in psi), which leads to the conclusion that MSE could be a function of the stress state at the borehole bottom. Since the pore pressure can also be defined as a stress, the hypothesis is that MSE can be correlated to the pore pressure (Pp). Currently, the MSE concept is utilized in industry only as a measurement of drilling efficiency, but not for determining pore pressure. The PSP[3] concept goes beyond the MSE measurement of efficiency to predict the pore pressure of the wellbore during drilling.

In summary, the stress state of a rock that is subjected to stresses by a drilled bit and by the drilling mud during drilling (at the very moment of failure onset) is determined by the principal stresses σ_{max} and σ_{min}. The effective stresses corresponding to the maximum and minimum principal stresses are determined from

$$\sigma'_{max} = S_c + P_h - P_p \tag{3.18}$$

$$\sigma'_{min} = P_h - P_p \tag{3.19}$$

respectively, where S_c is determined from drilling parameters according to Equation (3.16). It is important to note that, if the effective stresses are represented in a Mohr's circle as in Figure 3.10, the diameter of the Mohr's circle represents a magnitude equal to the cutting stress of the rock (see Figure 3.14).
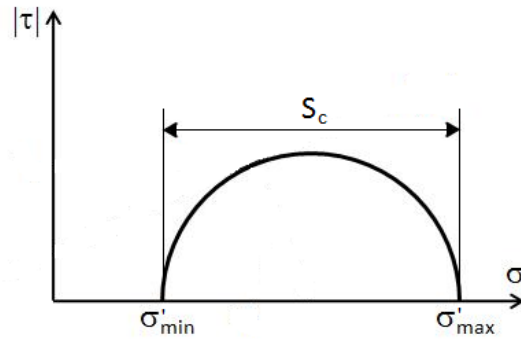
Figure 3.14 Graphical representation of the cutting stress in the Mohr's circle.

Once the stress state of the rock during drilling is determined in terms of the effective stresses, the Mohr-Coulomb failure criterion can be applied in combination to geometric relations from the Mohr's circle representation of the stress state of the rock in order to determine the relationship among pore pressure, drilling parameters, environmental parameters, and material properties. The development of this relationship is described in the next section.

3.2.2 PSP³ equation for pore pressure prediction

When the rock chip in Figure 3.9 reaches failure, the Mohr's circle that represents the effective stresses on the rock chip will tangentially intersect with the Mohr's envelope of that type of rock. Assuming a linear Mohr's envelope of the form given in Equation (3.9), and using the segment lengths defined in Figure 3.15, the minimum effective stress can be expressed in terms of the radius of the Mohr's circle (r_M) and the segments L_1 and L_2 as

$$\sigma'_{min} = L_1 - (L_2 + r_M) \tag{3.20}$$

where $L_1 = \dfrac{r_M}{\sin \phi}$, and $L_2 = \dfrac{S_0}{\tan \phi}$.
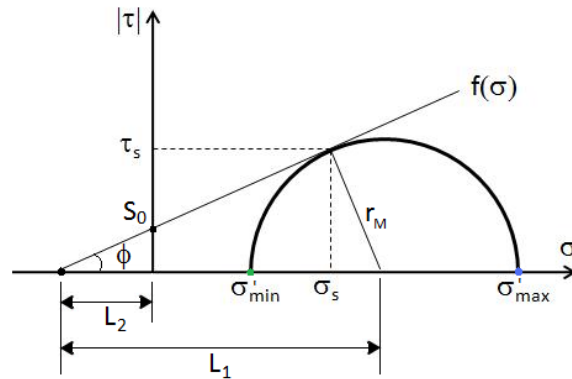
Figure 3.15 Geometric relations of the cutting stress in the Mohr's circle and Mohr's envelope.

The rock cohesion (S_0) represents the intercept of the Mohr's envelope with the shear stress axis at zero normal stress; whereas, the coefficient of internal friction (m) represents the slope of Mohr's envelope. The coefficient of internal friction is related to the angle of internal friction of the rock by

$$m = \tan \phi \tag{3.21}$$

Substituting the expressions for L_1 and L_2 into Equation (3.20), knowing that the diameter of the Mohr's circle is equal to the cutting stress, and solving for pore pressure, the following equation can be determined

$$P_p = \frac{S_c}{2}\left(1 - \frac{1}{\sin \phi}\right) + P_h + \frac{S_0}{m} \tag{3.22}$$

Equation (3.22) can be rearranged, using Equation (3.21), as

$$P_p = \frac{S_c}{2}\left(1 - \frac{\sqrt{1 + m^2}}{m}\right) + P_h + \frac{S_0}{m} \qquad (3.23)$$

It should be noted that the virgin pore pressure (P_p) is not physically a function of cutting stress (S_c). On the contrary, the hypothesis in the PSP[3] concept is that the cutting stress (which is a fraction of the MSE) depends on the virgin pore pressure. Since S_c can be calculated from drilling measurements, the pore pressure can be back calculated if the relationship among the cutting stress, the hydrostatic pressure, and pore pressure is identified. Equation (3.23) provides such a relationship and it is the final form of the PSP[3] concept to determine pore pressure at the bit during drilling from drilling parameters [cutting stress (S_c), Equation (3.16)], environmental parameters (P_h), and material properties (m, S_o). Attempts to validate Equation (3.23) have been conducted using drilling log data of three oil wells and compared to the post-drill pore pressure of each well. The results of the pore pressure determined with Equation (3.23) are presented in the next section.

3.3 Results of pore pressure prediction from the PSP[3] concept

Comparisons of pore pressure profiles of three oil wells determined from post-drill pore pressure analyses with predictions of pore pressure determined with the PSP[3] equation, Equation (3.23), are presented in this section. The post-drill pore pressure analysis of each well is considered as the true value of pore pressure for validation purposes.

The drilling and environmental parameters needed in Equation (3.23) are determined from drilling log data of the three oil wells considered, which are located in the Gulf of Mexico. The wells analyzed are termed Well 1, Well 2, and Well 3 in this dissertation. The cutting stress (which can be thought as the energy required to break the rock) was calculated using available data of torque, weight on bit, RPM, and rate of penetration data, from the drilling logs of each well. Well 1 has a sandstone lithology; whereas, Well

2 and Well 3 have a predominantly shale lithology. Rock properties are not available from the data, but typical values were assumed from the literature. As mentioned above, the failure envelope of rock is typically a non-linear function of principal stress (see Figure 3.7). However, the PSP[3] concept has been derived under the assumption that the failure envelope varies linearly with effective stress. In order to minimize the error introduce by this assumption, a spline function can be used for the failure envelope. With as spline function, a linear behavior can be assumed for small ranges of effective stress, and different linear functions can be assumed at different ranges of effective stress. The failure envelope parameters for Well 1 (sandstone) were estimated from data published by Murrell [51], as well as other works [2, 52-54]; whereas, the failure envelope parameters for Well 2 and Well 3 were estimated from the data in [55]. In order to estimate the failure envelope parameters, the cutting stress S_c was calculated from the drilling parameters. The cutting stress corresponds to the diameter of the Mohr's circle, as shown in Figure 3.14. If the diameter of the Mohr's circle is known [from Equation (3.16)], as well as the non-linear failure envelope from [2, 51-55], the line that tangentially touches the Mohr's circle at the point of contact with the non-linear failure envelope might be regarded as the linear approximation of the failure envelope at that normal stress. The values of failure parameters (rock properties) that were used in Equation (3.23) for each well are shown in Table 3.1.

Table 3.1 Assumed rock properties used in the validation of the PSP[3] concept.

Name of well	Angle of internal friction, ϕ	Cohesion, S_0
Well 1	47°	1,000 psi
Well 2	55° at depth ≤ 15,000 ft	900 psi at depth ≤ 15,000 ft
	45° at depth > 15,000 ft	1,800 psi at depth > 15,000 ft
Well 3	55° at depth ≤ 15,000 ft	900 psi at depth ≤ 15,000 ft
	50° at depth > 15,000 ft	1,200 psi at depth > 15,000 ft

Figure 3.16 is a plot showing a comparison of the pore pressure determined from Equation (3.23) with the pore pressure from a post-drill analysis (considered as the true value of pore pressure for validation purposes) for Well 1. The pore pressure determined from Equation (3.23) is plotted in green; whereas, the post-drill pore pressure is plotted in red. The pore pressure was determined in the range from 9,100 ft to 17,500 ft of depth. After calculating the cutting stress S_c along the depth of Well 1, it was determined that the failure envelope could be described with a single linear function rather than a spline function due to the small variation of Mohr's circle diameter. As mentioned in Table 3.1, the angle of internal friction was estimated to be ~47°, and the cohesion of the rock ~900 psi.
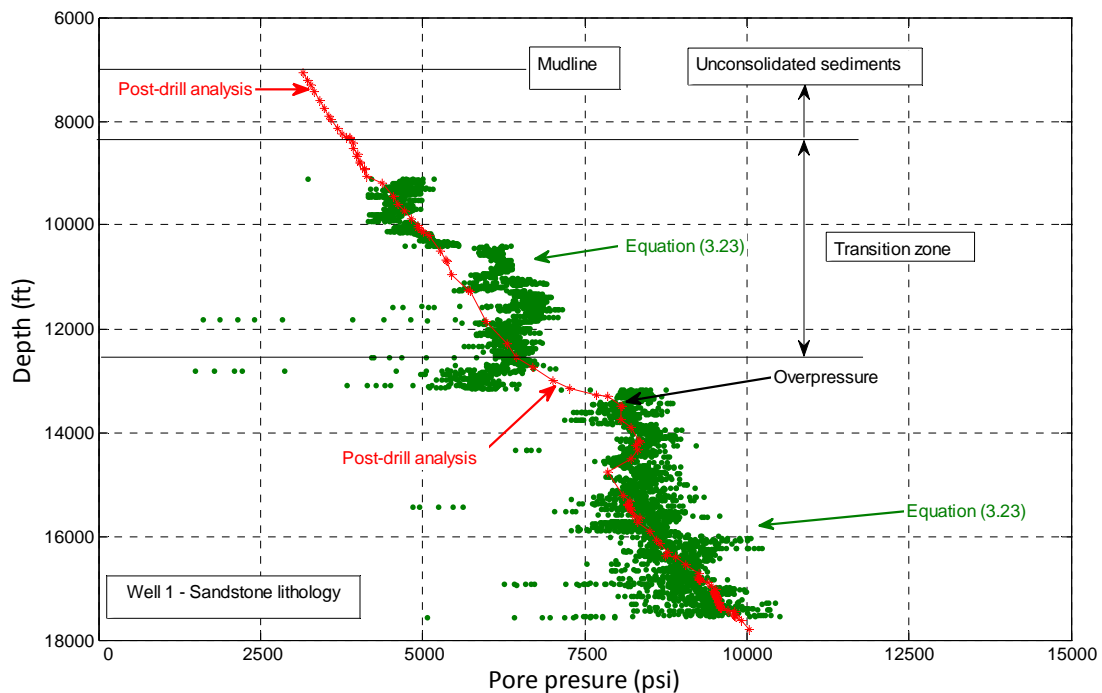
Figure 3.16 Comparison of pore pressure determined with Eq. (3.23) against post-drill pore pressure for Well 1, both as a function of depth.

It can be observed from Figure 3.16 that in general the pore pressure determined with Equation (3.23) follows the trend of the post-drill analysis along the depth of the well, except in the ranges from 10,400 ft to 12,000 ft and from 12,800 ft and 13,100 ft. The scattering in the data of pore pressure determined with Equation (3.23) is due to the scattering in the data of the drilling parameters (torque, rate of penetration, RPM). The bandwidth of the scattering in the pore pressure determined with Equation (3.23) is ~700 – 1000 psi at any given depth. Nevertheless, the average value of pore pressure determined with Equation (3.23) at any given depth is within 10% of the post-drill pore pressure, except in the ranges from 10,400 ft to 12,000 ft and from 12,800 ft and 13,100 ft. At these two regions (from 10,400 ft to 12,000 ft, and from 12,800 ft and 13,100 ft) the pore pressure determined with Equation (3.23) is over predicted by 15-20%. Data of the rock properties as a function of depth was not available. It is hypothesized that the over prediction of pore pressure might be due to the fact that these two regions have a different lithology than the one assumed for the rest of the well. Another potential reason of discrepancy between the pore pressure determined with Equation (3.23) and the post-drill analysis is the value of the efficiency assumed in the calculation of the cutting stress S_c. This efficiency is defined as the ratio of the energy required to break the rock to the input energy measured at the drill bit. Since downhole data was available (that is, drilling parameters were measured just above the drill bit), an efficiency of 100% was assumed in the calculation of the cutting stress. In other words, it was assumed that all the input energy measured at the drill bit was used to break the rock. However, this is assumption might not be appropriate if a wear bit is used or a significant amount of energy is lost by friction (or any other means) at the cutter-rock interface.

A second attempt to validate Equation (3.23) was conducted using drilling data from Well 2. The comparison of the pore pressure determined from Equation (3.23) with the post-drill analysis of Well 2 is presented in Figure 3.17. The pore pressure in Well 2 was determined from 7,000 ft to 16,500 ft. According to the drilling data, the rock composition in Well 2 is mainly shale, except from 9,600 ft to 15,300 ft where a salt

dome was found. Pore pressure was not determined at the salt dome. The failure envelope was estimated using a spline function with the parameters provided in Table 3.1. The drilling data used to determine the cutting stress was taken downhole. Therefore, an efficiency of 100% (defined as the ratio of the energy required to break the rock to the input energy measured at the drill bit) was assumed in the calculation of the cutting stress.
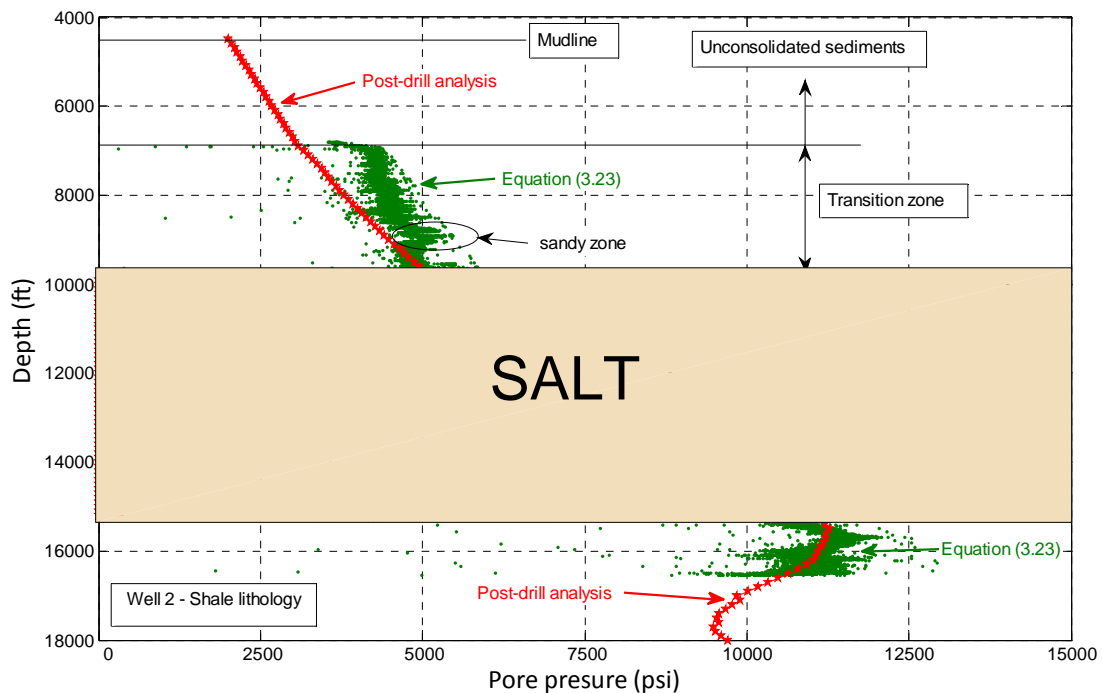
Figure 3.17 Comparison of pore pressure determined with Eq. (3.23) against post-drill pore pressure for Well 2, both as a function of depth.

It can be observed from Figure 3.17 that there is a considerable discrepancy in the pore pressure determined with Equation (3.23) with respect to the post-drill pore pressure at shallower depths (about 35% at 7,000 ft). However, the pore pressure prediction [from Equation (3.23)] significantly improves as the depth of the well increases. In fact, it can be observed that, from 9,300 ft and deeper (except at the salt dome), the pore pressured determined with Equation (3.23) predicts within 10% the post-drill pore pressure.

It was found from the calculated values of cutting stress at shallower depths (above 8,000 ft) that the Mohr's circles corresponding to the stress state at shallower depths are too small in comparison to the available data in [55] from which the failure enveloped was determined. This suggests that this region (above 8,000 ft) of Well 2 might be a region of poorly consolidated sediments; and therefore, the failure parameters in Table 3.1 might not be representative of this region. Further work is needed to determine whether choosing the appropriate failure parameters suffices to prove the validity of Equation (3.23).

A third comparison of the pore pressure determined from Equation (3.23) with the post-drill analysis is presented in Figure 3.18 for Well 3. According to the drilling data, the rock composition in Well 3 is mainly shale, except from 10,000 ft to 16,000 ft where a salt dome was found. The pore pressure in Well 3 was determined from 7,100 ft to 17,400 ft, except at salt dome and at the range from 16,300 to 17,000 ft where data was not available. The failure envelope was estimated using a spline function with the parameters provided in Table 3.1.

Downhole data was available only from 7,000 ft to 10,000 ft for Well 3. However, a zone of great interest for pore pressure prediction is the region below the salt dome (at 16,000 ft), since this is an over-pressured zone. Therefore, the cutting stress was calculated from drilling parameters measured at the surface, and the percentage of energy lost along the drill string was estimated by comparing the cutting stress at the regions where both, downhole data and surface data were available (from 7,000 ft to 10,000 ft). It was found that approximately 75% of the input energy measured at the surface is lost along the drill string. Thus, the cutting stress was calculated with surface data, and an efficiency of 25% (defined as the ratio of the energy required to break the rock to the input energy measured at the surface) was assumed. It is important to note that the definition of efficiency used for Well 1 and Well 2 (where the input energy is measured at the drill bit) is different than the definition of efficiency used for Well 3

(where the input energy is measured at the surface). The efficiency in Well 3 is used to estimate the energy loss along the drill string, and the reported efficiency is consistent with values reported in literature [30, 31]. Moreover, it is assumed that the cutting efficiency at the rock-cutter interface is 100% for all three wells. A detailed explanation of the definitions of these efficiencies is provided in Chapter V, Section 5.1.
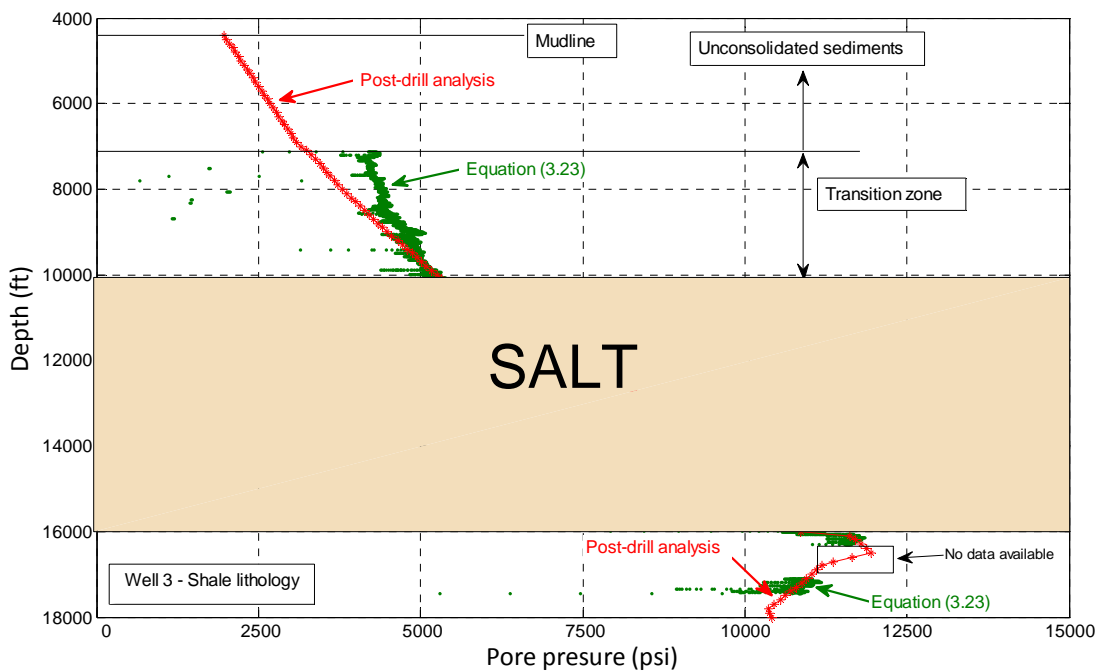
Figure 3.18 Comparison of pore pressure determined with Eq. (3.23) against post-drill pore pressure for Well 3, both as a function of depth.

It can be seen in Figure 3.18 that the pore pressure determined with Equation (3.23) for Well 3 exhibits a similar behavior as the predicted pore pressure for Well 2. A considerable discrepancy between the post-drill pore pressure and the predicted pore pressure is found at shallower depths (above 9,400 ft), with over predictions of up to 30% at 7,100 ft. Since Well 2 and Well 3 are located in the same field, it was expected to find a similar behavior in the predicted pore pressures for both wells. Moreover, the pore pressure determined with Equation (3.23) improves its prediction of the post-drill pore

pressure as it increases in depth. From 9,400 ft and below, the pore pressure determined with Equation (3.23) is always in agreement (within 5%) with the post-drill pore pressure. Unfortunately, there was no data available at the region from 16,300 ft to 17,000 ft to further validate the model in the over-pressured zone.

Figure 3.19 shows a comparison of predicted pore pressure with Equation (3.23) for Well 1, Well 2, and Well 3 to the post-drill pore pressure expressed in terms of a ratio of predicted to post-drill pore pressure. Note that a ratio of one would signify perfect agreement between predicted and post-drill values; whereas a value greater than one would signify over prediction.
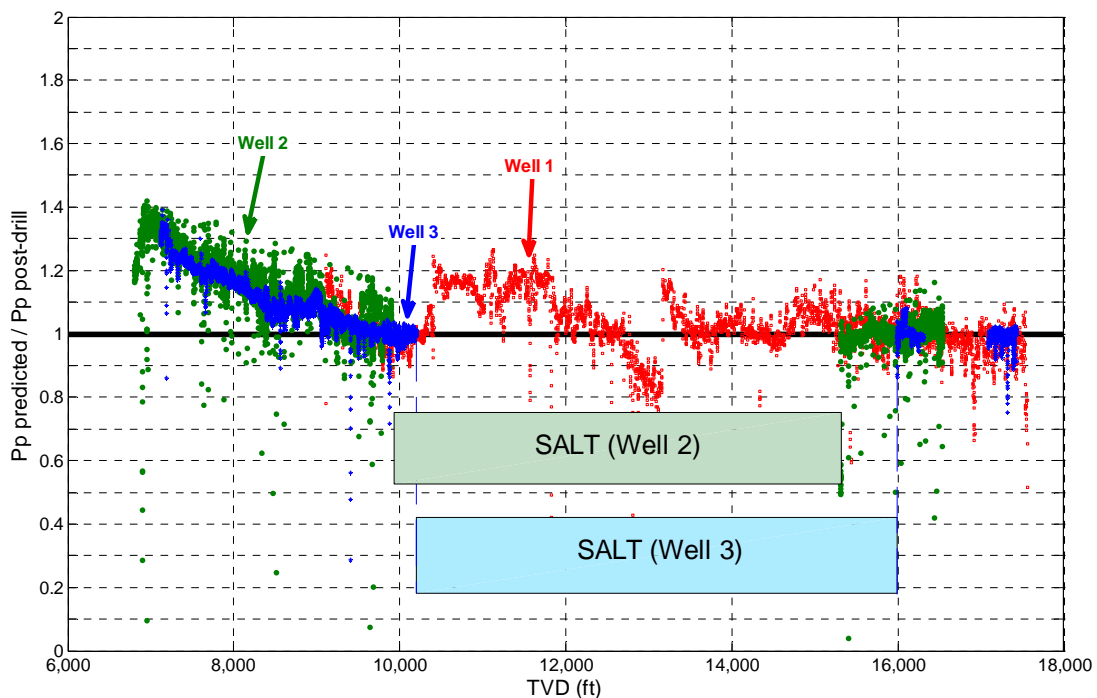
Figure 3.19 Ratio of predicted pore pressure from Equation (3.23) to post-drill pore pressure for Well 1, Well 2, and Well 3.

It can be observed that the prediction of pore pressure is in agreement to the post-drill analysis (within 10%) at depths greater than 13,500 ft for the three wells. It can be also

observed that the pore pressure is significantly over predicted for Well 2 (up to 35%) and Well 3 (up to 30%) at 7,000 ft of depth. However, as the depth increases the over prediction decreases until the trend is corrected from 9,300 ft and below. It was found that failure parameters used in Equation (3.23) can significantly affect the prediction of pore pressure. It is important to emphasize that the failure parameters used in this analysis were estimated from the information available in the drilling logs. However, specifics of the type of rock in each well were unknown. Further work is needed to determine whether the pore pressure can be correctly predicted at all depths if the actual failure parameters corresponding to the type of rock of each well are used. However, there is also the possibility that the PSP[3] concept does not capture the overall physics of the drilling process, and thus, the lack of correct prediction at shallow depths.

In this chapter, a description of the development of the PSP[3] concept to determine pore pressure at the bit from drilling parameters, environmental parameters, and material properties, as well as results of the attempts to validate the PSP[3] concept has been presented. Several plots are presented in order to visualize the comparison of the pore pressure determined from the PSP[3] concept [Equation (3.23)] with the post-drill pore pressure of each of the three oil wells. The lack of validation of the PSP[3] concept led to believe that this model might not capture the overall physics of the complex drilling process. It was recognized that there are other parameters that are not accounted for in Equation (3.23), such as the pore size, porosity, permeability of the rock, type of fluid in the pores, and temperature that might play a significant role in the physics of the drilling process. All these parameters might have an important effect in the formation pore pressure too. Furthermore, the model presented in Figure 3.9 might be oversimplified to represent the actual stress state of a rock during drilling.

These shortcomings suggest that a fundamental understanding of the parameters that affect or are affected by pore pressure is required in order to achieve a successful pore pressure prediction methodology. As a first step of a fundamental approach, a literature

review was conducted to identify if there were any prior fundamental studies of pore pressure prediction. Details of this literature review have been presented in Chapter II.

As a result of the ideas and work reviewed from the literature, a second approach was considered in this dissertation where a new way to mathematically describe the relationship between pore pressure and the energy required to break the rock (MSE) is suggested. It is important to remark that the second approach considered still focuses on the objective of determining whether or not it is possible to determine pore pressure at the bit from drilling parameters, environmental parameters, and material properties. Details of the second approach considered are presented in the next chapter.

CHAPTER IV
THE USE OF MSE IN EATON'S EQUATION
TO DETERMINE PORE PRESSURE

The second approach considered in this dissertation in order to determine whether or not it is possible to determine pore pressure at the bit from drilling parameters, environmental parameters, and material properties is presented in this chapter. The second approach is the development of the concept of using a fundamental parameter (the energy required to break the rock) in Eaton's equation. This new concept has been developed empirically, as a consequence of the lack of validation of the PSP^3 concept, by pursuing reasoning similar to Eaton [10].

The PSP^3 concept presented in Chapter III showed agreement with some post-drill data (for deeper regions), and inadequate prediction of pore pressure for other data (shallower depths). The inadequacy of the pore pressure prediction using the PSP^3 equation might be due to the fact that other parameters that possibly affect the virgin pore pressure have not been taken into account. A major concern is that the current PSP^3 equation is based on a theory that is applicable to rocks where the permeability is high enough to allow sufficient movement of fluid, and that connected systems of pores exist [47]. However, two (out of three) sets of data used in the attempt to validate the PSP^3 equation were obtained from wells for which the rock formation was predominantly shale (which is a low-permeability rock), and even for this data agreement with the post-drill pore pressure data was found at deeper regions. In order to clarify this behavior it has been recognized that a more fundamental understanding of the relationships among pore pressure, rock properties, drilling parameters, and environmental parameters is required.

As a first step of the initiation of a fundamental approach, a literature review was conducted to identify if there were any prior fundamental studies of pore pressure prediction. Although there are some investigations in literature that present a relationship

among pore pressure, drilling parameters, environmental parameters, and material properties [33, 39], the objective of these investigations did not focus on the pore pressure prediction. It was found from the literature review that Eaton's equation is one of the most commonly used relationships to determine virgin pore pressure [21]. Furthermore, current efforts to improve pore pressure prediction focus on improving the methods to measure or infer the parameters that can be used in Eaton's equation (resistivity, conductivity, wave velocity from sonic and seismic data, d-exponent). However, it is important to recall that Eaton's equation was developed empirically, rather than from basic principles. Thus, a review of the ideas that led Eaton to develop his equation for pore pressure prediction was conducted in detailed. From this review, and pursuing reasoning similar to Eaton, it is proposed in this work that a fundamental parameter (such as the energy required to break the rock) can be used in Eaton's equation.

In this chapter, a review of the development of Eaton's equation is described first. Subsequently, an analysis of the reasoning followed by Eaton to develop his equation for pore pressure prediction is presented. Then, a fundamental parameter is proposed to be used in Eaton's equation in order to predict pore pressure. Finally, results of pore pressure prediction using this fundamental parameter in Eaton's equation are presented.

4.1 Review of the development of Eaton's equation

In 1975, B.A. Eaton presented an equation for pore pressure prediction from well logs. This equation is one of the most commonly used relationships to predict pore pressure [21] in the formation. Eaton assumed that the effective stress in a low-permeability rock is a fraction of what it would be in high-permeability rock, because an additional part of the total stress is supported by the pore pressure in the case of the low-permeability rock. That is, when the permeability of the rock is very high, the pore pressure is equal to the hydrostatic pressure. However, in low-permeability rock the pore pressure is larger than the hydrostatic pressure and the effective stress is lower. To calculate the fraction of the

effective stress for the case of low-permeability rocks, Eaton proposed to consider the ratio of the electrical resistivity of the rock for a normal trend (representative the hydrostatic pressure) to the resistivity at an abnormal pore pressure.

Eaton's idea of comparing electrical resistivities was based on the observations of Hottman and Johnson for shale [18]. Hottman and Johnson were the first to observe that shale resistivity decreases in over-pressured zones. They reasoned that electrical resistivity is larger in the rock matrix than in the formation water. Thus, a well compacted shale containing less water is more resistive that a shale containing more water. Moreover, a sequence of normally compacted sediments should have a normally increasing resistivity trend. They supported their theory with resistivity plots from actual well logs, and established that any resistivity decrease from this normal trend was associated with abnormally high-pressure zones. However, this theory, which is the basis for the Eaton's equation, remains questionable [20].

It was obvious to Eaton, based on the observations from Hottman and Johnson, that there should be a relationship between abnormal pore pressure and any deviation of resistivity from the normal trend. Eaton used the effective stress concept, Equation (2.3), and expressed the pore pressure gradient (dividing all terms by depth, D) as

$$\frac{P_P}{D} = \frac{OB}{D} - \frac{\sigma'}{D}$$
(4.1)

where:

$\frac{P_p}{D}$ = virgin pore pressure gradient (psi/ft)

$\frac{OB}{D}$ = overburden stress gradient (psi/ft)

$\frac{\sigma'}{D}$ = effective stress gradient (psi/ft)

D = depth (ft)

Equation (4.1) expresses a relationship among pore pressure, overburden stress and effective stress for a sequence of normally compacted sediments. It was also recognized that normally compacted sediments allow the formation fluid to escape freely. Thus, the normal trend of pore pressure is the hydrostatic pressure normal trend, and the effective stress in such situation is expressed as

$$\left(\frac{\sigma'}{D}\right)_{normal} = \frac{OB}{D} - \left(\frac{P_p}{D}\right)_{normal} \tag{4.2}$$

Eaton hypothesized that the effective stress in an over-pressured zone should be a fraction of the normal effective stress, because part of the total stress is supported by the pore fluid. Since electrical resistivity seemed to track changes in pore pressure, Eaton suggested that the fraction of effective stress should be expressed in terms of a ratio of the resistivities of the actual to normal trends. He proposed the following equation form to describe the abnormal effective stress

$$\left(\frac{\sigma'}{D}\right)_{abnormal} = \left(\frac{\sigma'}{D}\right)_{normal} \left(\frac{Observed\ R_{sh}}{Normal\ R_{sh}}\right)^n \tag{4.3}$$

where $Observed\ R_{sh}$ is the actual value of resistivity at a given depth (see Figure 4.1), $Normal\ R_{sh}$ is the resistivity for the normal trend at the same depth (see Figure 4.1), and n is an exponent to fit the data.

It is important to mention that the form of Equation (4.3) was developed from trial-and-error fitting of data. The original value of the exponent was $n = 1.5$. Substituting Equation (4.2) into Equation (4.3), and Equation (4.3) into Equation (4.1), the expression to calculate abnormal pore pressure in shale formation [10] becomes

$$\frac{P_P}{D} = \frac{OB}{D} - \left[\frac{OB}{D} - \left(\frac{P_P}{D}\right)_N\right]\left(\frac{R_o}{R_N}\right)^n$$

(4.4)

where

$\frac{P_P}{D}$ = virgin pore pressure gradient (psi/ft)

$\frac{OB}{D}$ = overburden stress gradient (psi/ft)

$\left(\frac{P_P}{D}\right)_N$ = normal virgin pore pressure gradient (psi/ft)

R_o = observed resistivity at a given depth (ohm.m)

R_N = resistivity of normal trend at a the same depth as R_o (ohm.m)
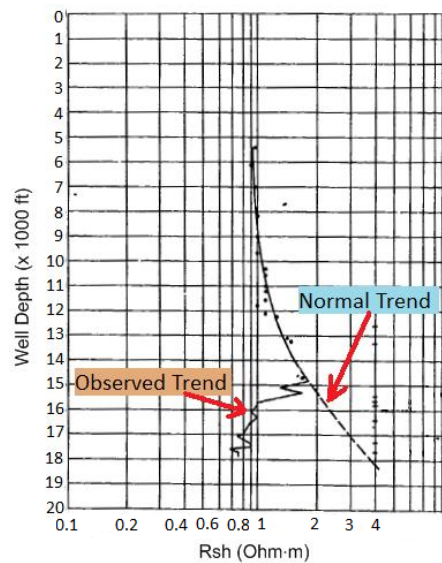
Figure 4.1 Log-resistivity data for a South Louisiana well presented by Eaton [10].
Reproduced with permission of the copyright owner, © SPE, 1975.

In Equation (4.4), the expression $\left[\frac{OB}{D} - \left(\frac{P_p}{D}\right)_N\right]$ represents the effective stress of the formation in normal compaction; whereas the n-th power of the ratio $\left(\frac{R_o}{R_n}\right)$ represents the ratio of the effective stress in the over-pressured zone to the effective stress in the hypothetical normal-pressured zone at the same depth. After evaluation of Equation (4.4)

with available data, Eaton found that the n coefficient with a value of 1.2 better fit the data. Eaton also recognized that the ratio of other measurements could be utilized in Equation (4.4) instead of electrical resistivity. He proposed the used of electrical conductivity (which is the inverse of resistivity), the corrected d-exponent (which produces a plot that is similar to the plot in Figure 4.1), and sonic-log data (with a value of 3 for the exponent). An analysis of the validity of the arguments that led Eaton to develop Equation (4.4) is presented in the next section.

4.2 Analysis of Eaton's equation

In principle, Eaton's reasoning to develop Equation (4.4) seems to be logical. When sediments in a saturated formation are compacted, the pore size decreases and fluids are expelled from the pores. If the pore fluid can escape and migrate to the surface at about the same rate as the rate of compaction, a normal pore pressure gradient is maintained. That is, if the formations are highly permeable, fluid within the pores would only support the weight of the water above. However, if the fluid in the pores is unable to communicate with other pores, the fluid must support a greater portion of the overburden load. That extra portion of the overburden load that is supported by the pore fluid corresponds exactly to the decrease of effective stress. By using the ratio of actual resistivity to the resistivity in a normal compaction situation, Eaton attempted to determine that portion of overburden load supported by the fluid. The question remains of whether or not electrical resistivity (or any of the other parameters used by Eaton) is the best parameter to track a change in the normal pore pressure trend.

It was reasoned originally that electrical resistivity would be a good indicator of the water content in the rock. Moreover, it was assumed that the more water content the higher pore pressure and the lower the resistivity would be. However, electrical resistivity is affected by other factors such as porosity of the rock, permeability, moisture content, concentration of dissolved electrolytes, temperature, phase of the pore fluid, clay content, among others. The important point is that there might be other parameters

that affect the resistivity value of a rock but have negligible effect on the pore pressure. In other words, a change in the value of resistivity from its normal trend might have, in certain occasions, nothing to do with abnormal pore pressure.

As an example, Figure 4.2 shows a plot of the electrical resistivity along with the pore pressure, both as a function of depth. The data corresponds to drilling logs from Well 2. As mentioned in Chapter III, the lithology of this well is mainly shale except for the salt dome clearly marked in Figure 4.2. The linear scale for the pore pressure curve is the horizontal red axis at the bottom (psi) of the plot, and the logarithmic scale for resistivity is the horizontal blue axis at the upper part of the plot (Ohm-m). It is important to note that this plot does not seek to compare pore pressure to resistivity, quantitatively. However, this plot is useful to determine qualitatively if there is any relationship between the trends of pore pressure and resistivity.
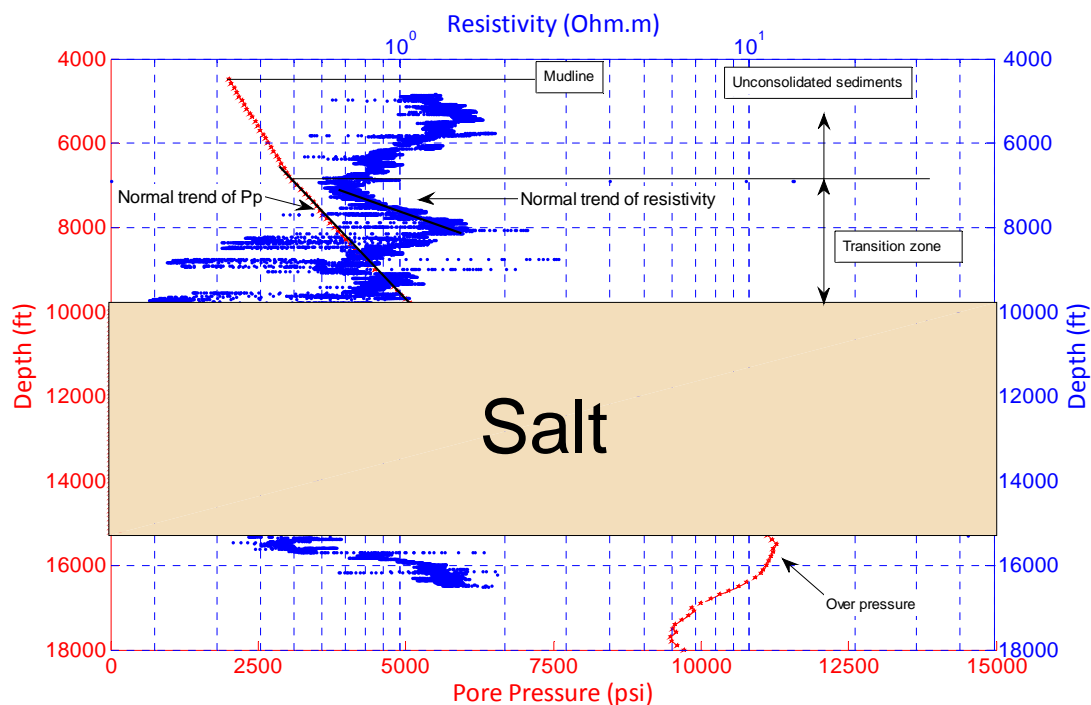
Figure 4.2 Comparison between electrical resistivity (log blue scale) and pore pressure (linear red scale) as a function of depth for Well 2.

Several observations can be made from the plot in Figure 4.2. First, it can be noticed that pore pressure increases with a constant gradient (constant slope of the pore pressure curve) at depths between 4,500 ft and 6,900 ft. This section of the curve corresponds to the shallow unconsolidated sediment that extends from the mudline (sea floor) down to the depth where the compaction disequilibrium dewatering (CDD) process begins [25]. The pressure gradient at this section of unconsolidated sediments is 0.447 psi/ft. It can be clearly seen that electrical resistivity at this region, between 4,500 ft and 6,900 ft, does not exhibit a constant slope. Moreover, resistivity increases from 4,800 ft to 5,400 ft, but then it decreases from 5,400 ft to 6,900 ft.

Second, the transition zone as defined in [25] is located in region from 6,900 ft to 9,700 ft. At this region, fluid flows upward as a result of the gradual pressure gradient increase (from 0.447 psi/ft to 0.73 psi/ft). This is the region where the normal compaction trend can be established. However, it can be seen from Figure 4.2 that the normal compaction trend of resistivity is present only in the range from 6,900 ft to 8,000 ft; whereas, the normal compaction trend for pore pressure extends to the entire transition zone (6,900 ft to 9,700 ft). This can be an indication that not all the changes in the resistivity are due to the pore pressure change.

Finally, the pore pressure is abnormally high at about 15,300 ft, that is, the pore pressure is higher than would be predicted from the normal trend. The resistivity at this point appears to respond to the increase in pore pressure by exhibiting a considerably lower value. However, it has already been observed that not all the changes in the resistivity are due to pore pressure.

Even though the electrical resistivity (or conductivity) of the rock might not be the best parameter to relate the change between normal and abnormal pore pressure, the form of Equation (4.4) seems to be appropriate if the following reasoning is considered. Equation (4.4) describes that the pore pressure at a given depth is equal to the

overburden (total stress) minus the actual effective stress in Equation (4.3). The effective stress at a *normally* pressured zone is always the difference between the overburden and the hydrostatic pressure. Equation (4.3) established that the actual effective stress would be equal to the effective stress in a hypothetically *normally* pressurized zone at the same depth multiplied by some factor. That factor should be less than unity in the common case of over pressurized zones, because a larger portion of the total stress is supported by the pore pressure. Furthermore, Eaton expressed that factor as the ratio of actual to normal resistivities raised to the *n*-th power.

Eaton's expression might work well if: (1) a hypothetical *normal* trend of the parameter used in the ratio (for example, resistivity) could be established, and (2) if any deviations of such parameter from the normal trend would be solely due to changes in pore pressure, rather than a multiplicity of factors.

A normal trend would be defined as a monotonic increase or decrease of the values of that parameter as a function of depth. Similarly, the normal trend of pore pressure is defined as the monotonic increase of pore pressure as a function of depth, which is usually the hydrostatic pressure encountered in high-permeability rock. Pursuing reasoning similar to that of Eaton, and using the above definition for a normal trend, a fundamental parameter is proposed to be used in Eaton's equation. That parameter is the mechanical specific energy, which has been previously defined as the energy (per unit volume) required to break the rock. This is a fundamental parameter that comes directly from thermodynamic principles. The development of this approach is presented in the next section.

4.3 Proposed fundamental parameter to be used in Eaton's equation

It has been previously mentioned that Eaton's expression might work well if: (1) a *normal* trend of the parameter used in the ratio of his equation could be established, and (2) if any deviations of such parameter from the normal trend would be solely due to

changes in pore pressure, rather than a multiplicity of factors. On the other hand, the PSP³ equation and the results from the attempt of validation of the PSP³ concept indicate that there might be a relationship between the energy required to break the rock (S_c, which is a portion of MSE) and the virgin pore pressure. It was reasoned that, if MSE is a function of the virgin pore pressure, then it could be used to track the changes of pore pressure. Therefore, instead of using electrical resistivity, a more fundamental parameter such as MSE could be used in Eaton's expression. Moreover, it was also reasoned that MSE may fit the definition of normal trend provided in the previous section, since it can be readily established that MSE increases nearly linearly as a function of depth, in the theoretical case where the pore pressure follows a normal trend and no changes in lithology are present. This reasoning led to believe that Equation (4.4) could be used to predict pore pressure behavior at a given depth using MSE as the parameter to use in the ratio of the equation. The proposed equation would be expressed as

$$\frac{P_P}{D} = \frac{OB}{D} - \left[\frac{OB}{D} - \left(\frac{P_P}{D}\right)_N\right]\left(\frac{MSE_o}{MSE_N}\right)^n$$

(4.5)

where MSE_o is the actual mechanical specific energy calculated with Equation (3.17) from drilling parameters, and MSE_n is the hypothetical value of MSE resulting if the normal trend were followed.

It seems from drilling log data that establishing a normal trend of MSE in a region of normal pore pressure is fairly straight forward. However, there is a more important issue that needs to be addressed so that Equation (4.5) can be used to predict pore pressure. This issue is whether it is realistic that any deviation in MSE from the established normal trend must result from changes in pore pressure. Moreover, if any other factors affect the normal trend of MSE, any changes due to those factors must be very small in comparison to the changes resulting from a change in pore pressure if MSE is to be an accurate predictor of pore pressure changes. Thus, Equation (4.5) could be a plausible expression to predict pore pressure for all types of rock provided that MSE is

significantly affected by changes in virgin pore pressure. At this point, it is worthwhile to recall that Detournay and Atkinson [33] concluded that MSE might be independent of virgin pore pressure for shale (see Chapter II), due to the low permeability of this type of rock. Therefore, if the hypotheses proposed in this section are correct, they would be contradictory to Detournay and Atkinson's theory. To address this issue, actual drilling data for shale has been analyzed to determine whether or not there is a relationship between MSE and virgin pore pressure.

Figure 4.3 shows the post-drill analysis of virgin pore pressure as a function of depth (in red), as well as the calculated MSE as a function of depth (in blue) for Well 2. The lithology of Well 2 is mainly shale, except for the salt dome clearly marked in the figure. However, no information on the actual permeability of this shale is available to the author. Figure 4.3 suggests, in a qualitative manner, that there is a relationship between MSE and virgin pore pressure.
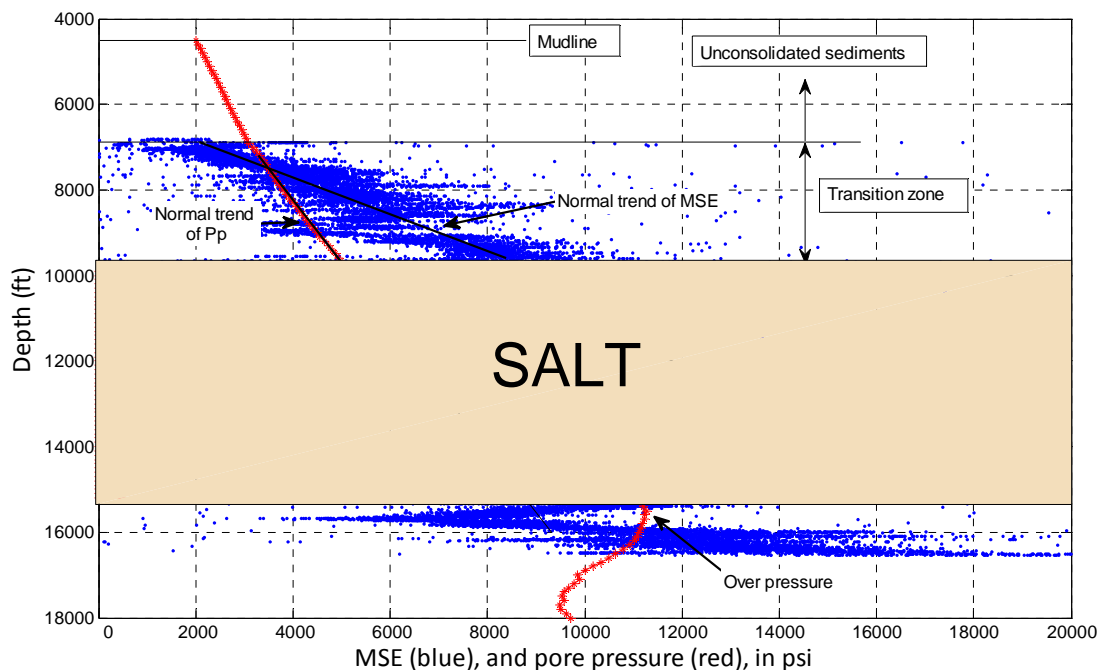
Figure 4.3 Comparison of the trends of MSE (blue curve) and Pp (red curve) as a function of depth for Well 2.

As explained above for Figure 4.2, at depths between 4,500 ft and 6,900 ft, the pore pressure corresponds to the hydrostatic pressure of seawater since this is a zone of unconsolidated sediments. At 6,900 ft the transition zone begins and there is a change in the slope of pore pressure that keeps increasing until the salt dome is reached (9,600 ft). It is at this region where the normal pore pressure trend is usually established, see [25]. It can be observed that a linear trend of MSE can be readily established at the region between 6,900 ft and 9,600 ft. That is, from 6,900 ft to 9,600 ft, both pore pressure and MSE increase linearly. Coming out of the salt dome, at about 15,300 ft, the pore pressure reaches values greater than the ones predicted by its normal trend (dotted black line). It can be clearly observed that in this region of abnormal pore pressure, MSE is decreased considerably from its normal trend, reaching values even smaller than pore pressure. Since a fundamental assumption is that increased pore pressure results in decreased MSE, the observed behavior is to be expected and it contradicts Detournay and Atkinson's conclusion (unless this is atypical shale with high permeability).

The MSE plotted in Figure 4.3 was calculated using downhole measurements of torque, ROP, RPM, and WOB. If downhole data is not available, MSE can still be calculated from surface data. However, it has to be considered that part of the calculated MSE (input energy) is not actually used to break the rock. It has been found in other works [30, 31] that only between 30-40% of this energy is actually utilized in breaking the rock formation, and the rest is lost resulting from other factors (for example, friction along the drill string or at the cutter-rock interface). Fortunately, this is not an issue for the use of Equation (4.5), since the ratio of MSE is what is needed. Therefore, if only a fraction of the energy input is used to break the rock, and this fraction remains constant, that factor cancels out when the ratio of actual to normal trend MSE is formed. The findings in Figure 4.3 suggest that the form of Equation (4.5) might be appropriate to relate pore pressure to mechanical specific energy. It is important to note that a previous work presented by Moore [56] describes a similar idea to the concept presented in this chapter. In his work, Moore [56] proposes that a change of pore pressure from the normal trend

can be track from the change in mud weight provided that the rate of penetration is maintained at the normal trend and the weight on bit and rotary speed are kept constant. However, the concept proposed in this chapter, Equation (4.5), relates the abnormal pore pressure to a fundamental parameter: the energy required to break the rock (MSE). Furthermore, the MSE accounts for the dependability of parameters such as rate of penetration, rotary speed, torque, and weight on bit. That is, instead of attempting to maintain any drilling parameters constant during drilling, as proposed by Moore [56], a fundamental parameter such as the MSE can take into account the dependable effects of all these drilling parameters at once.

Equation (4.5) describes the pore pressure in terms of the MSE by relating a change in the effective stress of the rock from the normal trend to a change in MSE from the hypothetical normal trend of MSE. However, an important question that is not answered in Figure 4.3 is: why is MSE a function of pore pressure? Nevertheless, it is reasonable to expect that the energy required to break the rock is a function of the stress state of the undisturbed rock, including the pore pressure. The exponent n in Equation (4.5) is another important aspect that requires a physical interpretation. In order to seek an answer to these questions, a fundamental approach based on basic principles is proposed and addressed in Chapter V. Even though it is not clear at this point why MSE is a function of pore pressure and the significance of the exponent n, Equation (4.5) has been used to determine pore pressure for the same three wells presented in Chapter III, and the results have been compared to a post-drill pore pressure analysis (which is considered the true value of pore pressure for validation purposes). Results from this attempt to validate Equation (4.5) are presented in the next section.

4.4 Results of pore pressure prediction using MSE in Eaton's equation

In an attempt to validate Equation (4.5), comparisons of the pore pressure determined with Equation (4.5) and the post-drill pore pressure are presented for the same three

wells presented in Chapter III. The parameters needed in Equation (4.5) to determine pore pressure were determined from drilling log data of each of the wells.

A plot similar to the one presented in Figure 4.3 was developed for each well analyzed, to establish the normal trends of pore pressure and MSE. For each well (Well 1, Well 2, and Well 3), regions were found with a monotonic increase of pore pressure (at the transition zone). That monotonic increase in pore pressure was assumed to be the normal trend of pore pressure, $(P_P)_n$, and a best fit curve was determined. At the same depths where the normal trend of pore pressure was established, the normal trend of MSE, MSE_n, was established and a best fit curve determined. Note that all normal trends, for MSE and pore pressure (for all wells), were found to be very close to linear functions.

The other parameter needed in Equation (4.5) (besides the normal pore pressure and the normal MSE) is the overburden, for which data was available and a best fit curve was also determined. Table 4.1 shows the linear functions of the normal trends for MSE and pore pressure, as well as the best fit curve of overburden, that were used in Equation (4.5) for each well analyzed.

Table 4.1 Normal trends (curve fits) of pore pressure and MSE, as well as the overburden function, for the three wells considered.

Name of well	Pp$_n$ (psi) z = depth (ft)	MSE$_n$ (psi) z = depth (ft)	Overburden (psi) z = depth (ft)
Well 1	$P_{p_n} = 0.602z - 1170$	$MSE_n = 0.908z - 9134$ (downhole data)	$OB = 4 \times 10^{-6}z^2 + 0.898z - 3365$
Well 2	$P_{p_n} = 0.713z - 1898$	$MSE_n = 2.4z - 14524$ (downhole data)	$OB = 2 \times 10^{-10}z^3 - 6 \times 10^{-6}z^2$ $+ 0.986z - 2356$
Well 3	$P_{p_n} = 0.713z - 1898$	$MSE_n = 7.2z - 35200$ (surface data)	$OB = 3 \times 10^{-10}z^3 - 8 \times 10^{-6}z^2$ $+ 1.021z - 2493$

It can be seen that the normal trend of pore pressure is the same for Well 2 and Well 3. Moreover, the overburden functions are similar for Well 2 and Well 3 as well. This is expected since both wells are located in the same field and have a very similar lithology. MSE is calculated using downhole data whenever possible. However, downhole data was not available in the drilling logs for Well 3 at depths greater than 16,000 ft. Therefore, a normal trend of MSE calculated from surface data is shown in the table. MSE calculated from surface data is greater than MSE calculated from downhole data, since the former also accounts for the energy required to overcome the friction all along the drill string. Fortunately, this is not an issue when using Equation (4.5) as long as the normal trend and the actual value of MSE are both consistently calculated with either surface or downhole data.

Figure 4.4 shows the pore pressure calculated with Equation (4.5) for Well 1. The lithology of this well is predominantly sandstone.

Figure 4.4 Comparison of pore pressure determined with Eq. (4.5) and $n = 1$ against post-drill pore pressure for Well 1, both as a function of depth.

The pore pressure determined from a post-drill analysis is also plotted in the figure. As it has been stated earlier in this dissertation, the pore pressure from the post-drill analysis is considered as the true value for validation purposes.

It can be observed from Figure 4.4 that the data of pore pressure determined from Equation (4.5) is considerably scattered at any given depth, but it forms a band that follows, in general, the same trend of the post-drill pore pressure. The bandwidth of the pore pressure increases with depth from ~500 psi (at 9,100 ft) up to 2,500 psi (at 15,200 ft and below). The scattering in the pore pressure data is due to the scattering in the torque data used to calculate MSE. It can be observed that post-drill pore pressure is on the middle of the pore pressure band determined from Equation (4.5), except in the zone that extends from 10,350 – 11,700 ft in depth. At this region, it can be seen that the post-drill pore pressure is slightly higher than the normal pore pressure (~100 psi). However, the pore pressure determined from Equation (4.5) over predicts the post-drill pore pressure by ~700 psi at this zone (10,350 – 11,700 ft in depth). It is interesting to note that the trend of pore pressure determined with Equation (4.5) in Figure 4.4 is remarkably similar to the trend of pore pressure determined with the PSP[3] equation (Figure 3.16). The trends of pore pressure determined from these two concepts [Equation (3.23) and Equation (4.5)] were similar only for Well 1. Thus, further work is recommended to investigate under which the circumstances both concepts would provide similar trends in pore pressure prediction. This knowledge could lead to a better understanding of the relationship between pore pressure and the energy required to break the rock.

It should be noted that the post-drill pore pressure for Well 1 is known as a function of the *true vertical depth* (TVD); however, the drilling data of Well 1 used to predict the pore pressure with Equation (4.5) was only available as a function of the total depth. Total depth is usually greater than the TVD because wells are not drilled perfectly vertical (the drill string can bent and even turn horizontally). However, the TVD is

important in determining the borehole pressures, which are caused in part by the hydrostatic pressure of fluid in the wellbore [57]. An estimation of the TVD for Well 1 was determined from a comparison of the *equivalent circulating density* (ECD) that was available both as a function of total depth and as a function of TVD. However, there might be a slight mismatch in depth between the post-drill and the predicted pore pressure profiles.

Interestingly, a value of 1 was used for exponent n in Equation (4.5), which suggests that the ratio $\frac{MSE_o}{MSE_n}$ is equal to the ratio of the effective stress in the over-pressured zone to the effective stress in the hypothetical normal-pressured zone at the same depth. It was found that the value of the exponent n, if varied from 0.5 to 1.5, does not significantly affect the trend of pore pressure. However, decreasing the value of the exponent reduces the scattering of the pore pressure data.

Figure 4.5 presents a comparison similar to Figure 4.4 of the pore pressure determined from Equation (4.5) with $n = 0.5$ for Well 1. It can be seen from Figure 4.5 that decreasing the value of the exponent n (from 1 to 0.5) decreases the scattering of the values of the predicted values while maintaining more or less the same trend. However, it can be deduced from Equation (4.5) that as the exponent n approaches a value of zero, the predicted pore pressure will approach the normal trend of pore pressure. Although not shown in the figure, it was also found that increasing the value of the exponent does not significantly affect the trend of the predicted pore pressure, but it results in even more scattering of the predicted values.
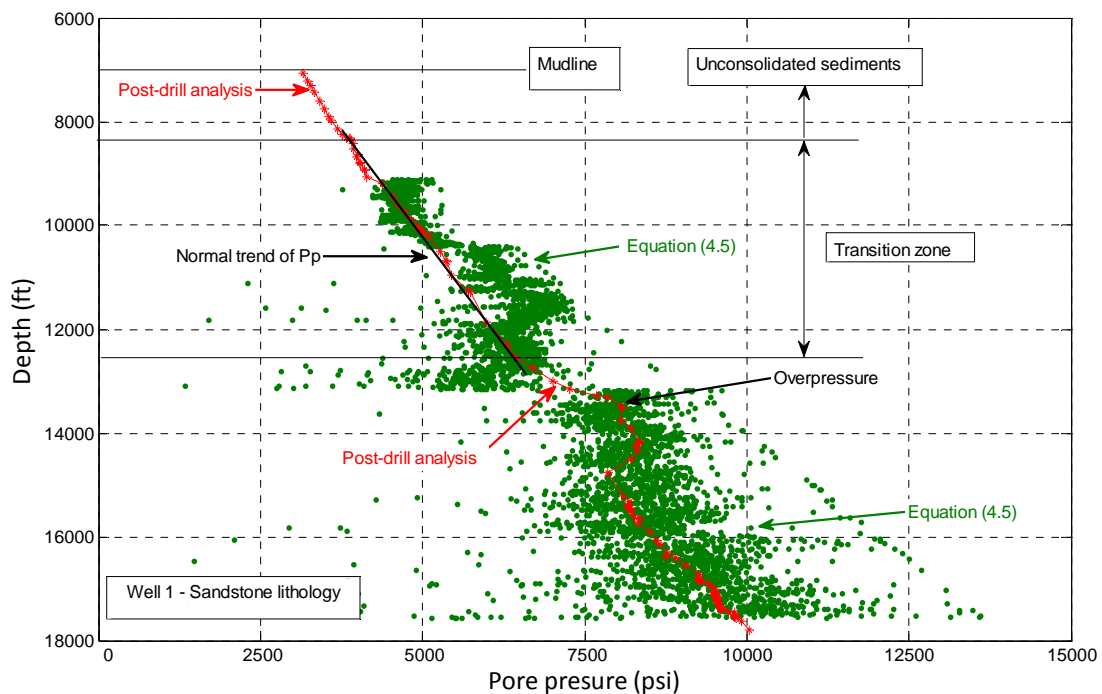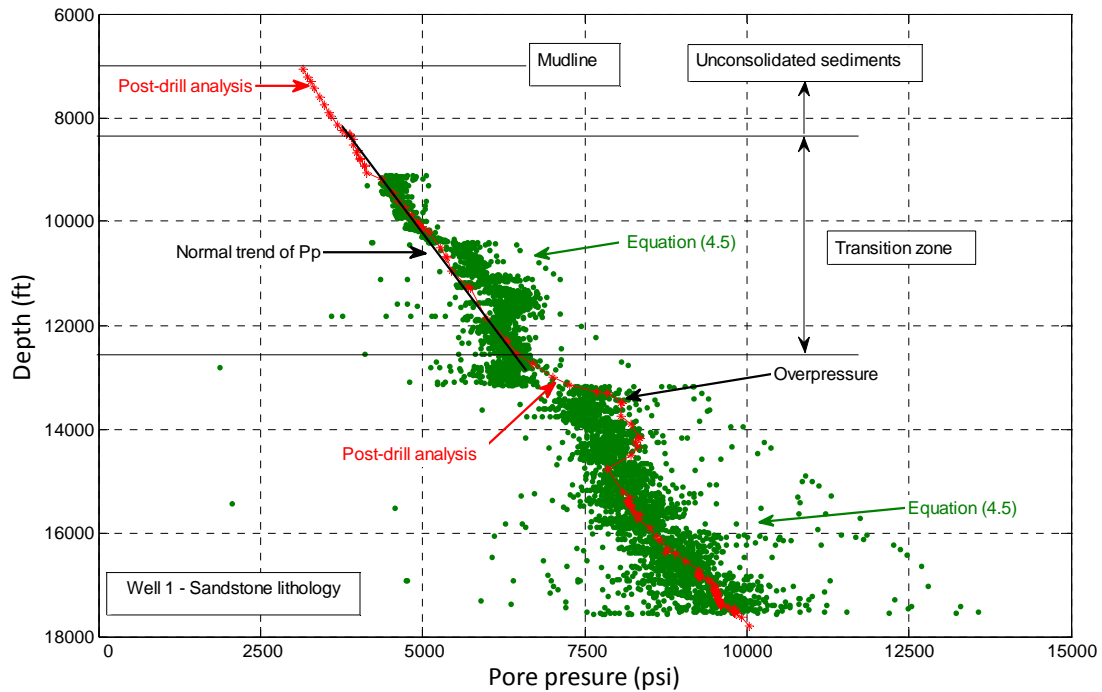
Figure 4.5 Comparison of pore pressure determined with Eq. (4.5) and $n = 0.5$ against post-drill pore pressure for Well 1, both as a function of depth.

A comparison of the pore pressure calculated with Equation (4.5) with the post-drill pore pressure for Well 2 is presented in Figure 4.6. The lithology of this well is primarily shale. It can be observed from Figure 4.6 that the trend of the pore pressure predicted with Equation (4.5) follows exactly the trend of the post-drill pore pressure. Moreover, the pore pressure band formed due to the scattering of the torque data has a width of about 600 psi along the well, which is considerable less than the band width for Well 1. It is important to remark that the pore pressure band determined with (4.5) is centered with respect to the post-drill pore pressure at each depth, except at the zone between 8,700 ft and 9,000 ft. At this zone, a change in lithology was found from shale to a sandy zone. This behavior suggests that Equation (4.5) could be used to predict pore pressure as long as the lithology does not change. Otherwise, a different normal trend of MSE must be established for the new lithology.
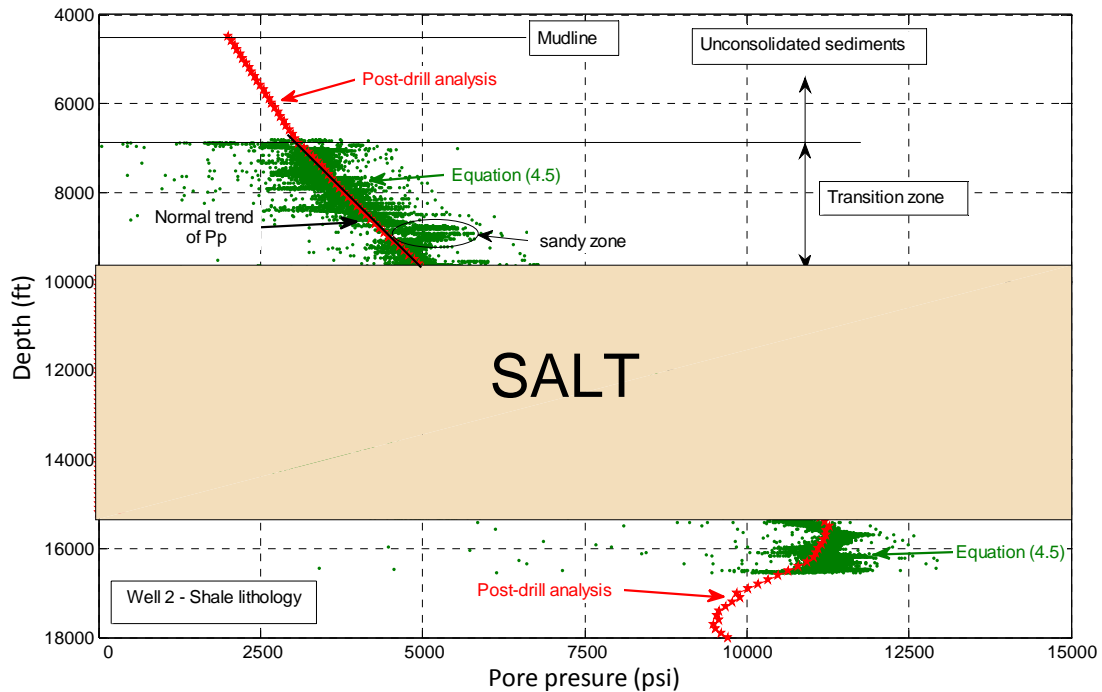
Figure 4.6 Comparison of pore pressure determined with Eq. (4.5) against post-drill pore pressure for Well 2, both as a function of depth.

It is important to recall that the pore pressure determined from the PSP[3] concept over predicts the post-drill pore pressure of Well 2 for up to 35% at 7,000 psi. However, the proposed new expression for pore pressure prediction, Equation (4.5), correctly predicts the trend of the post-drill pore pressure above the salt dome. Moreover, the pore pressure prediction below the salt dome also follows the trend of the post-drill pore pressure within ±300 psi (~10%). A value of 1 was used for the exponent n of Equation (4.5) in the determination of pore pressure, which surprisingly remarks the equality between the ratio $\left(\frac{MSE_0}{MSE_n}\right)$ and the ratio $\left(\frac{\sigma'_{abnormal}}{\sigma'_{normal}}\right)$. This suggests that a linear relation exists between the effective stress of the rock and the energy required to break it (MSE).

Figure 4.7 shows yet another comparison between post-drill pore pressure and pore pressure predicted from Equation (4.5). This comparison is for Well 3, for which the

lithology is very similar to the lithology of Well 2 (shale). Downhole data was not available for this well below the salt dome. Instead, surface data was used to calculate the MSE to be used in Equation (4.5).
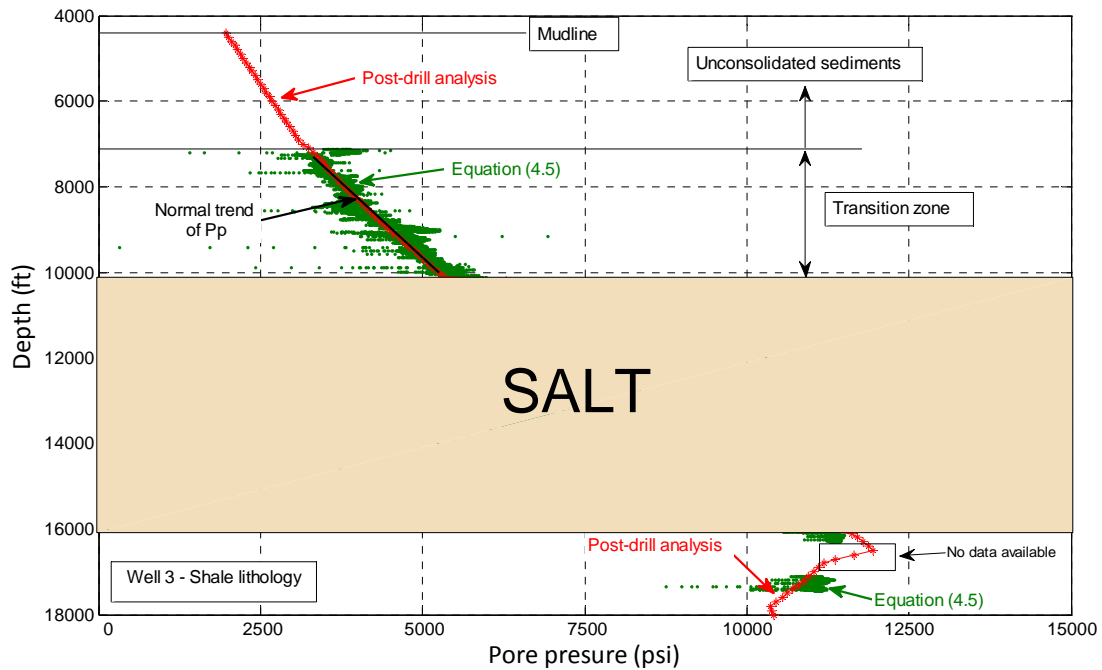
Figure 4.7 Comparison of pore pressure determined with Eq. (4.5) against post-drill pore pressure for Well 3, both as a function of depth.

Figure 4.7 shows that pore pressure calculated with Equation (4.5) follows exactly the trend of the post-drill pore pressure. The pore pressure band formed due to the scattering of the torque data has a width of about 300 psi (smaller than the one in Well 2). It can be observed that the pressure profile of Well 3 is very similar to the profile of Well 2, since both wells are located at the same field. Although there was not enough data available at some regions below the salt dome, the regions where the pore pressure could be calculated (below the salt dome) suggest a very good prediction of the actual pore pressure, within ±300 psi (<5%). As expected from results of Well 2, a value of 1 was used for the exponent of Equation (4.5).

Figure 4.8 shows a comparison of the pore pressure predictions from Equation (4.5) for Well 1 (for both $n = 1$ and $n = 0.5$), Well 2, and Well 3, with post-drill pore pressure data of each well. In the figure, the ratio of predicted pore pressure to actual pore pressure is shown for each well. A ratio value of one means perfect agreement between prediction and actual pressure. It can be seen that the ratios for the three wells oscillate around one. The ratio data has been smoothed to eliminate the random variations caused by the torque data used in the calculation of MSE. The data presented in Figure 4.8 corresponds to the moving average of the calculated ratios, which allows revealing the main feature of each curve.
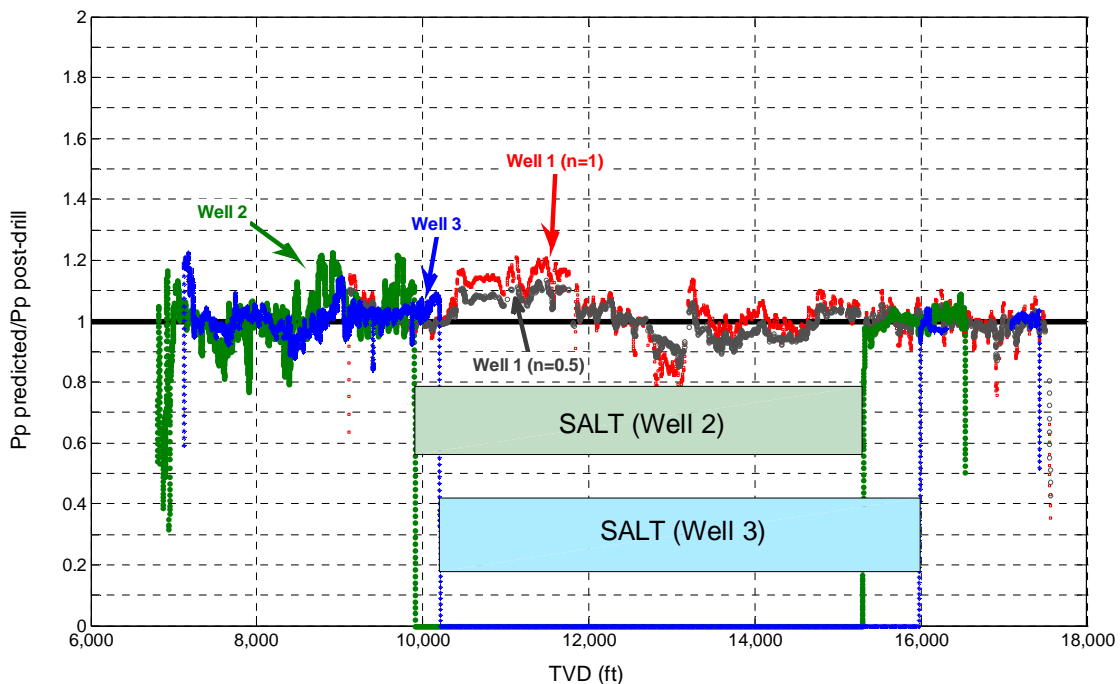
Figure 4.8 Ratio of predicted pore pressure to actual pore pressure using MSE as a new parameter in Eaton's equation for Well 1, Well 2, and Well 3.

The percentage variation of the predicted pore pressure to the post-drill pore pressure for Well 1 [for $n = 1$ in Equation (4.5)] is ~10% along the depth of the well, except in the ranges from $10,350 – 11,700$ ft and from $12,700 – 13,100$ ft. In the ranges from $10,350 –$

11,700 ft and from 12,700 – 13,100 ft, the percentage variation for Well 1 is the up to 20% [for $n = 1$ in Equation (4.5)]. The percentage variation for Well 1 [for $n = 0.5$ in Equation (4.5)] is slightly less than 10% along the depth of the well, including the ranges from 10,350 – 11,700 ft and from 12,700 – 13,100 ft. For Well 2, the percentage variation of the ratio of predicted pore pressure to post-drill post pressure is less than 10%, except at the sandy zone (~9,750 ft) where the over prediction goes up to 20%. The percentage variation of the ratio of predicted pore pressure to post-drill post pressure for Well 3 is ~8%, except at the sandy zone (~9,000 ft) where the over prediction goes up to 15%.

It is important to recall that the lithology of Well 2 and Well 3 is shale; whereas, the lithology of Well 1 is sandstone. Thus, it can be observed that the use of this new approach, Equation (4.5), seems to be promising for predicting pore pressure for different types of rock.

Several observations can be made from the results of the new equation, Equation (4.5), presented in the above figures. It has to be noted that the normal trends of pore pressure and MSE were established by analyzing plots of MSE and post-drill pore pressure as a function of depth for the entire well. However, even if the post-drill data is not available the normal trends may be inferred, as it is usually done, from information of adjacent exploratory wells that share similar lithology. Furthermore, if no information is available from adjacent well, the normal trends can be established while drilling in the transition zone and Equation (4.5) could be used to predict the pore pressure in the over-pressured zones.

Once the normal trends and the overburden are determined, the application of Equation (4.5) is straight forward. The only remaining open question is the appropriate value of the exponent n in the equation. The results presented above suggested that the exponent might not even be needed in the equation. However, the value of one for the exponent of

Equation (4.5) to determine the pore pressure of Well 1, Well 2, and Well 3 was an empirical finding. Nevertheless, the form of Equation (4.5), which relates pore pressure to drilling parameters (MSE), environmental parameters (overburden), seems to correctly predict the trends of pore pressure.

Another point to remark is the fact the material properties are not considered in Equation (4.5). Indeed, Equation (4.5) is only applicable to wells, or zones within a well, with the same lithology throughout. Moreover, it is hypothesized that the normal trend of mechanical specific energy (MSE_n) is a function of material properties. If this hypothesis is correct, a normal trend of MSE could be probably determined from the rock properties *a priori*. This would require a fundamental understanding of the role of material properties in the cutting process of rock.

From these observations, it is clear that further work is needed to validate Equation (4.5) with more data. Moreover, emphasis should be placed on understanding the reason why Equation (4.5) works well in predicting pore pressure. For these reasons, a fundamental approach, based on basic principles, to understand the mechanism of rock drilling is proposed. The development of this fundamental approach to determine whether or not it is possible to predict pore pressure from drilling parameters, environmental parameters and material properties is described in the next chapter.

CHAPTER V
FUNDAMENTAL APPROACH TO RELATING PORE PRESURE
TO DRILLING PARAMETERS, ENVIRONMENTAL PARAMETERS,
AND MATERIAL PROPERTIES

Two empirical approaches (first and second approaches considered) have been presented in previous chapters that attempt to establish a relationship among pore pressure, drilling parameters, environmental parameters, and material properties. Although both approaches suggest that such a relationship exists, neither approach have been validated to definitely prove the existence and form of the relationship. A fundamental approach is proposed in this chapter to investigate, from basic principles, the relationship among the mentioned parameters and material properties. A more fundamental way of viewing mechanical specific energy is described first. Then, a brief summary of the theory of Biot's poroelasticity is presented. Finally, a numerical model based on Biot's poroelasticity theory is proposed to describe the cutting process.

5.1 A more fundamental way of viewing MSE

In 1965, Teale introduced the term mechanical specific energy (MSE) to describe the energy required to break a volume of rock [9]. Teale expressed MSE in terms of drilling parameters with Equation (3.17). The equation derived by Teale accounts for two main contributions of input energy (per unit volume): (1) the mechanical (shaft) work done by the rotary movement of the drill bit [first term in Equation (3.17)], and (2) the work done on the rock by the vertical thrust of the drill bit [second term in Equation (3.17)].

The concept of mechanical specific energy has been used in the oil and gas industry as a quantifier of common drilling problems [30], as an indicator used to maximize the rate of penetration [31], and in general, as an index to evaluate the drilling performance [32]. However, there is no information available in current open literature (to the knowledge of the author) that suggests the use of MSE to predict virgin pore pressure. Although

MSE is not currently used to predict pore pressure, the use rate of penetration has been previously suggested in some investigations to predict pore pressure [56, 58]. Furthermore, a relationship between pore pressure and rate of penetration has been established in other investigations [59-61], and other works suggest that there is indeed a relationship between MSE and pore pressure [33, 39]. The PSP[3] concept and the concept of using MSE in Eaton's equation, described in Chapter III and Chapter IV, respectively, were developed under the premise that the MSE should be a function of the effective stress rather than the total stress of the rock, and from this relationship the virgin pore pressure could be predicted.

On the other hand, it can be recognized that drilling parameters (torque, rate of penetration, weight on bit, rotary speed) are not independent from each other. That is, the variation of one parameter affects the others. Thus, predicting pore pressure from a single parameter, such as the rate of penetration, has a limited applicability since it can be valid only if the other parameters are maintained constant. Fortunately, a fundamental parameter, the MSE, can be used to group the dependent parameters in one single parameter and account for the dependability of all the drilling parameters. Another important point to consider is the fact that MSE does not depend solely on the pore pressure. MSE depends on other factors (besides pore pressure) such as the type of the lithology being drilled, and the environmental parameters (such as the hydrostatic mud pressure and the confining stresses). Therefore, it is important to clearly establish all the factors that contribute to the energy required to break the rock.

It can also be recognized that the MSE calculated from drilling parameters that are measured at the surface is greater than the actual energy required to break the rock at the bottomhole, since a significant fraction of the MSE (calculated from surface parameters) is used to overcome friction of the drill string along the well. Furthermore, even if the MSE is calculated from downhole drilling parameters, a portion of this energy is not transfer from the drill bit to the rock since it is lost by friction at the cutter-rock

interface. It has been estimated that only 30-40% of the MSE calculated with Equation (3.17) (with surface parameters) is actually used to break the rock [31]. This suggests that there is an efficiency associated with energy input and the energy required to break the rock during drilling. If the drilling parameters to calculate MSE are measured at the surface, an overall drilling efficiency can be defined as

$$\eta_{overall} = \frac{MSE_{BR}}{MSE_{surface}} \tag{5.1}$$

where MSE_{BR} is the mechanical specific energy required to break the rock, and $MSE_{surface}$ is the mechanical specific input energy calculated from drilling parameters that are measured at the surface. The overall drilling efficiency in Equation (5.1) can be also thought as a product of two efficiencies

$$\eta_{overall} = \eta_{string} \cdot \eta_{cutter} \tag{5.2}$$

where η_{string} is the efficiency of the energy transfer along the drill string from the surface (where the torque is applied) to the bottomhole, and η_{cutter} is the efficiency of the energy transfer from the drill bit to the rock. Therefore, the efficiencies in Equation (5.2) can be expressed as

$$\eta_{string} = \frac{MSE_{downhole}}{MSE_{surface}} \tag{5.3}$$

where $MSE_{downhole}$ is the mechanical specific energy calculated from drilling parameters that are measured downhole, and

$$\eta_{cutter} = \frac{MSE_{BR}}{MSE_{downhole}} \tag{5.4}$$

The mechanical specific energy required to break the rock (MSE_{BR}) is of particular interest. Specifically, it is desired to know what factors contribute to the energy required to break the rock for a particular system. It is suggested that the value of MSE_{BR} for a particular system might depend on two main contributions

$$MSE_{BR} = MSE_{\substack{rock \\ matrix}} + MSE_{environment} \qquad (5.5)$$

where $MSE_{rock\,matrix}$ is the energy required to break the rock skeleton of a rock element that is subject to no external or internal (pore) stresses, and $MSE_{environment}$ is the energy required to overcome the environmental conditions to which the rock is subjected such as confining stress, temperatures, fluid in pores, pore pressure, and possibly others.

Therefore, it can be said that

$$MSE_{\substack{rock \\ matrix}} = f\left(MSE_{intrinsic_{rock\,grains}}, MSE_{rock\,structure}\right) \qquad (5.6)$$

where $MSE_{intrinsic_{rock\,grains}}$ is an intrinsic property of the material that constitutes the grains of the rock, and $MSE_{rock\,structure}$ is the energy required to counteract the structural characteristics of the rock skeleton in order to break it. Since $MSE_{intrinsic_{rock\,grains}}$ is an intrinsic property of the rock grains, it could be in principle determined by a thermodynamically defined strength criterion. An intrinsic property is defined as a macroscopic characteristic of a system to which a numerical value can be assigned at a given time without knowledge of the previous history of the system. The fundamental quantity that characterizes basic properties of a physical system, and which is a single-value function of the state of the system, is the internal energy of the system. Part of the applied MSE_{BR} is added to the internal energy of the solid matrix until a critical value is reached, which is determined by the strength of interatomic bonds ($MSE_{intrinsic_{rock\,grains}}$). A strength criterion can be thermodynamically defined as a

critical value of the stored internal energy that does not depend on the type or circumstances of deformation, but is a physical constant of the material (rock grains) [62]. On the other hand, the pore size, pore structure, and connectivity of the pores provide specific structural characteristic to the rock skeleton that modify the overall strength of rock. $MSE_{rock\ structure}$ is the energy required to counteract these structural characteristics of the rock skeleton in order to break it.

The other contribution to MSE_{BR} in Equation (5.5) is the energy required to overcome the environmental conditions to which the rock is subjected ($MSE_{environment}$). The environmental conditions of the rock are usually manifested as stresses applied on the rock. The environmental conditions may be internal or external. Thus, two main contributions to the ($MSE_{environment}$) can be distinguished

$$MSE_{environment} = MSE_{internal\ env.} + MSE_{external\ env.} \tag{5.7}$$

Internal environmental conditions (usually because of the presences of pore fluid) result in stresses on the pore walls such as pore pressure and thermal stresses (due to changes in temperature),

$$MSE_{internal\ env.} = f(Pp, T_f) \tag{5.8}$$

where Pp is the pore pressure, and T_f is the temperature of the pore fluid.

External environmental conditions subject the rock to stresses from overburden, hydrostatic mud pressure, Earth confining stresses, and thermal stresses. For example, a rock element in a drilling situation would be subjected to confining stresses from Earth and the hydrostatic mud pressure that can significantly increase the apparent strength of

the rock element. Thus, more energy to fracture the rock would be required, not because of the intrinsic nature of the material but to counteract the external conditions. That is,

$$MSE_{external\ env.} = f(OB, P_h, \sigma_c, T_s) \tag{5.9}$$

where OB is the overburden, P_h is the hydrostatic mud pressure, σ_c is the confining stress, and T_s is the temperature.

In summary, MSE_{BR} does not depend solely on the intrinsic strength of the grains that constitute the rock. Any physical conditions such as the pore size, pore structure, connectivity of the pores, type of fluid inside the pores, pore pressure, temperature, overburden, hydrostatic pressures, and confining stresses contribute to significant changes to the MSE_{BR}. That is,

$$MSE_{BR} = f\left(MSE_{intrinsic_{rock\ grains}}, MSE_{rock\ structure}, Pp, T_f, OB, Ph, \sigma_c, T_s\right) \tag{5.10}$$

Expression (5.10), and the explanation given for each of the contributions of MSE_{BR}, indicate that indeed, the virgin pore pressure in the rock element affects the energy required to break that rock (MSE_{BR}); and in turn, it affects the energy input, $MSE_{downhole}$ or $MSE_{surface}$, required. More importantly, the above explanations attempt to explain why $MSE_{downhole}$ or $MSE_{surface}$ could be a function of the virgin pore pressure.

It can be observed from Equation (5.10) that the energy required to break the rock depends on a multiplicity of factors. Since the interest is to determine the pore pressure during drilling, it has been recognized that a fundamental understanding of the rock cutting process, as well as the fluid-rock interactions during drilling, is required. It has been previously stated that a fundamental approach based on basic principles such fluid

mechanics, porous media, thermodynamics, and rock mechanics, could be used to explain the role of virgin pore pressure in the mechanical behavior of rock and eventually evolve into a methodology for virgin pore pressure prediction that would be reliable for all types of rocks, and situations. The general theory that is based on basic principles of fluid mechanics, porous media, thermodynamics, and rock mechanics to describe the two-way interactions between mechanical deformation and pore pressure is the Biot's poroelasticity theory. For these reasons, a model of the cutting process of rock (in a drilling situation) using Biot poroelasticity theory is proposed. Biot poroelasticity describes the hydo-mechanical coupled behavior of rock under external stresses, but it is used in this approach to describe such hydo-mechanical coupled behavior when the rock is undergoing failure (cutting process). The brief description of the poroelasticity theory is described in the next section. The proposed model of the cutting process using Biot poroelasticity theory is presented in Section 5.3, and results of the proposed poroelastic model are presented in Chapter VI.

5.2 Biot poroelasticity theory

The failure of rock during drilling is caused by the large stresses imposed on the rock by the drill bit. These stresses cause the rock to deform until failure is reached, but deforming the rock also results in a change in pore volume even before failure occurs. The permeability of the rock is a material property that accounts for the connectivity of the pores in a porous media. As the pore volume changes during deformation, the permeability of the rock affects how fast the pore fluid can be expelled from the pores (for a decrease of pore volume) or how fast new fluid can fill in the pores (for an increase in pore volume). A change in volume and amount of fluid in the pores is likely associated with a change in the pore pressure. Thus, depending on the permeability of the rock the local pore pressure at the cutting zone can either increase or decrease affecting the onset of failure.

It was mentioned in previous chapters, the pore pressure plays an important role in the mechanical behavior of rock, since part of the stresses applied to the rock are supported by the pore fluid. Thus, a change in pore pressure during drilling will result in a change in the mechanical behavior of rock, but a change in the mechanical deformation results in a change in pore pressure as well. That is, there is a two-way coupling between the mechanical deformation and the pore pressure of rock. The general theory that accounts for this coupled hydro-mechanical behavior is *poroelasticity* [1]. For many years, Biot's poroelasticity theory [16] was used only to solve problems involving consolidation of soils. However, a few decades later the equations of poroelasticity were successfully applied to solve problems in tectonophysics [43], petroleum-related rock mechanics [1], and even in the medical field to study the behavior of bones [44]. In petroleum-related rock mechanics, the effort has been concentrated on borehole stability, hydraulic fracturing, and compaction near pumping wells [45, 46]. However, to the best knowledge of the author, there are no investigations available in open literature that attempt to describe the cutting process of rock using poroelasticity equations. Nevertheless, there are no indications that suggest that the equations of poroelasticity should not be used to describe the process of cutting rock. In order to use Biot's poroelasticity theory to model the rock-fluid interactions during drilling, a brief description of this theory is presented in this section. Detailed explanation of the development of Biot's poroelasticity theory can be found elsewhere [1, 16, 42].

In order to describe the development of a linearized theory of poroelasticity (based on a continuum approach) for a macroscopic porous rock, it is convenient to first look into the micro-structure of the rock and establish the basic solid-fluid relations at the microscopic level. Figure 5.1, shows a two-dimensional view of a piece of porous rock that is subjected externally to a purely normal stress (confining pressure P_c), and the internal pore walls are subjected to a pore pressure (P_p), exerted by the pore fluid.
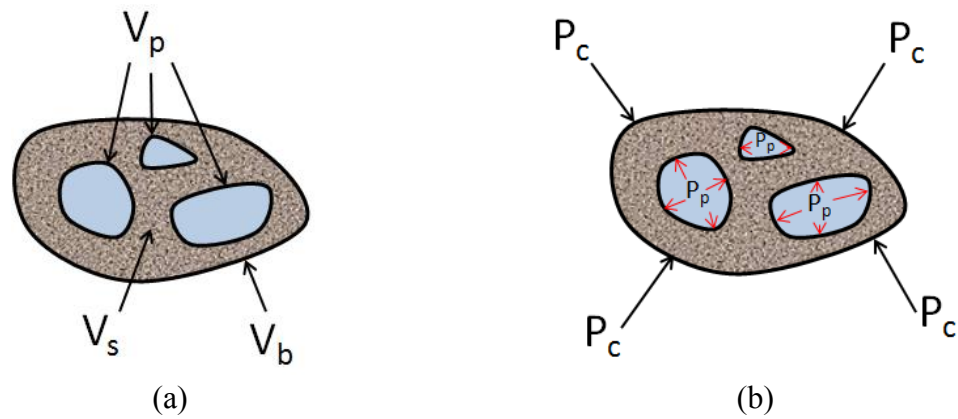
Figure 5.1 Two-dimensional view of a piece of porous rock, showing (a) the bulk volume, pore volume, and solid matrix volume, and (b) the confining and pore pressure, modified from Jaeger et al. [1].

The pore fluid is considered to be static and therefore it sustains no shear stresses. Thus, the internal pore walls are subjected only to normal stresses. If the model in Figure 5.1 is considered, it can be observed that there are two independent pressures acting on the rock, and the rock can be described by two independent volumes. Therefore, four independent compressibilities can be defined (in terms of the variables in Figure 5.1) as

$$C_{bc} = -\frac{1}{V_b^0}\left(\frac{\partial V_b}{\partial P_c}\right)_{P_p} \tag{5.11}$$

$$C_{bp} = \frac{1}{V_b^0}\left(\frac{\partial V_b}{\partial P_p}\right)_{P_c} \tag{5.12}$$

$$C_{pc} = -\frac{1}{V_p^0}\left(\frac{\partial V_p}{\partial P_c}\right)_{P_p} \tag{5.13}$$

$$C_{pp} = \frac{1}{V_p^0}\left(\frac{\partial V_p}{\partial P_p}\right)_{P_c} \tag{5.14}$$

where the superscript "0" denotes the initial, under-stressed state. The bulk and pore strains changes can be expressed in terms of the rock compressibilities as

$$d\varepsilon_b = -\frac{dV_b}{V_b^0} = C_{bc}dP_c - C_{bp}dP_p \tag{5.15}$$

$$d\varepsilon_p = -\frac{dV_p}{V_p^0} = C_{pc}dP_c - C_{pp}dP_p \tag{5.16}$$

where the bulk strain $d\varepsilon_b$ is equivalent to the macroscopic volumetric strain defined for any homogeneous material. The change in strain of the solid matrix can be deduced from the superposition concept assuming that a pore pressure and a confining pressure of the same magnitude act on the rock. That is, the strain in the solid matrix can be thought as the subtraction of the effects of a rock subjected to both confining and pore pressures (which affect both the solid matrix volume and the pore volume) minus a rock subjected to only pore pressures (which affects only the pore volume), such that

$$C_m = C_{bc} - C_{bp} \tag{5.17}$$

$$d\varepsilon_m = C_m dP = \frac{dP}{K_m} \tag{5.18}$$

where C_m is the compressibility of the solid matrix, K_m is the bulk modulus of the solid matrix, and $d\varepsilon_m$ is the volumetric strain change of the solid matrix. The compressibilities and volumetric strains defined above have been derived from a microscopic point of view. However, these concepts can be also be used to develop the equations that describe the mechanical behavior of rock at the macroscopic level.

In order to develop a linearized theory of poroelasticity that describes the behavior of a saturated porous rock, a small cubic element of rock which sides are parallel with the axes of the coordinate system is considered. This rock element should be large enough compared to the size of the pores so that it may be treated as a homogeneous and continuum medium. At the same time, the rock element should be small enough compared to the scale of the macroscopic phenomena of interest that it can be considered infinitesimal. For simplicity, the following equations used to describe the mechanical

behavior of rock are presented using the so-called *index notation,* where a comma followed by subscripts denotes differentiation with respect to spatial coordinates and repeated indices in the same monomial imply summation over the range of the indices (from 1 to n, where n is the number of dimensions considered in the analysis). From solid mechanics, it is well known that the stress-strain relations of a nonporous material can be expressed in terms of the shear modulus (G) and the Poisson ratio (v) as

$$\varepsilon_{ij} = \frac{\sigma_{ij}}{2G} - \frac{v}{2G(1+v)} \delta_{ij} \sigma_{kk}$$

(5.19)

where ε_{ij} is the strain tensor, σ_{ij} is the stress tensor, and δ_{ij} is the Kronecker delta ($\delta_{ij} = 1, if\ i = j;\ \delta_{ij} = 0, if\ i \neq j$). It can be seen from Equation (5.19) that a strain in the solid element that occurs in a direction parallel to one of the coordinate axes is due to the stress applied to the element in that direction (first term on the right-hand side of the equation) minus the effect of the normal stresses applied to the solid element (second term on the right-hand side of the equation). Any other strain along a direction not parallel to any of the coordinate axes is proportional only to the stress applied in that direction. The magnitude of the strain is affected by the material properties G (shear modulus) and v (Poisson's ratio).

If a displacement vector (u_{ij}) that tracks the movement of the solid element is defined, the stress tensor ε_{ij} can be expressed in terms of the displacement vector as

$$\varepsilon_{ij} = \frac{1}{2} \left(u_{i,j} + u_{j,i} \right)$$

(5.20)

Considering now a saturated porous rock which is macroscopically isotropic, it is first recognized that the pore pressure does not exerts shear stresses on the pore wall. It can be seen from Equation (5.15) that the total volumetric strain (ε_b) resulting solely from an

applied pore pressure is $-C_{bp}P_p$. Since the pore fluid only exerts normal stresses on the pore walls, a change in pore pressure results in equal extensions of the pore volume along each of the three mutually orthogonal directions of the coordinate system (assuming a three-dimensional rectangular system). This means that one third of the total volumetric strain that resulted from the pore pressure application must be added to each of the normal strain components. Thus, the equation for the stress-strain relations, Equation (5.19), for a saturated porous rock becomes

$$\varepsilon_{ij} = \frac{\sigma_{ij}}{2G} - \frac{v}{2G(1+v)}\delta_{ij}\sigma_{kk} - \frac{C_{bp}}{3}\delta_{ij}P_p \qquad (5.21)$$

It can be derived from Equation (5.17) that $C_{bp} = C_{bc} - C_m$. Additionally, the compressibility C_{bp} is related to the macroscopic bulk modulus as $C_{bp} = \frac{1}{K}$, where K is the bulk modulus of the rock. Therefore, Equation (5.21) can be rewritten as

$$\varepsilon_{ij} = \frac{\sigma_{ij}}{2G} - \frac{v}{2G(1+v)}\delta_{ij}\sigma_{kk} - \frac{\alpha}{3K}\delta_{ij}P_p \qquad (5.22)$$

where α is known as the Biot-Willis coefficient defined as $\alpha = 1 - \frac{C_m}{C_{bc}} = 1 - \frac{K}{K_m}$. Equation (5.22) shows that a normal strain is the result of the application of a normal stress in the same normal direction minus the combine effect of all other confining pressures and the pore pressure; whereas, the strain in all other directions depend only on the stress in that direction. An expression for the effective stresses in terms of the strains is determined by inverting Equation (5.22):

$$\sigma_{ij} - \alpha\delta_{ij}P_p = 2G\left(\varepsilon_{ij} + \frac{v}{1-2v}\delta_{ij}\varepsilon_{kk}\right) \qquad (5.23)$$

It can be deduced from Equation (5.23) that it is indeed the effective stress (left-hand side of the equation) in a saturated porous rock that is responsible of any volume changes in the rock (shown as strains in the right-hand side of the equation). In order to use the relationship established in Equation (5.23) to model complex, non-homogeneous domains, it is convenient to develop a differential set of equations from Equation (5.23). Combining conditions for stress equilibrium ($\sigma_{ij,j} = -F_i$), Equation (5.20), and Equation (5.23), the Navier equations of poroelasticity in terms of the displacement vector can be written as

$$G\nabla^2 u_i + \frac{G}{1 - 2v} u_{k,ki} = -F_i - \alpha P_{p,i} \tag{5.24}$$

or in vector form as

$$G\nabla^2 \boldsymbol{u} + \frac{G}{1 - 2v} \nabla(\nabla \cdot \boldsymbol{u}) = -\boldsymbol{F} - \alpha \nabla P_p \tag{5.25}$$

where $\boldsymbol{F} = F_i$ is a body-force vector (commonly due to gravity). Similar to Equation (5.23), Equation (5.25) implies that the deformation of the solid matrix is due to forces applied to the rock as well as any changes in pore pressure. In the absence of information of the shear modulus G, the Young's modulus can be used to characterized the rock using the relation $G = \frac{E}{2(1+v)}$.

It is important to note that Equation (5.25) is written in vector form; and therefore, it represents a set of equations with the same number of equations as the number of dimensions in the coordinate system considered for analysis. It can be also observed that the displacement vector has one component on each axis of the coordinate system. Therefore, there is always one more unknown in Equation (5.25) than the number of equations. For example, if a three-dimensional coordinate system is considered, Equation (5.25) will have three equations (one for each dimension) with four unknowns

(three displacements and the pore pressure). Therefore, an additional equation for pore pressure is needed in order to have a complete system of equations.

The additional equation for pore pressure is found from the conservation of mass for the pore fluid. The introduction of two new variables is required in order to develop the additional equation. First, the variable ζ is introduced to describe the variation of volumetric pore fluid content that is due solely to mass transfer. Second, the flux vector $\boldsymbol{q} = q_i$ is used to describe the rate of fluid volume that passes through a unit area of porous solid whose normal is in the x_i direction. It follows from a mass balance that

$$\frac{\partial \zeta}{\partial t} + \nabla \cdot \mathbf{q} = 0 \tag{5.26}$$

Equation (5.26) represents the conservation of mass for the pore fluid, even though it is derived based on volumetric quantities. This is because ζ is defined as the volumetric pore fluid content due solely to the mass transfer. It can be recognized that low flow rates are usually encountered in sedimentary rock. Thus, Darcy's law can be used to relate the flux vector $\boldsymbol{q}$ and the pore pressure. For the general anisotropic case, Darcy's law can be expressed as

$$\boldsymbol{q} = -\frac{\overline{\overline{\boldsymbol{k}}}}{\mu_f} \nabla (P_p - \rho_f \boldsymbol{g} \cdot \boldsymbol{x}) \tag{5.27}$$

where $\overline{\overline{\boldsymbol{k}}}$ is the permeability second-order tensor, μ_f is the dynamic viscosity of the fluid, ρ_f is the density of the fluid, and $\boldsymbol{g}$ is the gravitational acceleration vector. If the gravitational effects are disregarded and isotropic rock is considered, combining Equation (5.27) into (5.26) yields

$$\frac{\partial \zeta}{\partial t} = \frac{k}{\mu_f} \nabla^2 P_p \tag{5.28}$$

On the other hand, it can be recognized from the microscopic approach that the pore pressure is proportional to the dilation of the porous rock and the variation of the fluid content, such that

$$P_p \equiv M(\zeta + \alpha \varepsilon_b) \tag{5.29}$$

where M is known as the Biot modulus and it is defined from Equation (5.29) under constant bulk strain as

$$M = \left(\frac{\partial \zeta}{\partial P_p}\right)_{\varepsilon_b} \tag{5.30}$$

The inverse of the parameter M is termed the *storage coefficient* and it represents (physically) the amount of fluid which can be forced into the rock under pressure while the volume of the rock is kept constant [16]. For the case of an ideal porous material, the storage coefficient can be calculated from basic material properties using the relation

$$\frac{1}{M} = \frac{\phi_s}{K_f} + \frac{\alpha - \phi_s}{K_m} \tag{5.31}$$

where $\phi_s = \frac{V_p}{V_b}$ (from Figure 5.1) is the porosity of the rock, $K_f = \frac{1}{C_f}$ is the bulk modulus of the fluid, C_f is the compressibility of the fluid, $K_m = \frac{1}{C_m}$ is the bulk modulus of the solid matrix, and C_m is the compressibility of the solid matrix.

Finally, combining Equation (5.29) with Equation (5.28), the rate of change of pore pressure in the rock can be expressed as

$$\frac{\partial P_p}{\partial t} = \frac{kM}{\mu_f}\nabla^2 P_p + \frac{\alpha M \partial \varepsilon_b}{\partial t} \tag{5.32}$$

Equation (5.32) states that the rate of change in pore pressure is due to the flow in or out of the pore volume (first term on the right-hand side) and to the change in the bulk volume of the rock (second term on the right-hand side), which in turn affects the pore volume.

Equations (5.25) and (5.32) constitute the final form of the Biot poroelasticity theory. It can be observed that there is a two-way coupling of both sets of equation by the pore pressure and the total bulk strain of the rock. The physical meaning of this two-way interaction is that an increase of pore pressure induces a change in volume of the rock, but a change in the bulk volume of the rock (for example, by confining stresses) causes a change of pore pressure, which will depend on how easy the fluid can escape or enter the pores. That is, the change in pore pressure also depends on the permeability of the rock and viscosity of the fluid. It has been previously mentioned in this dissertation that the solid-fluid interactions in the rock affect the onset of failure, which in turn affect the amount of energy required to break the rock during drilling. In order to understand these interactions, and the extent of the effect they have on the cutting of rock, and analysis of the cutting process of rock using the Biot poroelasticity theory (which is derived from basic principles) is presented in the next section.

5.3 Numerical poroelastic model of the rock cutting process

It has been stated previously in this dissertation that a fundamental understanding of the rock cutting process is required in order to understand the role of pore pressure in the mechanical behavior of rock during drilling. In order to address this requirement, an analysis of the cutting process using Biot poroelasticity equations has been conducted.

One of the most important outcomes of this analysis is the identification the drilling parameters, environmental parameters, and material properties that play a significant role in the physics of the drilling process, which is a function required to satisfy the objective of this dissertation (see Figure 2.2). Parameters that play a role in the physics of the drilling process have already been recognized in Section 5.1, Equation (5.10). However, Equation (5.10) neither explains the extent to which each parameter affects the MSE_{BR}, nor provides the reason of the effect of these parameters on the MSE_{BR}. From Equations (5.25) and (5.32), it can be observed that a model of the drilling process using poroelasticity equations (which are derived from basic principles) could be used to explain the relationship between external stress (such as the cutting stress and the hydrostatic mud pressure) and pore pressure, while accounting for the rock-fluid interactions at the microscopic level. Furthermore, this model can be used to determine the extent of the effect of the drilling parameters, environmental parameters, and material properties on the drilling process. It is important to note that the effects of temperature are not considered in this model. Further work is recommended to use the extended thermoelasticity theory [1] to analyze the effects of temperature in the drilling process.

The model and analysis presented in this section are developed under the assumption that the cutting of rock occurs by shear. The cutting process of rock is a complex processes in which several cutters attached to the rotating drill bit (for PDC bits) shear the rock. In order to simplify the development of the model, the mechanism of rock shearing by a single cutter in a two-dimensional domain is considered. The simplified two-dimensional geometry to model the cutting of rock by a single cutter is shown in Figure 5.2. Notice that the geometry considered for this analysis is similar to the geometry in Figure 3.9 that was used to developed the PSP[3] model, except that the back-rack angle of the cutter (θ) is considered in the model in Figure 5.2.
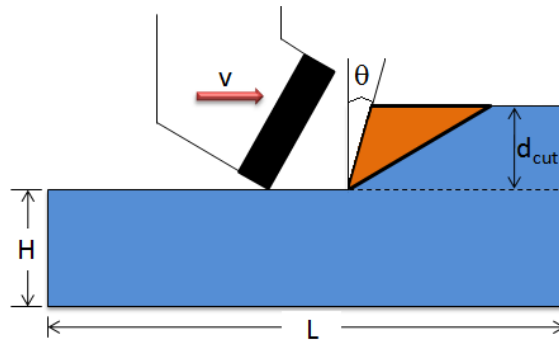
Figure 5.2 Two-dimensional geometry of the rock cutting process with a single cutter.

It can be seen in Figure 5.2 that the cutter moves from left to right with a velocity v against the rock at an angle θ (with respect to the vertical) and a depth of cut d_{cut}. It is assumed in this model that the cutting process starts when the cutter has already cut a layer of rock (of thickness equal to the depth of cut) approximately half-way $(L/2)$ from left to right. Moreover, any residual rock that has been previously separated from the bulk volume of the rock has been cleaned in such a way that the energy applied to the cutter transfers completely to the intact rock. It is important to mention that the sketch in Figure 5.2 is not to scale. The actual dimensions used in the poroelastic model have aspect ratios of $\frac{d_{cut}}{H} < 0.1$, and $\frac{d_{cut}}{L} < 0.04$. These dimensions ensure that edge effects of the geometry do not affect the analysis of stresses and pore pressure at the shearing zone.

Recalling that the objective of this dissertation is to determine whether it is possible to predict the pore pressure from drilling parameters, environmental parameters, and material properties, it can be observed that the model presented in this section is used to solve the inverse problem. That is, an initial value of pore pressure is assumed for the rock in Figure 5.2 and the poroelastic model is used to determine the energy required to break the rock (MSE_{BR}). The rock considered in the poroelastic model is characterized by its material properties and it subjected to environmental parameters. The poroelasticity model can provide an insight of the validity of Equation (5.10) for

different situations and types of rock. In order to determine MSE_{BR} for this model, Equations (5.25) and (5.32) are solved numerically using the commercial software COMSOL Multiphysics.

In general, the following protocol has been used to determine the energy required to break the rock (MSE_{BR}) using the poroelastic model proposed above:

(a) Material properties are assigned to the rock domain.

(b) A uniform initial value of (virgin) pore pressure is set to the rock domain.

(c) Environmental conditions (boundary conditions) are set at the boundaries of the rock domain.

(d) A cutting stress (as a function of time) is applied to the face of the rock that is in contact with the cutter (note that the cutter is not actually modeled, but only the stress transmitted to the face of the rock).

(e) The change in stresses within the rock is monitored as a function of time until any part of the rock reaches a stress that corresponds to the initiation of failure.

(f) The value of the cutting stress that caused the initiation of failure is recorded and considered to be the MSE_{BR}.

The rock in Figure 5.2 is characterized by the material properties in Table 5.1. Two sets of properties can be distinguished from the table, one for the solid matrix and one for the pore fluid. Notice how the properties of the solid matrix required for this model not only characterized the rock from the mechanical point of view, but also account for the pore structure and connectivity of the pores. The failure parameters S_0 and ϕ are not needed to solve the poroelasticity Equations (5.25) and (5.32). However, according to the protocol mentioned above, they are needed in order to determine the moment at which initiation of failure occurs after a cutting stress is applied. Since both failure parameters are specific for each type of rock, they are included in the set of material properties required to characterize the rock.

Table 5.1 Material properties of rock required for the poroelastic model.

Properties of solid matrix			Properties of pore fluid	
Symbol	Name	Comments	Symbol	Name
E	Young's modulus	mechanical behavior	μ_f	dynamic viscosity
v	Poisson's ratio	mechanical behavior	C_f	fluid compressibility
ρ_s	density of matrix	mechanical behavior		
ϕ_s	porosity	pore structure		
k	permeability	connectivity of the pores		
α	Biot-Willis coefficient	rock structure		
S_0	cohesion	failure parameter		
ϕ	angle of internal friction	failure parameter		

Two sets of boundary conditions and an initial condition are required for the solution of Equations (5.25) and (5.32), one for each equation. For Equation (5.25), which describes the solid mechanics behavior, it is assumed that boundaries of the geometry representing the rock are constrained (most likely by confining stresses) in the direction normal to each boundary, except for the top boundary which is subjected to the stress of the hydrostatic pressure (due to the drilling mud in a drilling situation). For Equation (5.32), which describes the fluid flow, it is assumed that the bottom boundary is subjected to the same value of the initial (virgin) pore pressure assumed for the rock. Moreover, it is assumed that there is no flow across the side boundaries (since it is assume that the pore pressure does not significantly vary in the horizontal direction), and the top boundary is subjected to the hydrostatic pressure of the drilling mud. Finally, a cutting stress S_c is applied as a function of time to the face of the rock that is in contact in an actual

situation with the cutter. All the boundary conditions considered in this numerical model are shown in Figure 5.3.
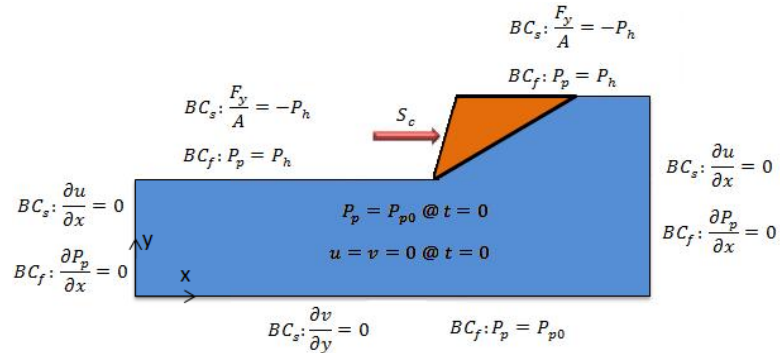
Figure 5.3 Boundary conditions for the poroelastic numerical model.

The Mohr-Coulomb failure criterion, Equation (3.9), is used to determine the moment at which failure initiates due to the application of the cutting stress. To facilitate the implementation of the failure criterion in the numerical model, the following expression can be derived from Equation (3.9) and the geometric relations in Figure 3.15:

$$\sigma'_{max} \geq \frac{2S_0 \cos \phi}{1 - \sin \phi} + \sigma'_{min} \frac{(1 + \sin \phi)}{1 - \sin \phi} \tag{5.33}$$

where initiation of failure occurs when the maximum principal effective stress (σ'_{max}) is equal or greater than the expression on the right-hand side of Equation (5.33). In the numerical model, the solution of Equations (5.25) and (5.32) is determined as a function of time. Since the cutting stress S_c is also applied as a function of time, the principal stresses are monitor at each time. The solution is stop when the criterion in Equation (5.33) is met. The energy required to break the rock MSE_{BR} corresponds to the cutting stress S_c at the moment of failure initiation.

Attempts to validate the model proposed in this section with available data from the literature are presented in the next chapter. Once the model is validated it can be used to: (1) identify the parameters and material properties that play a significant role in the cutting process for different types of rock and situations, (2) verify if the PSP^3 concept complies with the basic principles of rock mechanics and fluid mechanics used in the poroelasticity theory, and (3) verify if the concept of using MSE in Eaton's equation complies with the basic principles of rock mechanics and fluid mechanics used in the poroelasticity theory. Results of these analyses are presented in the next chapter as well.

CHAPTER VI
RESULTS OF THE POROELASTIC MODEL

The results of the numerical analyses of the cutting process using the poroelasticity equations (poroelastic model) are presented in this chapter. The solution of the equations of poroelasticity was determined with the aid of the commercial software COMSOL Multiphysics. Different types of rock and situations were analyzed in an attempt to validate the model, and subsequently to better understand the effect of different parameters on the cutting process of rock. Each analysis done in COMSOL Multiphysics is a virtual simulation of the actual process of cutting a rock by a single cutter. Thus, the simulations run for the numerical analyses presented in this chapter are termed *numerical experiments.* Results of the validation of the poroelastic model are presented first. Then, results of the numerical experiments that were conducted to determine the significant parameters that play a role in the physics of the drilling process are presented. Subsequently, the results of the verification of the PSP[3] concept using the poroelastic model are presented. Finally, comments on the insights gained from the results of the poroelastic model on the concept of using MSE in Eaton's equation are presented.

6.1 Validation of the poroelastic model

Two sets of numerical experiments were conducted in order to validate the poroelastic model described in the previous chapter. The first set consisted of three-dimensional numerical experiments that simulated the compression experiments conducted by Murrell [51] on Darley Dale sandstone. The second set consisted of a two-dimensional simplification of the experiments conducted by Rafatian et al. [63, 64] on Indiana Limestone. Details of both sets of experiments are presented in the next sections.

6.1.1 Validation of the poroelastic model with data from Murrell [51]

Murrell conducted an extensive series of tri-axial experiments on cylindrical samples of Darley Dale sandstone to determine the effect of pore pressure on the strength of the

rock. His experiments involved both extension and compression tests. Data from the compression experiments conducted by Murrell has been borrowed and used to validate the poroelasticity equations proposed in Section 5.2. Numerical experiments using the poroelasticity equations were conducted following a similar protocol described in Section 5.3. However, the rock geometry used for this set of experiments is different from the one proposed in Figure 5.2. Instead, a cylindrical geometry with the same dimensions of the cylindrical samples used by Murrell is simulated. The material properties of Darley Dale used in the experiments can be seen in Table 6.1.

Table 6.1 Poroelastic properties of Darley Dale sandstone.

Properties of solid matrix		
Symbol	Property	Value
E	Young's modulus	12.8×10^6 psi
ν	Poisson's ratio	0.15
ρ_s	density of matrix	2.28 g/cm^3
ϕ_s	porosity	0.21
k	permeability	56 mD
α	Biot-Willis coefficient	0.79
S_0	cohesion	1990 psi at $0 \leq \sigma_n' < 4000$ [psi] 3600 psi at $4000 \leq \sigma_n' < 17000$ [psi] 5177 psi at $17000 \leq \sigma_n' < 25000$ [psi]
ϕ	angle of internal friction	45.5° at $0 \leq \sigma_n' < 4000$ [psi] 37° at $4000 \leq \sigma_n' < 17000$ [psi] 31° at $17000 \leq \sigma_n' < 25000$ [psi]
Properties of pore fluid		
Symbol	Property	Value
μ_f	dynamic viscosity	6.9×10^{-4} Pa · s
C_f	fluid compressibility	3.8×10^{-10} 1/Pa

As mentioned above, the commercial software COMSOL Multiphysics was used to numerically solve the poroelasticity equations. COMSOL Multiphysics uses finite element numerical techniques to solve partial differential equations. In order to find a solution, a discretization of the domain into small elements must be made. These elements are known as the *mesh* of the domain. The mesh of the geometry considered in the first set of numerical experiments used for the validation of the poroelastic model is shown in Figure 6.1.
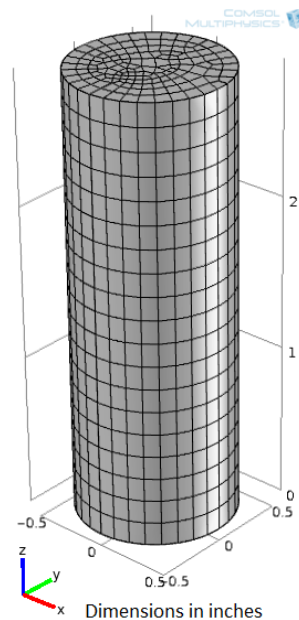
Figure 6.1 Mesh of geometry of rock domain for numerical experiments on Darley Dale.

According to the information provided in [51], the cylindrical samples used in the experiments had dimensions of 1 in. in diameter and 2.875 in. of length. The mesh shown in Figure 6.1 consisted of 2,812 hexahedral elements. Even though this seems to be a fairly small number of elements, it is important to point out that the mesh was used to solve the coupled system of Equations (5.25) and (5.33), which is coupled by the pore pressure and the volumetric bulk strain of the rock. A more representative parameter (indicative of the computational resources required to solve the system of equations) is

the number of degrees of freedom (DOF) for which the equations are solved for. The number of DOF solved for the mesh presented in Figure 6.1 was 97,500. This mesh was the result of an optimization procedure to balance the demanding computational resources of the coupled system of equations to the independence of results from a mesh with different number of elements.

The numerical experiments were conducted using the same combination of confining pressure and pore pressure used by Murrell for each experiment. In the experiments, the confining pressure was applied to the side walls of the cylindrical sample. A load was then applied at the top surface to compress the sample until it fails. The experiments were conducted under drained conditions. Except for this variation (the application of the load in the vertical direction to the top surface of the sample), the protocol described in Section 5.3 was followed for each numerical experiment.

Figure 6.2 shows an image from the numerical solution determined from the poroelastic model as compare to images of the broken samples from the actual experiments conducted by Murrell [51]. In the image from the numerical experiments, the surface in red indicates all locations where failure can potentially occur; whereas, the surface in blue indicates locations within the rock that are less susceptible to failure (at the given conditions). Based on the shape of the red surface, it can be deduced that several possible paths for a crack have the potential to occur. The lines in green and yellow indicate only two of the possible failure paths. The similitude between the indicated possible failure paths and the actual paths in the samples from Murrell is remarkable.

A plot of the load required to break each sample as a function of pore pressure at different confining pressures is presented in Figure 6.3. In this figure, the load determined from the numerical model (dotted line) is compared with the load determined experimentally by Murrell [51].
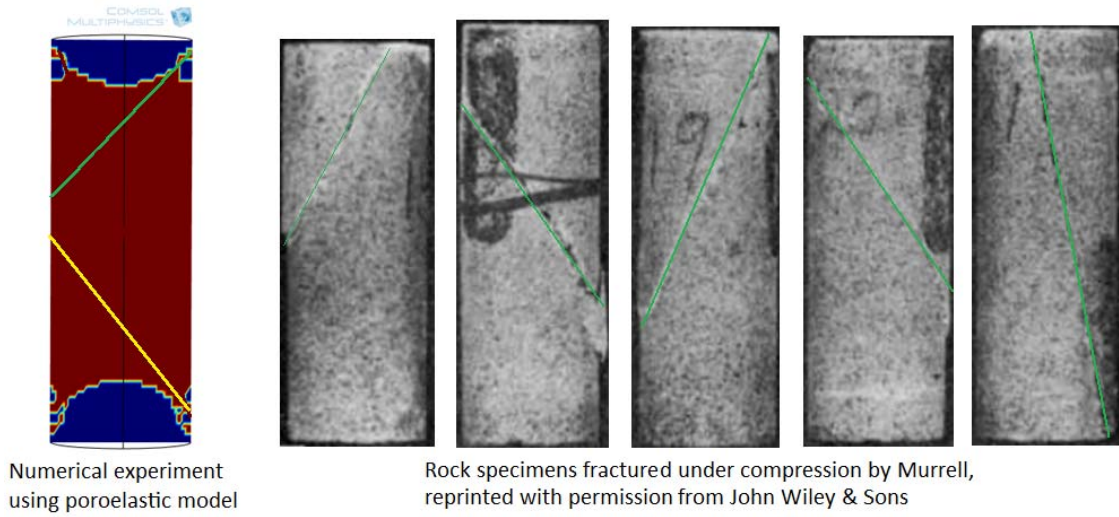
Figure 6.2 Visual comparison of rock failure between numerical experiments using poroelastic model and actual experiments conducted by Murrell [51].
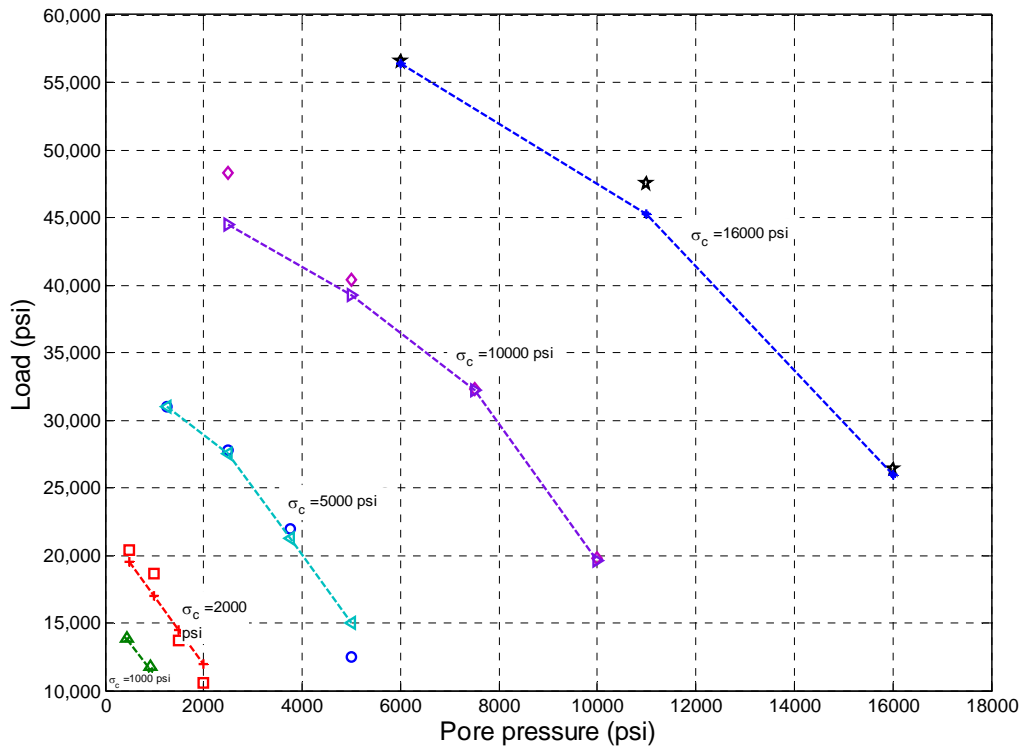
Figure 6.3 Comparison of the load determined from poroelastic model with the load determined experimentally by Murrell [51], as a function of pore pressure for several confining pressures.

It can be observed from Figure 6.3 that the load required to break the rock decreases as the pore pressure increases, which confirms the hypothesis of the relationship between CCS and pore pressure. Moreover, the load is also dependent on the confining pressure, since the load increases as the confining pressure increases even if the pore pressure is kept constant. This behavior is well known to be exhibit in sandstones, due to the high permeability of this type of rock, but it is important to remark that the poroelastic model is able to predict this behavior as seen in Figure 6.3. Furthermore, results in Figure 6.3 confirm the validity of Equation (5.10). In order to visualize the degree of agreement between the experimental data from Murrell and results from the poroelastic model, Figure 6.4 presents the same results of Figure 6.3, but presented as the ratio of load from the poroelastic model to the load found experimentally as a function of pore pressure. As mentioned in Chapters III and IV, a ratio equal to one signifies a perfect agreement between the experimental and numerical data.
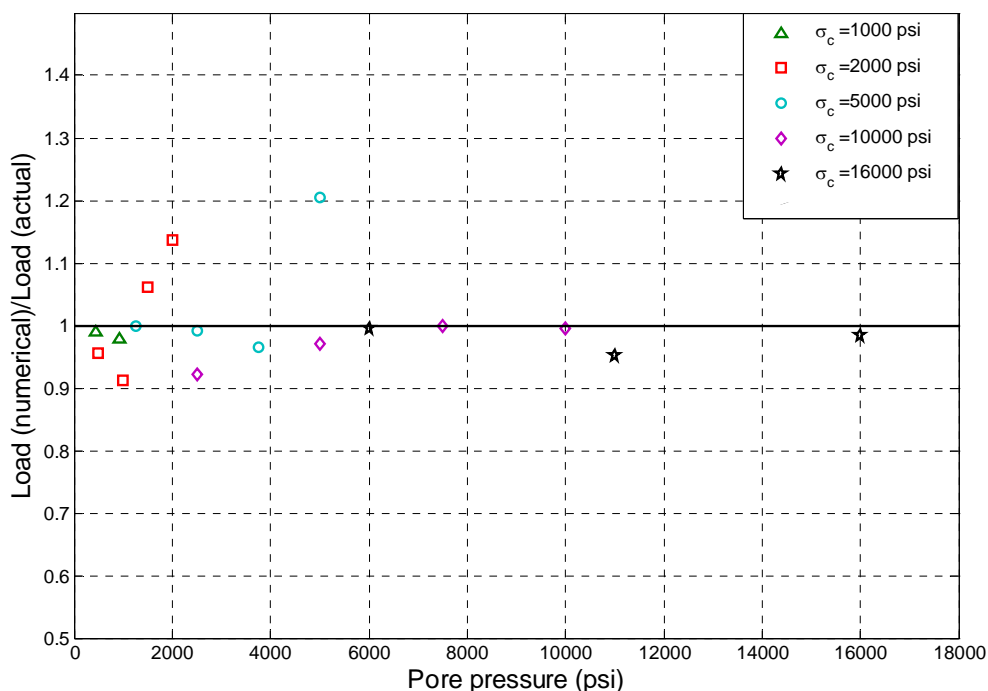
Figure 6.4 Ratio of the load determined from poroelastic model to the load determined experimentally by Murrell [51], as a function of pore pressure for several confining pressures.

It can be observed from Figure 6.4 that the load determined numerically from the poroelastic model is always in agreement with the load determined experimentally within a $\pm 10\%$, except for two data points where the load determined numerically over predicts the load determined experimentally by ~14% (at $Pp = 2,000$ psi, $\sigma_c = 2,000$ psi) and ~ 20.5% (at $Pp = 5,000$ psi, $\sigma_c = 5,000$ psi), respectively.

Results from Figures 6.2-6.4 indicate that poroelasticity theory can be successfully used to model the mechanical behavior of rock (or at least for Darley Dale sandstone) subjected to different pore pressures and confining pressure. However, it is important to note the model proposed in Section 5.3 does not resemble the conditions of the experiments conducted by Murrell. Moreover, the breakage of rock under the conditions tested by Murrell does not correspond to a true tri-axial test, since the confining stresses in two of the three principal directions are equal. In an actual drilling situation, the stresses acting on the rock (environmental conditions) do not resemble the situation tested by Murrell. The model proposed in Figure 5.2, however, attempts to simulate an actual drilling situation with a 2-D simplification of the cutting process. A second set of numerical experiments was conducted as an attempt to validate this model (explained in Section 5.3). The second set consisted of a two-dimensional simplification of the experiments conducted by Rafatian et al. [63, 64] on Indiana Limestone. Details of these numerical experiments are presented in the next section.

6.1.2 Validation of poroelastic model with data from Rafatian et al. [63, 64]
The second set of numerical experiments conducted to validate the poroelasticity equations is presented in this section. The model used in this analysis has been described in Section 5.3. The poroelastic model has been used to conduct numerical experiments that simulate the conditions of the experiments recently conducted by Rafatian et al. [63, 64] on Indiana limestone. An agreement between the numerical experiments using the poroelastic model and the data gathered by Rafatian et al. [63, 64] would further validate the poroelasticity equations. The geometry considered in this validation is shown in

Figure 5.2, and the boundary conditions are shown in Figure 5.3. The protocol described in Section 5.3 has been followed in order to determine the cutting stress required to break the rock under the simulated conditions. The material properties of Indiana limestone used for the numerical experiments are presented in Table 6.2. The failure parameters (S_o and ϕ) were estimated from the confined compressive strength (CCS) provided by Rafatian et al. [63, 64].

Table 6.2 Poroelastic properties of Indiana limestone.

Properties of solid matrix		
Symbol	Property	Value
E	Young's modulus	3.6×10^6 psi
ν	Poisson's ratio	0.25
ρ_S	density of matrix	2.3 g/cm^3
ϕ_S	porosity	0.15
k	permeability	10 mD
α	Biot-Willis coefficient	0.8
S_0	cohesion	2800 [psi]
ϕ	angle of internal friction	38°
Properties of pore fluid		
Symbol		Value
μ_f	dynamic viscosity	1×10^{-3} Pa · s
C_f	fluid compressibility	3.8×10^{-10} 1/Pa

The mesh utilized for the numerical experiments in order to simulate the conditions of the experiments conducted by Rafatian et al. [63, 64] is presented in Figure 6.5. The mesh consisted of 2,446 quadrilateral elements and 29,985 degrees of freedom. A greater

element density can be observed in the area of the domain where the cutting stress is applied and shearing occurs.
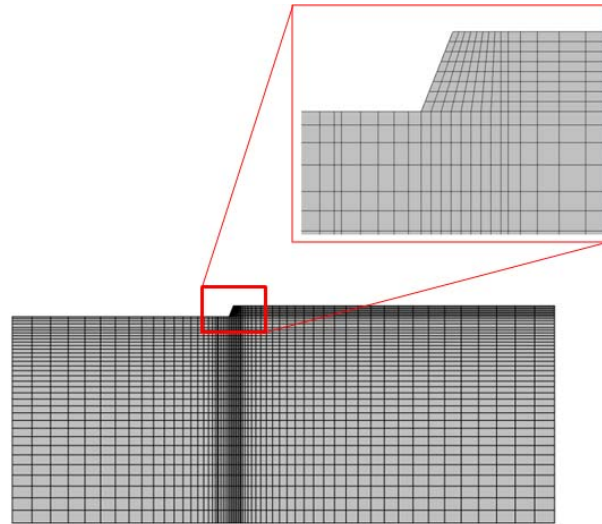
Figure 6.5 Mesh of geometry domain for numerical experiments on Indiana limestone.

A comparison of MSE_{BR} determined from the poroelastic model with the MSE_{BR} estimated experimentally by Rafatian et al. [63, 64] is presented in Figure 6.6, as a function of confining pressure. A pore pressure equal to the confining pressure was considered for each experiment, according to Rafatian's experimental setup. It can be observed from the figure that MSE_{BR} determined from the poroelastic model under-predicts the MSE_{BR} estimated by Rafatian et al. [63, 64] as the confining pressure increases. Rafatian et al. [63, 64] found that the actual value of MSE (termed MSE_{actual} in the plot) required to fracture the rock was significantly higher than the estimated confined compressive stress (MSE_{BR}). As mentioned by Rafatian et al. [63, 64] and others [65, 66], it seems that the energy spent in the plastic deformation of the crushed rock in front of the cutter is much more significant than the elastic energy of failing the virgin rock, even under ideal laboratory conditions.
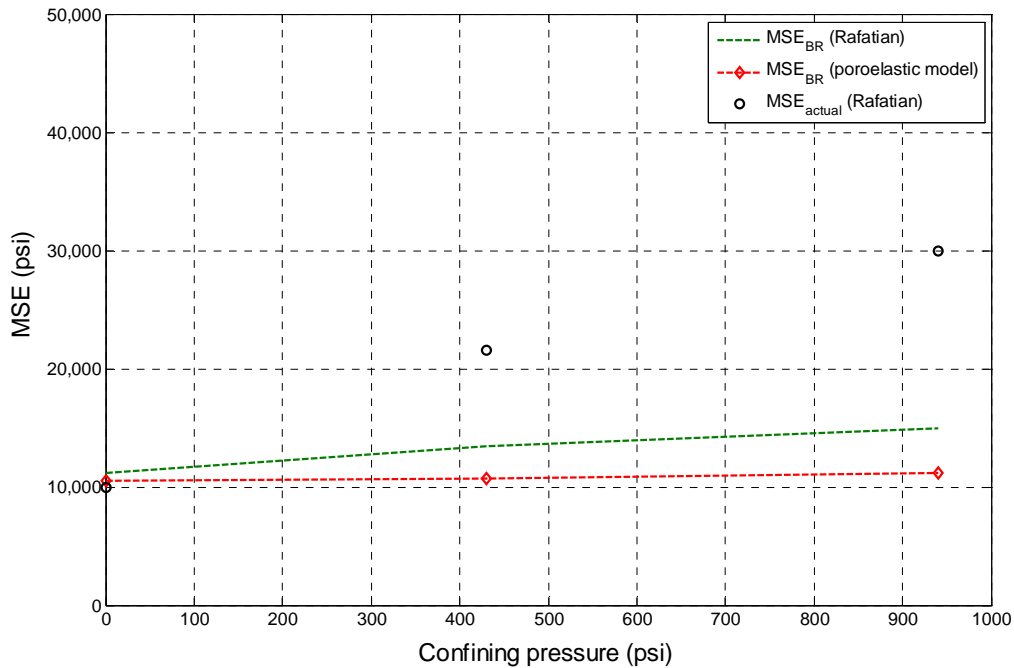
Figure 6.6 Comparison of the MSE_{BR} determined from poroelastic model with the MSE_{BR} and MSE_{actual} determined experimentally by Rafatian et al. [63, 64], as a function of confining pressure.

Unfortunately, the poroelastic model proposed in this dissertation models neither the plastic deformation of rock nor the crushed rock in front of the cutter. This might explain why the poroelastic model correctly predicts the MSE_{BR} at atmospheric conditions (unconfined compressive stress) where the crushed rock is immediately removed from the face of the cutter. Furthermore, it can be seen from Figure 6.6, that the MSE_{BR} determined from the poroelastic model does increase as the confining pressure increases, but with a smaller slope than the experimental trend of MSE_{BR} determined experimentally. The increase in the MSE_{BR} determined from the poroelastic model as the confining pressure increases it due solely to the additional elastic energy required to break the rock as the confining pressure increases.

A plot of the ratio of the MSE_{BR} determined from the poroelasticity model to the confined compressive strength (CCS) of Indiana limestone estimated experimentally by Rafatian et al. [63, 64] is presented in Figure 6.7, as a function of confining pressure. Similar to previous plots, a value of one indicates perfect agreement.
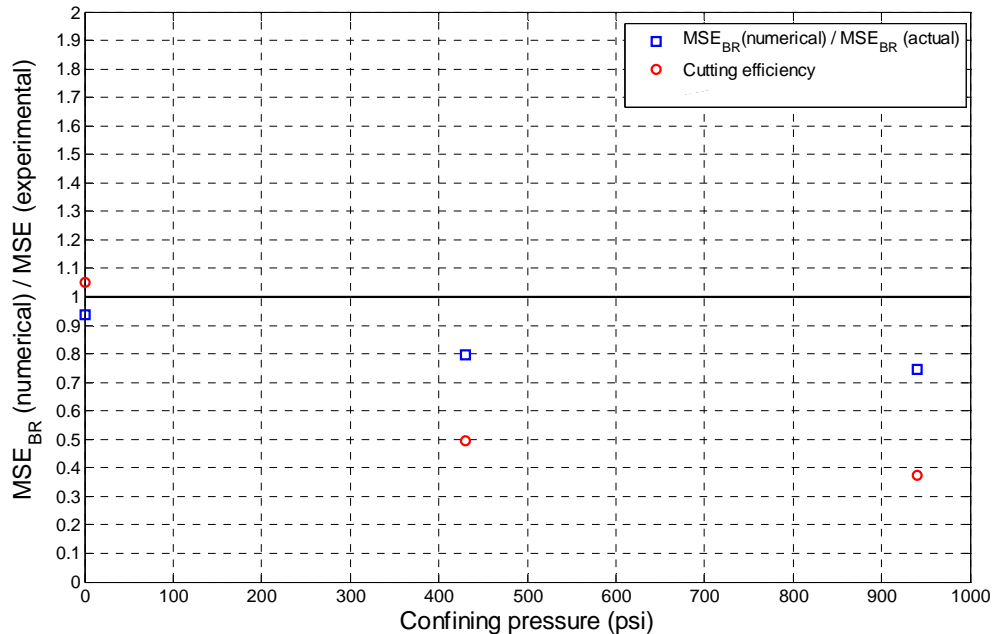
Figure 6.7 Ratio of the MSE_{BR} determined from poroelastic model to the MSE_{BR} and MSE_{actual} determined experimentally by Rafatian et al. [63, 64], as a function confining pressure.

It can be seen that the poroelasticity model correctly predicts the UCS strength of the rock within ~6%, but as the confining pressure increases the under-prediction of the CCS with the poroelasticity model increases up to ~25% at 950 psi. The ratio of the MSE_{BR} determined theoretically from the poroelasticity model to the actual value of MSE determine experimentally is also presented in Figure 6.7. This ratio corresponds to the efficiency of the cutting process as defined by Equation (5.4), where the variable $MSE_{downhole}$ has been substituted with MSE_{actual}. It can be observed that under atmospheric pressures, all the energy applied to the rock contributes to its failure.

However, as the confining pressure increases the efficiency of the cutting process decreases to less than 40% at 950 psi.

In summary, it can be concluded from the comparisons of the numerical experiments using the poroelasticity model against the experimental data gathered by Murrell [51] and Rafatian et al. [63, 64] that the poroelasticity model seems to correctly predict the theoretical value of MSE_{BR} required to break a rock subjected to external confining pressures under ideal conditions. However, the energy applied to break the rock in an actual drilling situation is usually significantly greater than the theoretical MSE_{BR}, since much more energy is required to plastically deform the crushed rock and to overcome friction at the rock-cutter interface. Further work is recommended to modify the model proposed in this dissertation in such a way that it can account for these factors.

Even though the poroelastic model can only predict the theoretical value of MSE_{BR} due to the elastic deformation, it can still be used to determine the parameters that have a significant effect in the cutting process. The identification of the significant parameters in the cutting process is described in the next section.

6.2 Identification of significant parameters in the rock cutting process

In order to determine whether or not it is possible to predict pore pressure during drilling from drilling parameters, environmental parameters, and material properties, it is important to determine the extent to which each parameter affects the drilling process. Moreover, if a parameter such as MSE (which groups drilling parameters) is to be used for the prediction of pore pressure (as proposed in Chapters III and IV), it is important to determine what other parameters, besides pore pressure, affect the value of MSE and to what extent. In order to identify the parameters that play a significant role in the cutting process, a sensitivity analysis of the model described in Section 5.3 has been conducted.

A sensitivity analysis consists in determining the variation in the *response* (output) of a model due to the variation of the input parameters of that model. There are several procedures to conduct a sensitivity analysis. A sensitivity analysis based on the analysis of variance (ANOVA) has been conducted in this dissertation, which is used to determine the extent of the effect of each input parameter on the response of the model by the use of statistical methods. In order to collect data that can be analyzed by statistical methods, a statistical design of experiments (DOE) needs to be planned.

One strategy of experimentations used when several input parameter affect the response is to select a baseline value for all input parameters and then successively vary each parameter (termed *factor*) over a range with the other factors held constant at the baseline. However, any possible *interaction* between factors will not be considered if this approached is followed. An interaction between factors is defined as the failure of one factor to produce the same effect on the response at different *levels* of another factor [67]. Thus, a preferred approach is to conduct a *factorial experiment* in which all factors are varied together instead of one at a time. Details on the concept of factorial experiments can be found in [67]. For these reasons, a factorial design of experiments was developed to determine the number of numerical experiments, and conditions of each experiment, that need to be conducted for the sensitivity analysis of the poroelastic model.

The first step is to identify all the factors (input parameters) that are accounted for in the model, as well as the desired response (output). A list of all the input parameters considered in the poroelastic model is presented in Table 6.3. The parameters are categorized in geometric parameters, material properties, environmental parameters, and drilling parameters. The response of the poroelastic model is the MSE_{BR}.

Table 6.3 List of input parameters for the poroelastic model.

Properties of solid matrix		Properties of pore fluid	
Symbol	Property	Symbol	Property
E	Young's modulus	μ_f	dynamic viscosity
ν	Poisson's ratio	C_f	fluid compressibility
ρ_s	density of matrix	Geometric parameters	
ϕ_s	porosity	θ	back rake angle (Figure 5.2)
k	permeability	d_{cut}	depth of cut (Figure 5.2)
α	Biot-Willis coefficient	Environmental parameters	
S_0	cohesion	P_h	confining pressure (hydrostatic pressure of drilling fluid)
ϕ	angle of internal friction	P_p	pore pressure
		Drilling parameters	
		$\dot{S}_c$	rate of stress application

It can be observed from Table 6.3 that fifteen input parameters (factors) are considered in the poroelastic model. If a full factorial design of experiments were conducted considering only two levels for each of the factors in Table 6.3, a total of 32,768 numerical experiments would have to be conducted. However, it is recognized that the majority of the factors are material properties which normally do not vary independently. For example, different types of rock are characterized with an specific set of properties, but some of these properties (such as the density of rock, Poisson ratio and Young's modulus) may not vary significantly from one type of rock to another, and others (such as Biot-Willis coefficient, permeability, and porosity; and cohesion and angle of internal friction) are dependent on each other. Similarly, pore fluid in rock is commonly either brine or gas, which can be described by a specific set of properties. Therefore, in order to reduce the number of numerical experiments that need to be conducted, the material

properties were grouped in two main factors: type of rock, and type of fluid. This reduces the number of factors from fourteen to seven factors. Two levels were considered in this design of experiments for each of the seven factors, which resulted in a matrix of 128 numerical experiments that needed to be conducted. The two levels of each parameter were chosen from typical values encountered in rock drilling. The seven factors considered in the design of experiments along with the two levels considered for each factor is presented in Table 6.4.

Table 6.4 List of factors considered for the design of experiments.

Symbol	Factor	Low level	High level
	Type of rock $E = 4 \times 10^6$ psi $v = 0.2$ $\rho_s = 2.3 \frac{g}{cm^3}$	Shale $\alpha = 1$ $k = 1$ nD $\phi_s = 0.05$ $S_0 = 950$ psi $\phi = 45.2°$ at $0 \le \sigma_n' < 2800$ [psi] $S_0 = 2324$ psi $\phi = 27.3°$ at $2800 \le \sigma_n' < 5600$ [psi] $S_0 = 3748$ psi $\phi = 14.45°$ at $5600 \le \sigma_n' < 10700$ [psi]	Sandstone $\alpha = 0.8$ $k = 50$ mD $\phi_s = 0.2$ $S_0 = 1990$ psi $\phi = 45.5°$ at $0 \le \sigma_n' < 4000$ [psi] $S_0 = 3600$ psi $\phi = 37°$ at $4000 \le \sigma_n' < 17000$ [psi] $S_0 = 5177$ psi $\phi = 31°$ at $17000 \le \sigma_n' < 25000$ [psi]
	Type of fluid	Gas $\mu_f = 2 \times 10^{-5}$ Pa·s $C_f = 1 \times 10^{-8} \frac{1}{Pa}$	Liquid $\mu_f = 1 \times 10^{-3}$ Pa·s $C_f = 4 \times 10^{-10} \frac{1}{Pa}$
θ	back rake angle	0°	40°
d_{cut}	depth of cut	0.05 inches	0.2 inches
Pp	pore pressure	500 psi	5,000 psi
P_h	confining pressure	$P_h = P_p$	$P_h = 1.3 \times P_p$
$\dot{S}_c$	rate of stress application	$1,000 \frac{psi}{s}$	$100,000 \frac{psi}{s}$
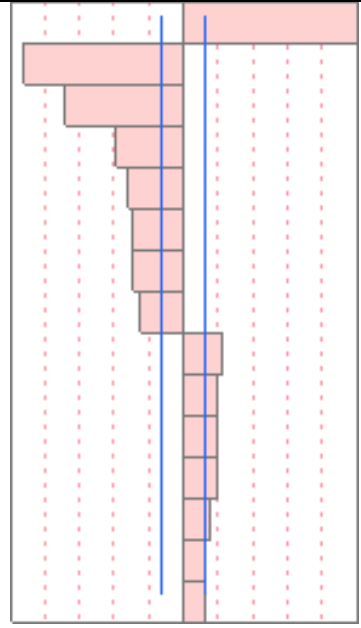
The MSE_{BR} was determined from the poroelastic model (developed in COMSOL Multiphysics) using the procedure described in Section 6.1.2, for each of the 128 combinations of the seven two-level factors in Table 6.4. The results of MSE_{BR} determined from the poroelastic model where analyzed statistically using the commercial software JMP 8. An analysis of variance (ANOVA) was performed in order to determine what input factors (and their interactions) have a significant effect on the MSE_{BR}. The analysis conducted considers only the main effect of each factor and the effect of second-order interactions between factors (that is, the effect of varying any combination of two factors at the same time on the response). A stepwise model was used to determine the significant factors and second-order interactions, and remove the non-significant interaction terms. Once these significant parameters were determined, a standard least square method was used to develop a regression model for predicting the MSE_{BR} with the significant terms (main factors and second-order interactions). The regression model for prediction the MSE_{BR} had the form

$$M\hat{S}E_{BR} = \hat{\beta}_0 + \hat{\beta}_1 x_1 + \hat{\beta}_2 x_2 + \cdots + \hat{\beta}_{12} x_1 x_2 + \hat{\beta}_{13} x_1 x_3 + \cdots \epsilon \qquad (6.1)$$

where $M\hat{S}E_{BR}$ is the estimated value of MSE_{BR} from the regression model; $\hat{\beta}_0, \hat{\beta}_1, \hat{\beta}_2, \ldots, \hat{\beta}_{12}, \hat{\beta}_{23}, \ldots,$ are the coefficient estimates of the regression model; $x_1, x_2, \ldots,$ are the main factors of the model; $x_{12}, x_{13}, x_{23}, \ldots,$ are the second-order interactions between factors, and ϵ is a random error. Once the coefficient estimates were determined, a series of statistic tests (F-ratio and t-ratio) were performed in order to test the effect of each factor and second-order interaction on the response (MSE_{BR}). Details of the procedure for this type of analysis can be found elsewhere [67, 68].

It was determined from this analysis that fifteen terms (including main effects and second-order interactions) play a significant role in the determination of MSE_{BR} using the poroelasticity model. A list of these parameters is presented in Table 6.5.

Table 6.5 Significant parameters of the poroelastic model.

Term	Estimate	Std Error	t-ratio	t-ratio	Prob>|t|
P_p	2021.52	129.32	15.63		<0.0001
$Rock$	-1874.65	129.32	-14.50		<0.0001
θ	-1395.35	129.32	-10.79		<0.0001
$\theta * P_p$	-777.77	129.32	-6.01		<0.0001
$Fluid * d_{cut}$	-637.30	129.32	-4.93		<0.0001
d_{cut}	-591.60	129.32	-4.57		<0.0001
$Rock * d_{cut}$	-591.60	129.32	-4.57		<0.0001
$d_{cut} * \dot{S}_c$	-515.43	129.32	-3.99		<0.0001
P_h	457.77	129.32	3.54		0.001
$\dot{S}_c$	387.30	129.32	2.99		0.003
$Rock * \dot{S}_c$	387.30	129.32	2.99		0.003
$P_p * P_h$	386.29	129.32	2.99		0.003
$Fluid * \dot{S}_c$	324.41	129.32	2.51		0.014
$Fluid$	262.30	129.32	2.03		0.045
$Rock * Fluid$	262.30	129.32	2.03		0.045

The first column in Table 6.5 corresponds to each term in the regression model (either a factor or an interaction between two factors), Equation (6.1). The coefficient estimates of each term of the regression model are presented in the second column, along with the standard error in the third column. The standard error is calculated as the square root of the mean square error divided by the number of experiments conducted $\left(\sqrt{\frac{\bar{e}^2}{2^k}} \right)$. The **t-**statistic is presented in the fourth column and is equal to the ratio of the coefficient estimate to the standard error. The greater the t-ratio is, the more significant the term is on the response. A very low value of the t-ratio could indicate that the value of the coefficient is zero. The chart to the right of the t-ratio values is a plot of the t-ratios for each term. It can be observed that the terms have been sorted by the absolute value of the t-ratio, showing the most significant effect at the top. Finally, the last column in Table 6.5 presents the probability (in absolute value) of getting an even greater t-ratio. Probabilities less than 0.05 are often considered as significant evidence that the

coefficient estimate is not zero; and therefore, that term significantly contributes to the value of the response. The two lines in blue in the t-ratio chart correspond to the ± 0.05 significance level of the probability of the t-statistic.

It can be observed from Table 6.5 that out of the fifteen terms that play a significant role in the poroelastic model, the pore pressure, the type of rock, and the back rake angle of the cutter are the three factors that have the greatest effect on the MSE_{BR}. Another important point to remark is that all seven factors considered in the analysis and shown in Table 6.4 play a significant role in the determination of the MSE_{BR} with the poroelastic model. Fortunately, pore pressure is among the parameters that have the greater effect on the MSE_{BR}, which could be helpful in developing a method to determine pore pressure from these parameters. Figure 6.8 present a series of charts with all the possible second-order interaction between the factors considered in this analysis. The charts of the significant interactions (which are included in Table 6.5) are presented with a grey background for easy identification. Each chart presented in Figure 6.8 has two curves. Each curve is a plot of the MSE_{BR} as a function of the corresponding factor at the bottom of the figure, for one of the two levels of the corresponding factor to the far right of the figure. The scale of MSE_{BR} is shown on the left side of the figure.

Several important observations can be made from Figure 6.8. First, it can be observed that all the plots presented with a colored background (in grey) have trends of MSE for each level that are not parallel to each other. This behavior confirms the interaction between the two factors. Moreover, any other interaction charts (shown on a white background) have trends of MSE for each level that are parallel to each other. Another observation is the fact that the pore pressure and the confining pressure are presented as a nested parameter. That is, the confining pressure in a drilling situation depends on the expected value of the formation pore pressure, and it is usually kept above the pore pressure as a margin of safety.
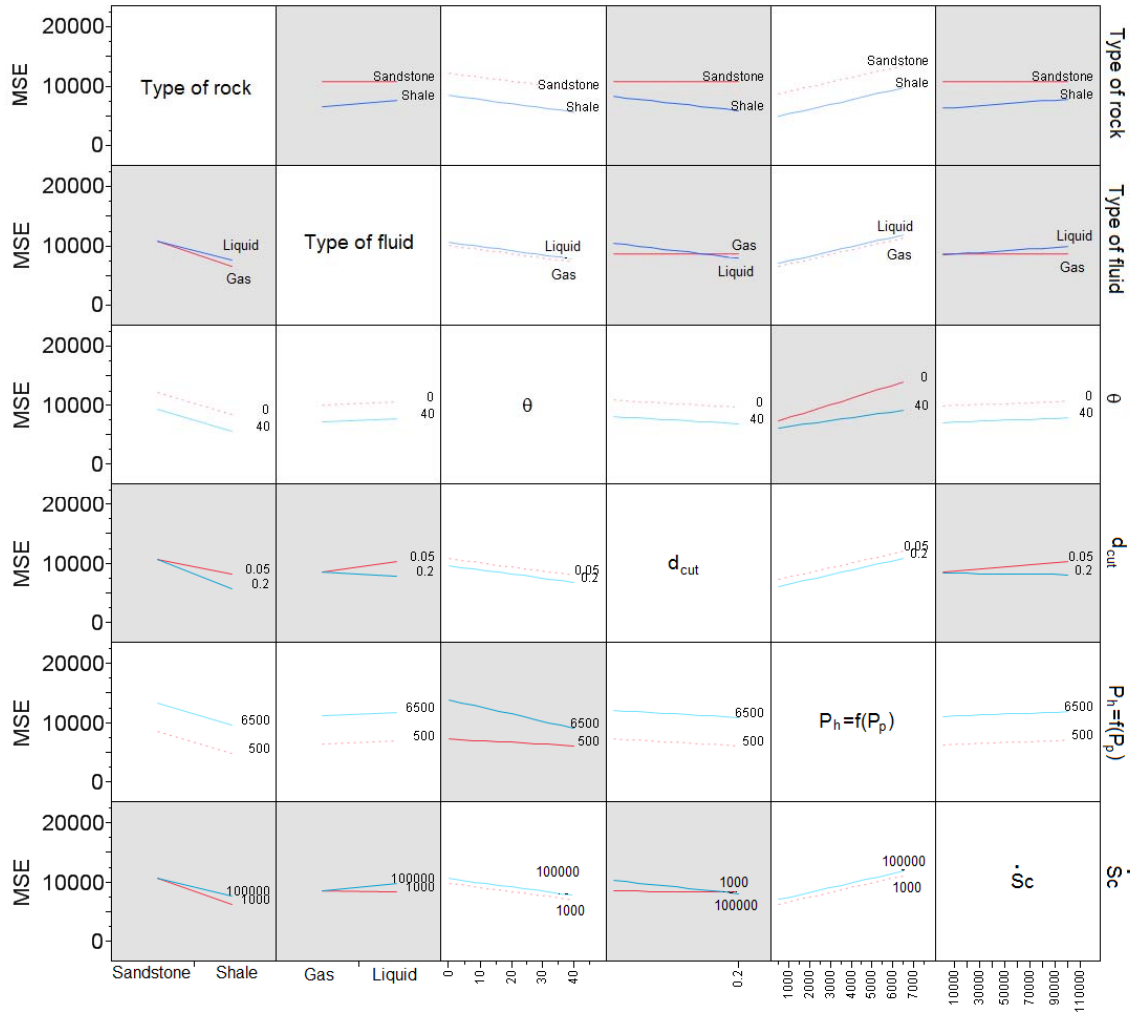
Figure 6.8 Effects of second-order interactions between the factors considered in the poroelastic model on the MSE_{BR}.

This poses a problem for analysis, since the effect of increasing pore pressure and confining pressure results in an increase of the MSE_{BR}. However, the increase of MSE_{BR} is most likely due to the differential pressure (confining minus pore pressure), as has been determined before for rocks with high permeability [33]. It can be also observed that any variations of the type of fluid, the depth of cut, and the rate of cutting stress result in a negligible effect on the MSE_{BR} when a typical sandstone is considered. The greatest effect on the MSE_{BR} when cutting a sandstone is caused indeed by the

differential pressure, even though the bake rake angle of the cutter also affects the energy required to break the rock but to a lower extent than the differential pressure.

This behavior is not observed in the (simulated) cutting of shale. It can be observed from Figure 6.8 that not only the differential pressure and bake rake angle of the cutter, but also the type of fluid, depth of cut, and rate of cutting stress have a noticeable effect on the required MSE_{BR} when a shale is considered. In fact, the different behaviors between typical sandstone and typical shale are the cause of the three significant interactions on the top row in Figure 6.8. It was found from the numerical experiments that the difference in mechanical behavior of the sandstone and shale considered in this analysis is due mainly to the difference in permeability between the two types of rock, which has been discussed before by Detournay and Atkinson [33]. In order to understand the different behaviors of rock due to their different permeability, Figure 6.9 and Figure 6.10 show the distribution of pore pressure at the shearing zone just before failure occurs at two rates of cutting stress, 1,000 psi/s and 100,000 psi, respectively.

Figure 6.9 shows the pressure distribution of rock during cutting (just before failure occurs) at a relatively low cutting rate of 1,000 psi/s for sandstone and shale. Figure 6.9a and Figure 6.9b show the comparison of the pore pressure distribution in sandstone and in shale with virgin pore pressure (initial pore pressure at time zero) of 500 psi, and hydrostatic mud pressure of 650 psi after 5 seconds of cutting stress application. It can be observed in Figure 6.9a that the pore pressure in a sandstone quickly equilibrates and becomes equal to the mud pressure at the shearing zone, and decreases uniformly in the downward direction due to the influence of the far-field pore pressure which is equal to the virgin pore pressure.
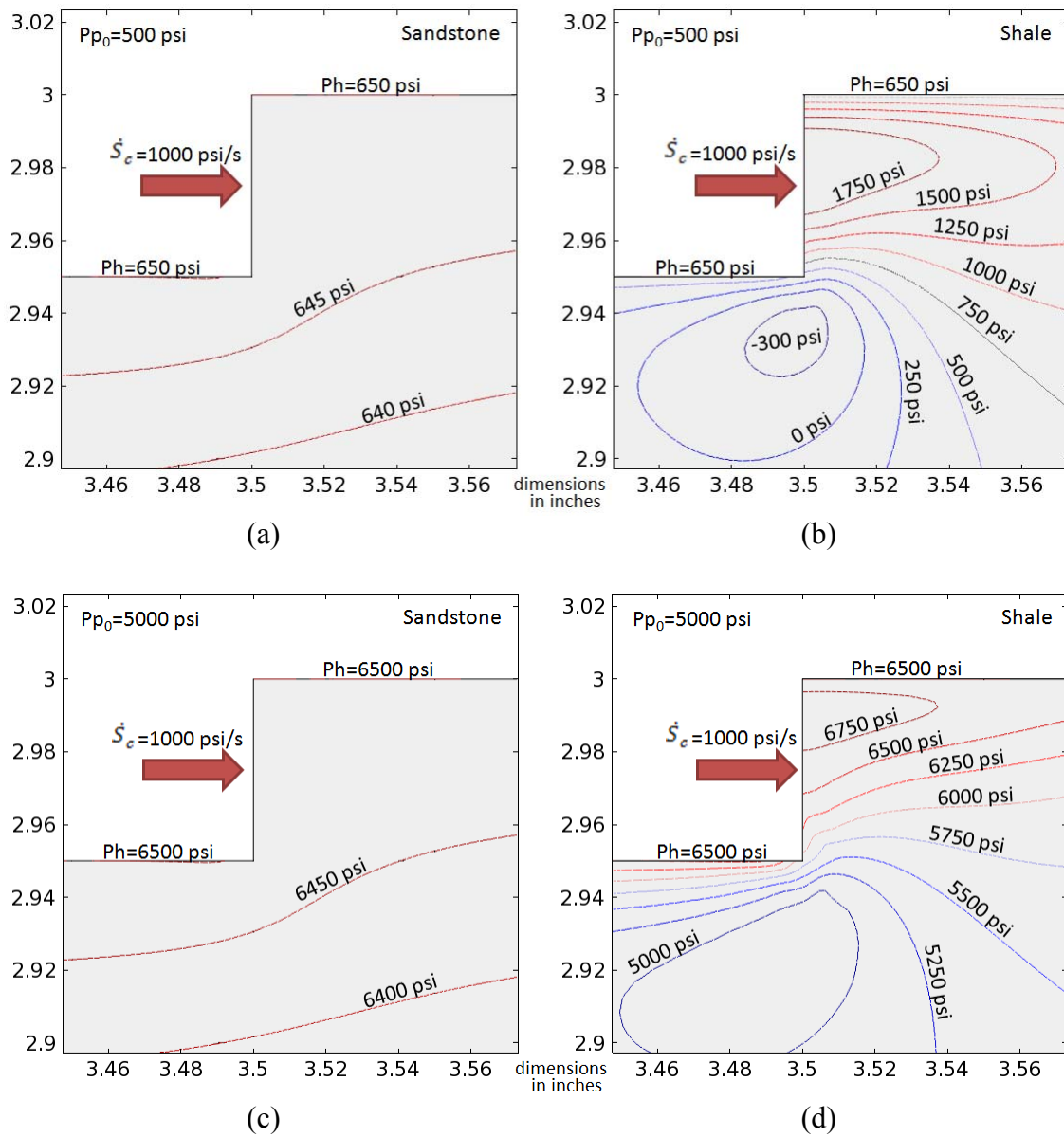
Figure 6.9 Pore pressure distribution during simulated rock cutting at 5 seconds and a cutting rate of 1,000 psi/s, for: (a) sandstone with virgin pore pressure of 500 psi, (b) shale with virgin pore pressure of 500 psi, (c) sandstone with virgin pore pressure of 5,000 psi, and (d) shale with virgin pore pressure of 5,000 psi.

The compression of the rock in sandstone due to the action of the cutter seems to have a negligible effect on the pore pressure distribution, since as the pore volume is reduced at the shearing zone the fluid is expelled from the pores easily due to the high permeability of the sandstone. Furthermore, at regions just below the shearing plane where tension might be expected, the expansion of the pores can rapidly accept fluid from the neighboring shearing zone. A different effect can be observed for the shale shown in Figure 6.9b under the same circumstances. As the cutting stress is applied on shale at a relatively low rate (1,000 psi/s), the pore pressure at the shearing zone increases considerably (nearly three times the value of the mud pressure). Contrary to sandstone, the shale considered in this set of numerical experiments has a very low permeability (1nD), which signifies that there is a poor communication among the pores in the rock. Thus, as the rock is compressed by the action of the cutter, the pores are compressed but the pore fluid cannot escape rapidly, and as a result, the pressure in the pores increases. Another interesting behavior is found just below the shearing zone, where the pore pressure decreases to even negative values. This behavior is consistent with the work of Detournay and Atkinson where they found that cavitation might occur in shale at the shearing zone if the virgin pore pressure is not sufficiently high [33].

Figure 6.9c and Figure 6.9d show a similar comparison as Figure 6.9a and Figure 6.9b, but for a virgin pore pressure of 5,000 psi and a hydrostatic mud pressure of 6,500 psi. A similar behavior is found for both sandstone and shale, respectively, when the pore pressure is increased. However, the zone of low pressure in shale does not reach cavitation when the pore pressure is higher. Nevertheless, the pore pressure below the shearing zone in shale reaches values lower than the virgin pore pressure.

A similar set of contour plots as the one presented in Figure 6.9 is presented in Figure 6.10 for a rate of cutting stress of 100,000 psi/s. It can be observed that increasing the rate of cutting stress from 1,000 to 100,000 psi/s has a negligible effect on the pore pressure distribution in the sandstone. The pore pressure distribution in the sandstone is

determined only by the pressure difference between the mud pressure (at the boundary of the rock) and the virgin pore pressure at the far-field.
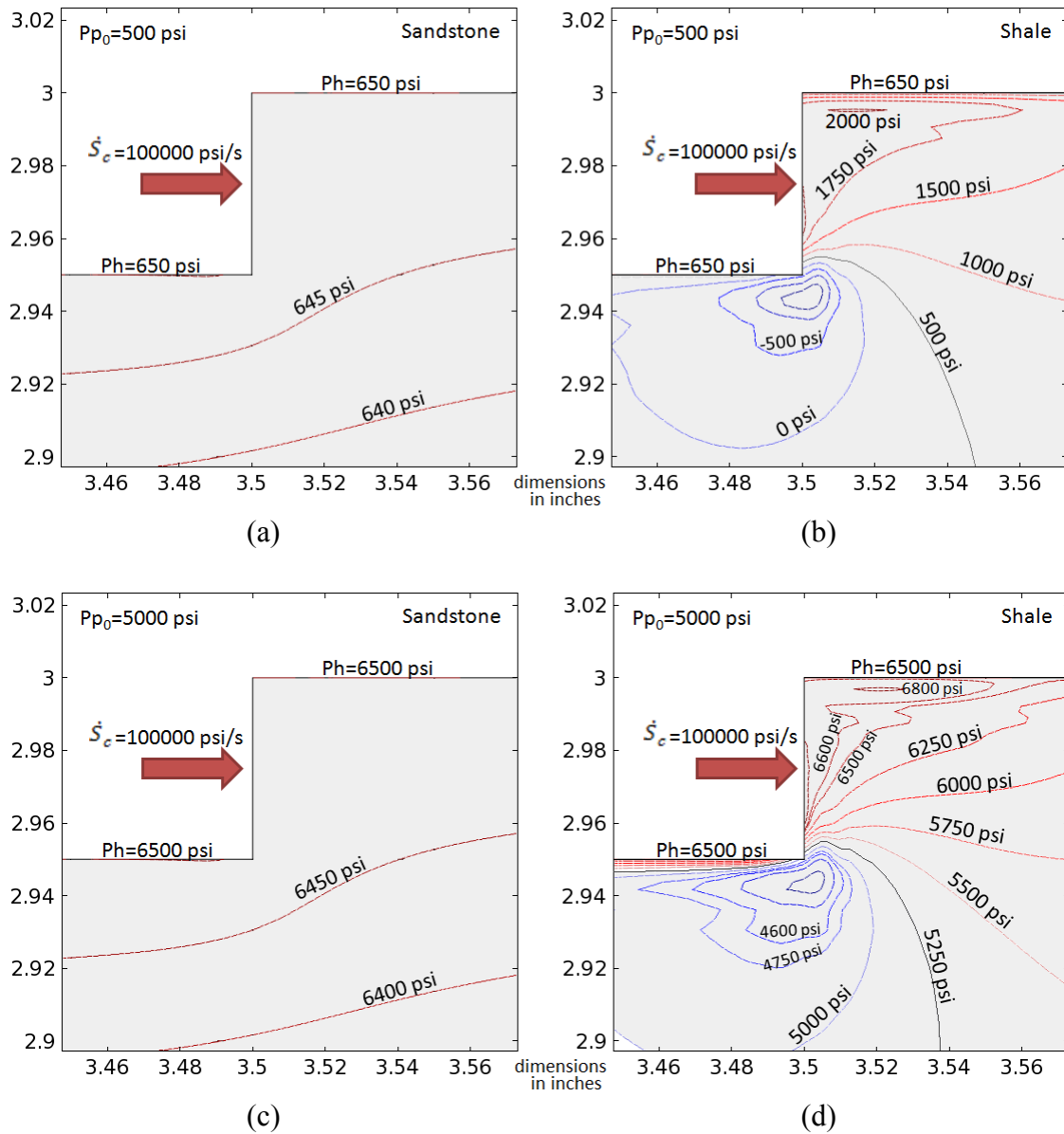

Figure 6.10 Pore pressure distribution during simulated rock cutting at 0.05 seconds and a cutting rate of 100,000 psi/s, for: (a) sandstone with virgin pore pressure of 500 psi, (b) shale with virgin pore pressure of 500 psi, (c) sandstone with virgin pore pressure of 5,000 psi, and (d) shale with virgin pore pressure of 5,000 psi.

Increasing the rate of cutting stress from 1,000 psi/s to 100,000 psi/s does not significantly affect the pore pressure distribution in shale. However, it can be noticed that the pore pressure contours in shale are slightly less uniform when a higher rate of cutting stress is considered. Also, the zone of low pressure occupies a slightly greater surface (in this 2-D view), and has lower values of pore pressure when cutting occurs at 100,000 psi/s.

As mentioned above, the behavior of shale under cutting found in the numerical experiments presented in this dissertation is similar to the behavior described before by Detournay and Atkinson [33]. However, two important distinctions have to be made: (1) the zone of low pressure (or probable cavitation) are found below the shearing zone and not at the shearing zone as stated by Detournay and Atkinson, (2) the different pore pressure distribution in shale does affect the mechanical behavior of rock, but the energy required to break a rock is still a function of the initial value of pore pressure (virgin pore pressure).

The numerical experiments presented in this section to identify the significant parameters that play a role in the cutting process of rock should be considered as the first step of a fundamental understanding of the cutting process of rock. From the results presented in this section, it was found that several parameters play a significant role in the cutting process. Therefore, further work is recommended to investigate the extent of the effect of each significant parameter and its interactions. Fortunately, this investigation shows that the pore pressure is one of the most significant parameters affecting the cutting process, at least in ideal conditions. Further work is also recommended to investigate the amount of energy that is spent in the plastic deformation of crushed rock when the cutting process is conducted under pressure. The knowledge gain from the current and future investigations can evolve into a methodology to predict pore pressure in actual drilling situations. Next section presents the results of verifying the PSP^3 concept with the poroelastic model.

6.3 Use of the poroelastic model to verify the PSP^3 concept

The poroelastic model proposed in Section 5.3 was used to verify if the PSP^3 concept comply with the basic principles of poroelasticity. Specifically, the results of the numerical experiments presented in Section 6.2 were used to verify the PSP^3 concept. In the experiments presented in Section 6.2, a value of virgin pore pressure is assumed as the initial value of pore pressure, and the MSE_{BR} is determined with the poroelastic model for the different combinations of the factors in Table 6.4. Therefore, the PSP^3 concept can be verified with the poroelastic model if the virgin pore pressure is determined with Equation (3.23) (using the MSE_{BR} determined from the poroelastic model) and compared with the original value of pore pressure that was assumed in the poroelastic model. It is important to note that the cutting stress assumed in the numerical experiments was applied only in the horizontal direction. Thus, the cutting stress defined with Equation (3.16) is equivalent to the MSE defined with Equation (3.17) under these circumstances.

Results of the verification of the PSP^3 concept with the poroelastic model are presented in the following three plots. The results are presented as the ratio of pore pressured determined from the PSP^3 concept, Equation (3.23), to the virgin pore pressure assumed in the numerical experiments, as a function of confining (mud) pressure. As mentioned before, a ratio equal to one signifies an excellent agreement between the PSP^3 concept and the poroelastic model. The results of the verification of the PSP^3 concept with the poroelastic model for sandstone with the properties described in Table 6.4 (with either gas or liquid as the pore fluid) are presented in Figure 6.11.

Figure 6.11 Ratio of pore pressure determined from the PSP^3 concept to the virgin pore pressure of the poroelastic model as a function of confining pressure, for the sandstone described in Table 6.4 with either gas or liquid as the pore fluid.

It can be observed from Figure 6.11 that the pore pressure determined with PSP^3 concept is in agreement with the virgin pore pressure assumed in the poroelastic model within 25%, for a back rake angle of the cutter of 0°. If the back rake angle of the cutter increases to 40°, the pore pressure from the PSP^3 concept over predicts up to 90% the virgin pore pressure of the poroelastic model at confining pressures of 500 psi. At this point is important to recall that the PSP^3 concept has been developed under the assumption that the back rake angle of the cutter is 0°. Therefore, it is not surprising (although not expected) that the increasing the back rake angle to 40° results in a worse prediction of the pore pressure. However, it is interesting to see that the effect of a large back rake angle is diminished as the confining pressure increases. On the other hand, it is important to point out that a total of thirty two data points are actually plotted in Figure 6.11, even though only eight data points can be observed. That is, each data point seen in the figure actually corresponds to four data points. The data points are collapsed into a

single data point since factors such as depth of cut, and rate of cutting stress have a negligible effect on the MSE_{BR} determined from the poroelastic model. Furthermore, results shown Figure 6.11 are identical regardless of the type of pore fluid considered (either the gas or the liquid described in Table 6.4). This behavior was only found in sandstone. Results of the verification of the PSP[3] concept with the poroelastic model for shale with the properties described in Table 6.4 and gas as the pore fluid are presented in Figure 6.12.
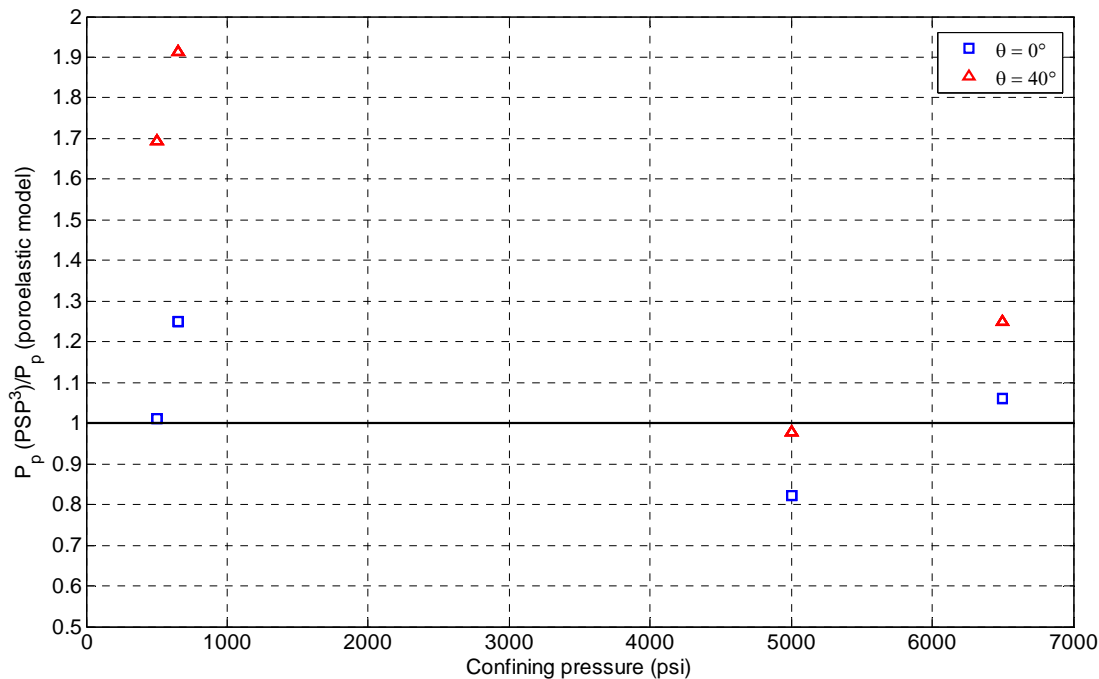

Figure 6.12 Ratio of pore pressure determined from the PSP[3] concept to the virgin pore pressure of the poroelastic model as a function of confining pressure, for the shale described in Table 6.4 with gas as the pore fluid.

It can be observed from Figure 6.12 that, similar to the case of sandstone, the pore pressure determined with PSP[3] concept is in agreement with the virgin pore pressure assumed in the poroelastic model within 25%, for a back rake angle of the cutter of 0°. The PSP[3] concept over predicts the virgin pore pressure of the poroelastic model up to

65% at confining pressures of 500 psi, if the back rake angle of the cutter increases to 40°. However, the prediction of pore pressure from the PSP^3, when back rake angles of 40° are considered, improves at larger values of confining pressure (a maximum over-prediction of 20% of the virgin pore pressure at 6,500 psi of confining pressure).

It can be observed from Figure 6.12 that, contrary to the case of sandstone, depth of cut and rate of cutting stress have an effect on the MSE_{BR} determined from the poroelastic model which results in the spread of data points at the same conditions of back rake angle and confining pressure. That is, different values of the ratio $\left(\dfrac{P_{p(PSP3)}}{P_{p(poroelastic)}}\right)$ are found if the depth of cut and rate of cutting stress is varied while maintaining the bake rake angle and confining pressure constant. Variation of the ratio of pore pressure prediction due to changes in depth of cut and rate of cutting stress show that the prediction of pore pressure from the PSP^3 concept can vary up to 15%, at low confining pressures, due to these two factors. This implies that the PSP^3 concept fails to capture all the significant parameters that affect the drilling process (for this type of shale). For example, if the virgin pore pressure is to be determined from the PSP^3 concept for a situation where shale is drilled using cutters with a back rake angle of 0°, differences in depth of cut and angular velocity of the drill bit during drilling (assuming a constant pore pressure) can result in variations of the predicted pore pressure from the PSP^3 concept of up to 15% at low confining pressures (~500 psi). Furthermore, it the effect of the back rake angle is introduced (that is, a cutter with a back rake angle different from 0° is used) the pore pressure prediction from the PSP^3 concept can be up to 65% above the virgin pore pressure of the formation at low confining pressures. This over-prediction of pore pressure from the PSP^3 concept when the back rake angle is not 0° can be lower as the confining pressure increases. These findings are under the assumption that the pore fluid in the shale is a gas. However, the results are similar if a liquid is considered as the pore fluid. Results of the verification of the PSP^3 concept with the poroelastic model for the shale of Table 6.4 with liquid as the pore fluid are presented in Figure 6.13.
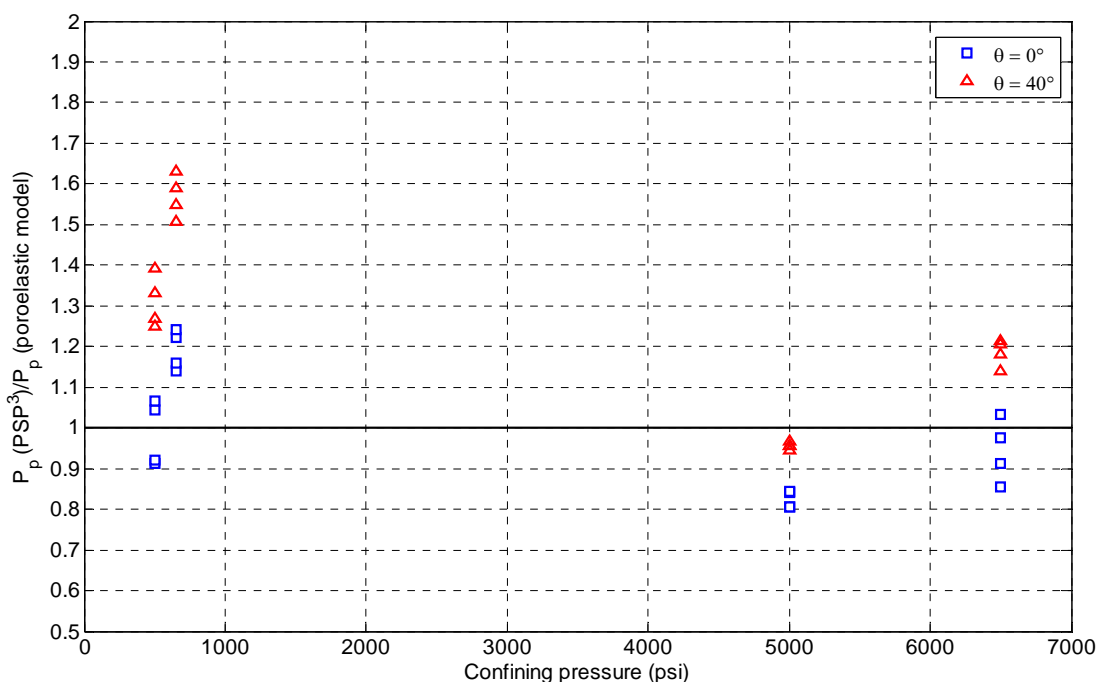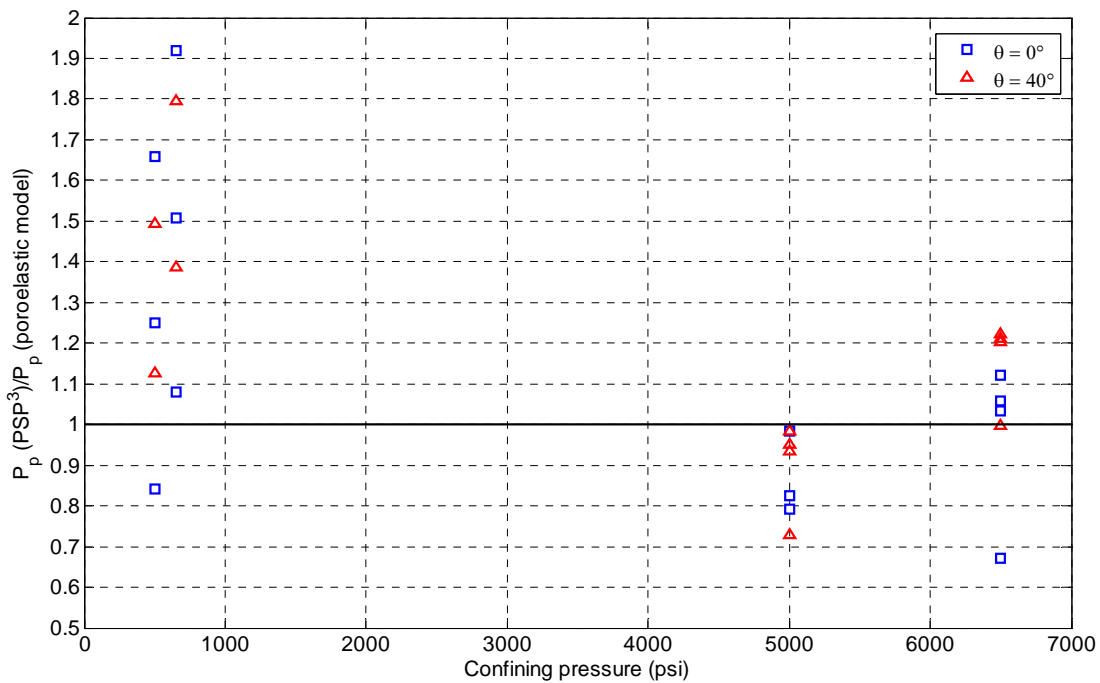
Figure 6.13 Ratio of pore pressure determined from the PSP^3 concept to the virgin pore pressure of the poroelastic model as a function of confining pressure, for the shale described in Table 6.4 with liquid as the pore fluid.

It can be observed from Figure 6.13 that the effects of depth of cut and rate of cutting stress are even more significant when liquid is considered as the pore fluid instead of gas (assuming low permeability shale). At confining pressures of ~500 psi, the pore pressure predicted from the PSP^3 concept can be between -20% to +92% of the virgin pore pressure of the poroelastic model, even for back rack angles of 0°. However, it is interesting to see that as the confining pressure increases the prediction of pore pressure with the PSP^3 concept improves nearly to the same degree as in the case of shale with gas as the pore fluid ($\pm$25% of the virgin pore pressure). This behavior might explain why the pore pressure prediction from the PSP^3 concept shown in Chapter III, Figure 3.17 and Figure 3.18, improves as a function of depth, since the confining pressure increases as a function of depth as well. However, it is clear from the results presented

above that the PSP^3 concept fails to capture the overall physics of the drilling process. Therefore, further work is recommended to redefine the PSP^3 model to include the effects of the type of fluid, back rack angle, and permeability of the rock if it is to be used as a methodology for pore pressure prediction that could be reliable for all types of rocks and situations. Nevertheless, the insights gained from comparing the poroelastic model to the PSP^3 concept are extremely valuable. Insights gained from the poroelastic model to understand whether the concept of using MSE as a fundamental parameter in Eaton's equation complies with basic principles of rock mechanics and fluid mechanics are presented in the next section.

6.4 Insights from the poroelastic modeling on the concept of using MSE in Eaton's equation

One of the improvements made by Eaton [10] to the model proposed by Hottman and Johnson [18] for pore pressure prediction based on resistivity and sonic logs was to include the effect of the overburden on the abnormal pore pressure. Eaton recognized that there are zones where the compaction and abnormal pore pressures are caused by increasing overburden loads [10]. Moreover, Eaton also recognized that the overburden stress is a function of depth in areas such as the Gulf of Mexico. For this reason, the poroelastic model cannot be directly compared to the concept of using MSE as a fundamental parameter in Eaton's equation, since the effect of compaction as a function of depth is not considered in the poroelastic model. However, several observations from the results of the numerical experiments conducted using the poroelastic model can be useful to verify if the concept of using MSE (instead of resistivity or sonic data) in Eaton's equation complies with the basic principles that the poroelasticity theory is based on.

Hottman and Johnson [18] recognized that in regions where a normal pore pressure trend could be found, a normal trend of electrical resistivity could be determined if plotted on a logarithmic scale. Moreover, a deviation of the pore pressure from its normal trend was

accompanied by a deviation of the normal trend of resistivity. Eaton [10] included the effect of overburden and proposed Equation (4.4) to determine the abnormal pore pressure based on the establishment of normal trends of pore pressure and resistivity. The cornerstone of Equation (4.4) is Equation (4.3), which relates the effective stress in an abnormally pressured region to the normal effective stress and the ration of resistivities. However, it is important to note that there is not a linear relation between the effective stress and resistivity. Rearranging Equation (4.3), it can be observed that

$$\log\left(\frac{\sigma'_{abnormal}}{\sigma'_{normal}}\right) = n \cdot \log\left(\frac{R_0}{R_n}\right) \tag{6.2}$$

which implies

$$\log\left(\frac{\sigma'_{abnormal}}{\sigma'_{normal}}\right) \propto \log\left(\frac{R_0}{R_n}\right) \tag{6.3}$$

Equation (6.3) is the basis for the development of Eaton's Equation (4.4). Disadvantages of using resistivity measurements in Equation (4.4) are explained in Chapter IV. Moreover, it is also proposed in Chapter IV that a fundamental parameter such as MSE could be used in Equation (4.4) instead of resistivity. Results from the concept of using MSE instead of resistivity in Eaton's equation indicated that Equation (4.5) could correctly predict the post-drill pore pressure (within ~20% at location of less than 14,000 ft and ~10% at deeper locations) of three oil wells, if a value of one was used in the exponent of the equation. A value of one in Equation (4.5) has an important implication: it implies that the relation between the ratio of effective stresses (abnormal to normal) and the ratio of MSEs (observed to normal) is linear. This is not surprising, since it is generally assumed that the energy required to break the rock is directly proportional to the effective stress of the rock. Moreover, it is generally accepted that the minimum MSE required to break the rock is equal to the confined compressive stress (CCS) of the

rock being drilled [9, 30, 31]. Results from the poroelastic model also confirm this behavior. In order to illustrate this idea, the poroelastic model was used to determine the variation of MSE_{BR} due to a change in pore pressure, assuming all other parameters constant. A baseline value of pore pressure was chosen as the normal pore pressure, and three other simulations were run for increasing values of pore pressure (considered as the abnormal pressures). The effective stress in the vertical direction was assumed as the confining pressure minus the virgin pore pressure (for either the abnormal or normal pressures). The results are presented in Figure 6.14, as the ratio of the MSE required to break the rock in the abnormal situation (when pore pressure is higher than the baseline pressure) to the MSE required in the normal situation (baseline pore pressure), as a function of the ratio of abnormal effective stresses to normal effective stress.
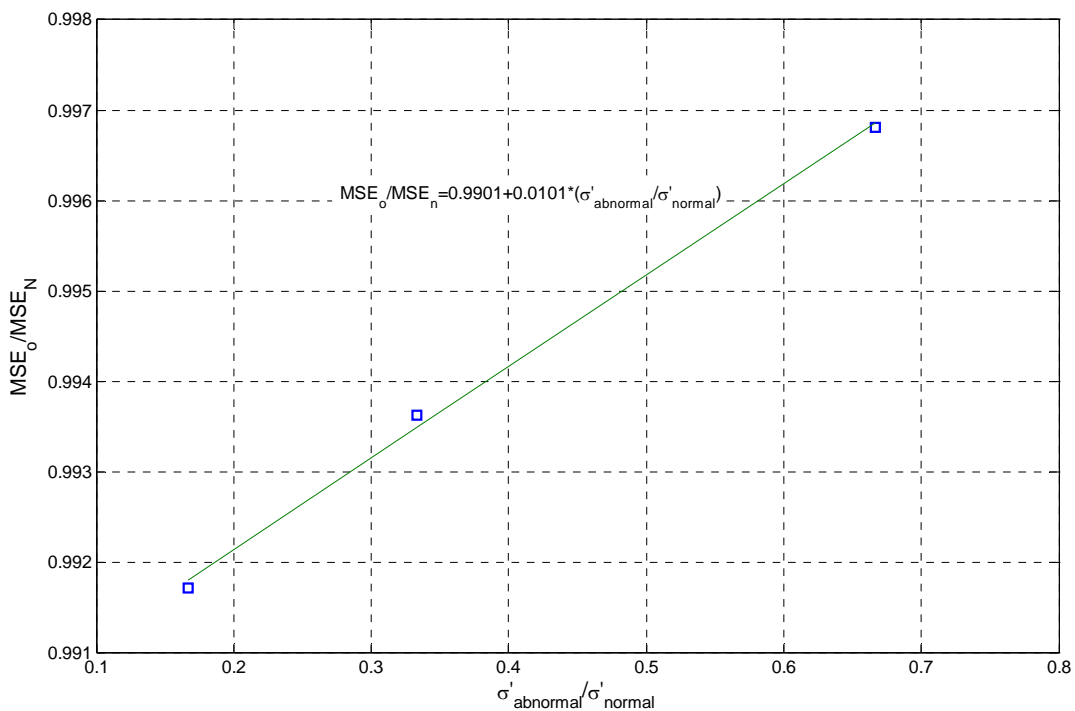
Figure 6.14 Ratio of MSE abnormal to MSE normal determined from the poroelastic model as a function of ratio of abnormal effective stress to normal effective stress.

It can be seen Figure 6.14 that there is a small difference in the MSE_{BR} among the three data points presented; and thus, the ratio $\frac{MSE_o}{MSE_N}$ is close to one. This small variation of MSE_{BR} is due to the fact that the pore pressure was varied in a small range (from 5,000 to 6,250 psi). The hydrostatic mud pressure was considered to be 6,500 psi. Nevertheless, it is important to note that the variation of the ratio of MSEs is a linear function of the ratio of effective stresses. Therefore, it can be hypothesized from the results presented in Chapter IV, and results from the poroelastic model that

$$\left(\frac{MSE_o}{MSE_N}\right) \propto \left(\frac{\sigma'_{abnormal}}{\sigma'_{normal}}\right) \tag{6.4}$$

and from Figure 6.14, rearranging terms

$$\left(\frac{\sigma'_{abnormal}}{\sigma'_{normal}}\right) = a + b\left(\frac{MSE_o}{MSE_N}\right) \tag{6.5}$$

where a and b are the coefficients of the linear function that relates the ratio of effective stresses to the ratio of mechanical specific energies.

It has to be pointed out that physically it is the MSE_{BR} that depends on the effective stress. However, Equation (6.5) has been rearranged because the interest is to determine the effective stress from the MSE in order to predict the pore pressure. Using Equation (6.5), the equation for pore pressure prediction would have a different form than Eaton's Equation (4.4), and Equation (4.5) proposed in Chapter IV. The new equation for pore pressure prediction based on Equation (6.5), and considering the effect of the overburden stress could be expressed as

$$\frac{P_P}{D} = \frac{OB}{D} - \left[\frac{OB}{D} - \left(\frac{P_P}{D}\right)_N\right]\left[a + b\left(\frac{MSE_o}{MSE_N}\right)\right] \tag{6.6}$$

Even though results from Equation (4.5) (presented in Chapter IV) provided an adequate agreement between the predicted pore pressure and the post-drill pore pressure, insights gained from the results of the poroelastic model suggest that Equation (6.6) could described the relation among pore pressure, overburden stress, and mechanical specific energy. However, the proposal of this new equation does not disprove the results presented in Chapter IV, since it can be noticed that if the relation between the ratio of effective stresses and the ratio of mechanical specific energies is one-to-one, Equation (6.6) is equivalent to Equation (4.5) with an exponent value of one.

Unfortunately, the information presented in this dissertation is not enough to prove or disprove the validity of Equations (4.5) and/or (6.6). Further work is recommended to investigate the relationship between the effective stress of the virgin rock and the mechanical specific energy as a function of depth for different lithologies.

In this chapter a fundamental approach to relating pore pressure to drilling parameters, environmental parameters, and material properties has been presented. The use of mechanical specific energy as a fundamental parameter that groups drilling parameters has been emphasized. Moreover, factors affecting the mechanical specific energy that is required during drilling have been identified. On the other hand, a 2-D poroelastic model of drilling process was proposed. Two important findings can be remarked from the results of the poroelastic model: (1) the theoretical amount of energy required to break the rock under pressure, assuming elastic deformation, is much less than the actual amount of energy required to break the rock (determined experimentally) even under ideal situations; (2) there are several factors, and interactions between factors, that significantly affect the amount of energy that is required to break the rock, assuming elastic deformation. If was found that the pore pressure, the type of rock, and the back rake angle of the cutter are the three factors that have the greatest effect on the MSE_{BR}. Importantly, the pore pressure is one of the most significant parameters that affect the

energy required to break the rock, which confirms a relationship between pore pressure and mechanical specific energy.

The results presented in this chapter (and in general in this dissertation) suggest that it can be possible, in principle, to predict pore pressure from drilling parameters, environmental parameters, and material properties. However, it has been also found from this investigation that the cutting of rock is a very complex process in which several factors play a significant role even when a simplified model, such as the poroelastic model, is considered. Further work is required to improve this model so that it accounts for other effects found in actual drilling situations (such as the plastic deformation of rock under pressure, the plastic deformation of the crushed rock, the friction at the cutter-rock interface, and effects of temperature). That is, the poroelastic model described in this chapter should be extended to a thermo-poroplastic model. If a model is developed that can correctly describe the cutting process of actual drilling situations (not only ideal situations), it could be used to establish a quantitative relation among pore pressure, drilling parameters, environmental parameters, and material properties. Moreover, this information could be used to develop a methodology for pore pressure prediction from drilling parameters, environmental parameters, and material properties for all types of rock and situations.

CHAPTER VII
SUMMARY AND CONCLUSIONS

An investigation of whether or not it is possible to predict pore pressure from drilling parameters, environmental parameters, and material properties has been conducted and presented in this dissertation. A functional decomposition allowed for the identification of the functions that need to be satisfied in order to satisfy the objective (see Chapter II). Three approaches were considered as possible means to satisfy the objective of this investigation. A summary of the developments and findings of each approach considered is presented in this chapter. Findings of the PSP^3 concept (first approach considered) are described first. Then, the findings of the concept of using MSE as a fundamental parameter in Eaton's equation (second approach) are presented. Subsequently, findings of the fundamental approach to relating pore pressure to drilling parameters, environmental parameters, and material properties (third approach) are presented. Finally, the conclusion of this investigation is presented.

7.1 Findings of the PSP^3 concept

The Principal Stress Pore Pressure Prediction (PSP^3) concept was developed under the hypothesis that the virgin pore pressure at the drill bit could be determine during drilling by identifying the effective stress (from drilling and environmental parameters) of the rock being drilled, in combination with the Mohr-Coulomb failure criterion (defined by rock properties). An expression was developed, Equation (3.23), that conveniently expresses the pore pressure as a function of the cutting stress (drilling parameters), the hydrostatic mud pressure (environmental parameters), and failure parameters (material properties).

In an effort to validate the PSP^3 concept, Equation (3.23) was used to determine the pore pressure from drilling log data of three oil wells located in the Gulf of Mexico. The pore pressure determined with Equation (3.23) was then compared against a post-drill

analysis of pore pressure of each well, which was considered as the true value of pore pressure for validation purposes. The lithology of one of the three wells (Well 1) was sandstone, whereas the other two wells (Well2, and Well3) were shale. Results for Well 1 indicated that the pore pressure determined with Equation (3.23) predicts the post-drill pore pressure within $\pm20\%$ for deeps shallower than 14,000 ft and within $\pm10\%$ at deeper regions (>14,000 ft). Results for Well 2 and Well 3, indicated that the pore pressured determined with Equation (3.23) over predicts the post-drill pore pressure up to 35% at ~7,000 ft. However, the pore pressure determined with Equation (3.23) improves its prediction as the depth increases, such that below 10,000 ft and deeper the pore pressure from Equation (3.23) is within $\pm10\%$ (or less) the post-drill pore pressure.

Insights from the results of the poroelastic model presented in Chapter VI, showed that there other factors not considered in Equation (3.23), such as the back rake angle of the cutters, the type of rock, and the type of fluid in the rock, that affect the drilling process and in turn the prediction of pore pressure from Equation (3.23). Furthermore, it was found from the results of the poroelastic model that Equation (3.23) tends to over predict the virgin pore pressure of rock with low permeability (for example, shale) at low values of confining pressure, and the prediction of pore pressure with Equation (3.23) improves as the confining pressure increases. These findings were consistent with the results of the attempt for validation of the PSP[3] concept. Unfortunately, this is a clear indication that the PSP[3] concept should not be used in its current form to predict virgin pore pressure at bit during drilling for all types of rocks and situations. Nevertheless, results from the poroelastic model confirm that there exists a relationship among pore pressure, drilling parameters, and material properties, as attempted to be described with the PSP[3] concept.

The second approach considered in this investigation is the concept of using MSE as a fundamental parameter in Eaton's equation. The findings of the second approach considered are presented in the next section.

7.2 Findings of the concept of using MSE in Eaton's equation

The concept of using mechanical specific energy (instead of electrical resistivity or sonic data) as a fundamental parameter in Eaton's equation has been proposed and described in Chapter IV. Pursuing reasoning similar to that of Eaton, it was recognized that MSE could be used to track any changes in the effective stress of the rock, since the MSE should be (at least in principle) a function of the effective stress. Then, the pore pressure could be determined from the effective stress concept. Following this reasoning, Equation (4.5) was proposed to determine the virgin pore pressure in abnormally pressured zones from the overburden stress and the MSE.

Equation (4.5) was used with the drilling log data of Well 1, Well 2, and Well 3 to determine the virgin pore pressure and compare it to the post-drill pore pressure of each well. Surprisingly, the pore pressure profile determine with Equation (4.5) for Well 1 was almost identical to the pore pressure profile determine with Equation (3.23) for the same well. That is, the pore pressure determined with Equation (4.5) predicts the post-drill pore pressure within $\pm 20\%$ for deeps shallower than 14,000 ft and within $\pm 10\%$ at deeper regions ($>14,000$ ft). However, it was found that the virgin pore pressure for Well 2 and Well 3 determined with Equation (4.5) is in closer agreement to the post-drill analysis ($\pm 10\%$) than the pore pressured profile determined with Equation (3.23) at each depth.

Interestingly, a value of one for the exponent in Equation (4.5) was found to be the best fit between the post-drill analysis and the predicted pore pressure for the three wells considered. This finding suggests that there is a linear relation between the effective stress and the MSE. Results from the poroelastic model confirmed this hypothesis. However, the relation between the ratio of effective stresses $\frac{\sigma'_{abnormal}}{\sigma'_{normal}}$ (effective stress of the abnormally pressured zone to the effective stress of the normally pressured zone) and the ratio $\frac{MSE_O}{MSE_N}$ (the MSE at the abnormally pressured zone to the MSE at the normally

pressured zone) might not necessarily be one to one. Thus, a new expression for pore pressure prediction is proposed in Equation (6.6). Even though it seems to be clear that a relationship of the form of Equation (6.4) exists, further work is required to determine if Equation (6.5) is correct. Moreover, further work is required to determine the coefficients of Equation (6.5), provided it is correct, for different lithologies and situations.

7.3 Findings of fundamental approach to relating pore pressure to drilling parameters, environmental parameters, and material properties

A fundamental approach to relating pore pressure to drilling parameters, environmental parameters, and material properties from basic principles has been proposed and presented in Chapters V and VI. First, a new way of viewing MSE has been proposed in which different factors that affect the energy required to break the rock are identified. This information helped recognizing the complexity of the cutting process of rock and the interactions that occur between the pore fluids and the solid matrix of the rock during cutting. Thus, it was proposed that the cutting process could be described, as a first step, with Biot's poroelasticity theory which describes the coupled hydro-mechanical behavior of rock. A simplified two-dimensional model of the cutting process using poroelasticity theory was then proposed.

The poroelastic model was validated with data from Murrell [51], and Rafatian et al. [63, 64]. Results from the validation with data from Murrell [51] showed that the poroelastic model could predict the load required to break the rock in closer agreement ($\pm 10\%$) with the load determined experimentally in a tri-axial test. However, comparisons of the results from the poroelastic model to experiments conducted by Rafatian et al. [63, 64] indicated that the MSE_{BR} determined from the poroelastic model is even lower than the confined compressive strength determined by Rafatian et al. [63, 64]. In other words, it seems that the poroelastic model correctly predicts the MSE_{BR} at unconfined conditions (within $\pm 5\%$), but fails to predict the MSE_{BR} as the confining pressure increases. These

findings suggest that a more complex mechanism occurs when cutting a rock under pressure; and thus, it is not capture with the poroelastic model. Furthermore, it was found from other investigations [63-66] that the energy spent (when cutting under confining pressures) in the plastic deformation of the rock in front of the cutter is much more significant than the elastic energy of failing the virgin rock, even under ideal laboratory conditions. Further work is required to investigate the effect of plastic deformation of the rock under these conditions in order to improve the poroelastic model. From these findings, it was assumed that the poroelastic model could be useful in predicting the theoretical value of MSE_{BR} under ideal conditions where the crushed rock is immediately clean out from the face of the cutter.

A sensitivity analysis (using an analysis of variance) was then conducted on the poroelastic model to determine the significant factors that affect the cutting process. It was found from the sensitivity analysis that the seven factors considered in the analysis (and seven out of fifteen interactions between factors) play a statistically significant role on the determination of MSE_{BR}. It was also found that the factors with the greatest influence on the MSE_{BR} are the pore pressure, the type of rock, and the back rake angle of the cutter. Furthermore, results indicated that the type of rock is a significant factor in the determination of MSE_{BR} not only because of the mechanical strength of the rock (defined by the Mohr-Coulomb failure parameters) but also because of the permeability and porosity of the rock. It was found that the rate of cutting stress, depth of cut, and type of fluid have a negligible influence on the MSE_{BR} when a rock of high permeability (such as sandstone) is cut. However, each one of these factors (the rate of cutting stress, depth of cut, and type of fluid) and its interactions become important when a rock of low permeability (and low porosity), such as shale, is cut.

Results also showed that cavitation might occur below the shearing zone if a low permeability rock is cut under low pore and confining pressures. Even if cavitation does not occur, a zone of pore pressure lower than the virgin pore pressure is developed

during cutting just below the shearing zone. Increasing the rate of cutting stress seems to move this zone of low pore pressure upwards, closer to the shearing zone.

The developments and findings of each approach considered in this work led to formulate a conclusion to the objective of this dissertation established in Chapter I. The conclusion is described in the next section.

7.4 Conclusions

The primary conclusion of this investigation is that, in general, there exists a relationship among pore pressure, drilling parameters, environmental parameters, and material properties. Therefore, it will be possible in principle to determine the virgin pore pressure at the drill bit from drilling parameters, environmental parameters, and material properties.

Additionally, it was concluded from the results described in this dissertation that:

- pore pressure, type of rock, and back rake angle of the cutter will be the most significant factors affecting the energy required to break the rock
- rate of application of cutting stress, depth of cut, and type of pore fluid (gas or liquid) will become significant factors of the cutting process only when a low-porosity, low-permeability rock is considered
- the model resulting from the first approach will not provide an adequate pore pressure prediction for all types of rocks and situations
- the model resulting from the first approach will fail to capture the effect of factors such as permeability, porosity, back rake angle of cutter, which significantly affect the cutting process
- there will be a linear relation between the effective stress and the mechanical specific energy
- the energy required to break the rock (under confining pressures) determined from the poroelastic model will be much less than the actual energy required to

break the rock, even under ideal laboratory conditions, since part of the actual energy will be used to plastically deformed the crushed rock in front of the cutter

- several interactions between the factors considered in the poroelastic model will significantly affect the cutting process.

CHAPTER VIII
RECOMMENDATIONS FOR FUTURE RESEARCH

Several recommendations for future research have been generated from the findings of the current investigation, in order to satisfy the need of a method to determine the virgin pore pressure ahead of the bit during drilling. A functional decomposition allowed identifying two top-level functions for the design of such methodology. The two top-level functions are: (1) to provide means to determine the virgin pore pressure at the bit, and (2) to provide means to relate the virgin pore pressure at the bit to the virgin pore pressure at the far-field. The work presented in this dissertation focuses on determining whether or not it is possible to determine the virgin pore pressure at the bit from drilling parameters, environmental parameters, and material properties. That is, the work presented in this dissertation attempts to determine if the function (1) can be satisfied if drilling parameters, environmental parameters, and material parameters are known.

The results from this investigation indicated that it is possible, in principle, to determine the virgin pore pressure at the drill bit from drilling parameters, environmental parameters, and material properties. However, a more extensive theoretical and experimental investigation of the factors affecting the cutting process of rock is required before a methodology to predict pore pressure from drilling parameters, environmental parameters, and material properties can be developed for all types of rock and situations. Specifically, it is recommended to:

- extend the scope of the fundamental approach described in Chapter V in order to include, in the modeling of the cutting process of rock, the effects of:
    - the plastic deformation of rock under confining pressures
    - the crushed rock in front of the cutter
    - the properties of the drilling fluid (since depending on its properties, the mud can infiltrate the rock at different rates affecting the local pore pressure)

- o   the temperature of the rock and the drilling fluid
- design experiments of rock cutting by a single cutter that allow to gather data that can be used to validate the model developed from the recommendations mentioned above. An experimental setup similar to the one described by Rafatian et al. [63, 64] is recommended, but considering the following factors:
    - o   different types of rock (considering rocks of low and high permeability, and low and high porosity)
    - o   different types of pore fluid (preferably a gas and a liquid)
    - o   different properties of the drilling fluid
    - o   different values of the back rack angle of the cutter
    - o   different values of pore pressure while maintaining a constant value of confining pressure
    - o   different values of confining pressure while maintaining a constant value of pore pressure
- further investigate the interactions of the different factors considered in the rock cutting process when a rock of low permeability and low porosity is considered

Additionally, validation of the concept of using MSE (instead of electrical resistivity or sonic log date) in Eaton's equation against post-drill pore pressure, using drilling log data from three oil wells, showed promising results if a value of one is used in the exponent of the equation. These findings, along with results from the numerical experiments using the poroelastic model, suggest that there is a linear relationship between the effective stress of the undisturbed rock and the mechanical specific energy required to fracture the rock. Further work is recommended to investigate the nature of such a relationship. Specifically, it is recommended to:

- determine whether the relationship between the effective stress of the undisturbed rock and the MSE is different for different the lithology (type of rock)

- further validate Equation (4.5) with new data, or determine whether Equation (6.6) provides a better way to relate pore pressure to overburden stress and MSE

Finally, it is envisioned that the top-level function (2) could be satisfied from a theoretical perspective using Darcy law for low velocity flows and the principle of mass conservation. The sketch in Figure 8.1 can be helpful to illustrate the way this function could be satisfied. The sketch shows the drilling of a well for which two values of pore pressure were determined at the bit (when the drill bit was drilling that location). Considering the situation in Figure 8.1, it is desirable to satisfy the top-level function (2) in order to be able to predict the pore pressure at the far-field (Pp_z).
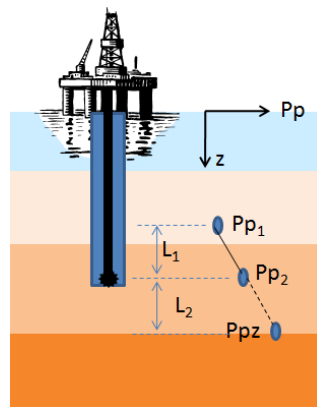
Figure 8.1 Sketch showing the drilling of a well and the virgin pore pressure (P_{p1} and Pp_2) determined at the drill bit, as well as the unknown virgin pore pressure at the far-field (Pp_z).

If a methodology to determine pore pressure at the drill bit during drilling were available, the pore pressure P_{p1} and P_{p2} could be determined when the drill bit was drilling at each location. In order to determine the virgin pore pressure at the far-field (Pp_z), it is assumed that the low velocity flows in the undisturbed formation have been in equilibrium for a long time. Under this condition, the change in the fluid content in the pores with respect to time is effectively zero (steady-state conditions), and the mass balance in Equation (5.26) reduces to

$$\nabla \cdot \mathbf{q} = 0 \tag{8.1}$$

If only the z-direction is considered (as shown in Figure 8.1), Equation (8.1) implies that under steady-state conditions the fluid flux q_z is constant, and from Darcy's law, Equation (5.27), it follows that

$$q_z = -\frac{\kappa}{\mu_f}\frac{dP_p}{dz} + \frac{\kappa \rho_f g_z}{\mu_f} \tag{8.2}$$

where κ is the permeability of the rock that has been considered constant for simplicity, and all other variables are the same as defined for Equation (5.27).

For a constant fluid flux, Equation (8.2) can be re-written in terms of the virgin pore pressures determined at the drill bit as

$$q_z = -\frac{\kappa}{\mu_f}\frac{P_{P2} - P_{P1}}{L_1} + \frac{\kappa \rho_f g_z}{\mu_f} \tag{8.3}$$

or in terms of the virgin pore pressure at the bit

$$q_z = -\frac{\kappa}{\mu_f}\frac{P_{Pz} - P_{P2}}{L_2} + \frac{\kappa \rho_f g_z}{\mu_f} \tag{8.4}$$

and combining Equations (8.3) and (8.4), the virgin pore pressure at the far-field can be determined as

$$P_{Pz} = P_{P2}\left(\frac{L_2 + L_1}{L_1}\right) - \frac{L_2}{L_1}P_{P1} \tag{8.5}$$

It can be observed from Equation (8.5) that the pore pressure P_{PZ} located at a vertical distance L_2 from the location of P_{P2} (that is, at the far-field) can be easily determined if the two values of virgin pore pressure are known, as well as the vertical between those two values. Equation (8.5) has been developed under the assumption of constant pore fluid properties, constant permeability, and steady-state conditions (constant fluid flux). However, if the properties are not constant, it can be demonstrated the pore pressure at the far-field could be determined from

$$P_{Pz} = \frac{\mu_{f2}}{\mu_{f1}}\frac{\kappa_1}{\kappa_2}L_2\left(\frac{P_{P2} - P_{P1}}{L_1} - \rho_{f1}g_z\right) + L_2\rho_{f2}g_z + P_{P2} \tag{8.6}$$

where the subscript "1" indicates mean properties at the location between P_{P1} and P_{P2}, and the subscript "2" indicates the mean properties at the location between P_{P2} and P_{Pz}. Even though Equation (8.6) is developed under the assumption of constant fluid flux, the same equation can be used if the fluid flux is not constant provided that small increments Δz are considered. That is, Equation (8.6) is still valid if the fluid flux is not constant, provided that the vertical distances L_1 and L_2 are small.

In an actual drilling situation, drilling log data is taken at intervals of less than 1 ft. If a methodology to determine pore pressure at the drill bit during drilling were available, Equation (8.6) could be used to predict the pore pressure ahead of the fit (at least a few feet ahead) based on the previous pore pressures determined at the drill bit. Therefore, it is recommended that future work include an investigation of the procedure proposed in this section to relate the virgin pore pressure at the bit to the virgin pore pressure at the far-field. With this information, the ultimate goal of predicting virgin pore pressure ahead of the bit during drilling would be satisfy.

REFERENCES

1.   Jaeger JC, Cook NGW, and Zimmerman RW. Fundamentals of rock mechanics, 4th ed. Malden, MA: Blackwell Publishing; 2007.

2.   Fjaer E, Holt RM, Horsrud P, Raaen AM, and Risnes R. Petroleum related rock mechanics, 2nd ed. London: Elsevier; 2008.

3.   Terzaghi K. Stress conditions for the failure of saturated concrete and rock. Proceedings of the American Society for Testing and Materials, 1945; 45: 777-792.

4.   Standifird W, Paine K, and Matthews M. Improving drilling success requires better technology and models. World Oil 2004; 225: 51-56.

5.   Bollfrass C, Lalk T, Marotta E, Richardson K, Silva C, et al. Pore pressure determination ahead of the bit during drilling. Report. BP-36380, BP America, Houston, TX, 2007.

6.   Marotta E, Bollfrass C, Lalk T, Silva C, Rivas-Cardona A, et al. Pore pressure determination ahead of the bit during drilling. Report. BP-36380, BP America, Houston, TX, 2008.

7.   Rivas-Cardona A, Lalk T, Silva C, Talapatra A, Bollfrass C, et al. Pore pressure determination ahead of the bit during drilling. Report. BP-36380, BP America, Houston, TX, 2009.

8.   Richardson KW. Principal stress pore pressure prediction: Utilizing drilling measurements to predict pore pressure. M.S. Thesis, Texas A&M University, College Station, TX, 2008.

9.   Teale R. The concept of specific energy in rock drilling. International Journal of Rock Mechanics and Mining Science & Geomechanics Abstracts 1965; 2: 57-73.

10.   Eaton BA. The equation for geopressure prediction from well logs. In: Fall Meeting of the Society of Petroleum Engineers of AIME, Dallas, Texas, 1975; SPE 5544: 1-9.

11.   Goodman HE. Method for determining rock mechanical properties using electrical log data. Patent US 5416697, 1995.

12.   Osborne MJ and Swarbrick RE. Mechanisms for generating overpressure in sedimentary basins: A reevaluation. AAPG Bulletin 1997; 81: 1023-1041.

13. Yassir N and Addis MA. Relationships between pore pressure and stress in different tectonic settings: Pressure regimes in sedimentary basins and their prediction. AAPG Memoir, 2002; 76: 79-88.

14. Yu G. Pore pressure prediction sees improvements. E&P Magazine, Houston, TX, September, 2008. Available from: http://www.epmag.com/Magazine/2008/9.

15. Terzaghi K, Peck RB, and Gholamreza M. Soil mechanics in engineering practice, 3rd ed. New York: Wiley; 1996.

16. Biot M. General theory of three-dimensional consolidation. Journal of Applied Physics 1941; 12: 155-164.

17. Bruce B. An introduction to this special section: Pore pressure. The Leading Edge 2002; 21: 169-177.

18. Hottman CE and Johnson RK. Estimation of formation pressures from log-derived shale properties. Journal of Petroleum Technology 1965; 17: 717-72.

19. Hubbert MK and Rubey WW. Role of fluid pressure in mechanics of overthrust faulting: I. Mechanics of fluid-filled porous solids and its applications to overthrust faulting. Geological Society of America Bulletin 1959; 70: 115-166.

20. Lyons WC and Zaba J. Standard handbook of petroleum and natural gas engineering, 6th ed. Houston, Texas: Gulf Publishing Company; 1996.

21. Sayers CM. An introduction to velocity-based pore-pressure estimation. The Leading Edge 2006; 25: 1496-1500.

22. Wang C-x, Cao W-l, and Wang X-r. Pressure gradient computation and application of the wireline formation tester. Petroleum Exploration and Development 2008; 35: 476-481.

23. Cranganu C. Using artificial neural networks to predict the presence of overpressured zones in the Anadarko basin, Oklahoma. Pure and Applied Geophysics 2007; 164: 2067-2081.

24. Lei Z and Kaiki Z. Prediction of formation and downhole pressures by using computer intelligent calculation analysis. In: SPE Latin American and Caribbean Petroleum Engineering Conference, Buenos Aires, Argentina, 2001; SPE 69528, 1-4.

25.   Shaker S. Calibration of geopressure predictions using the normal compaction trend: Perception and pitfall. CSEG Recorder 2007; 32: 29-35.

26.   Alberty MW and McLean MR. Emerging trends in pressure prediction. In: Offshore Technology Conference, Houston, TX, 2003; OTC 15290: 1-7.

27.   Solano YP, Uribe R, Frydman M, Saavedra NF, and Calderon ZH. A modified approach to predict pore pressure using the d-exponent method: An example from the carbonera formation, Colombia. CT&F - Ciencia, Tecnología y Futuro 2007; 3: 103-111.

28.   Jayaraman SB. Kaiser effect study on rocks. Report. Pennsylvania State University, State College, PA, 2001. [cited May 14, 2011]. Available from http://www.personal.psu.edu/sbj110/research/html.

29.   Simon R. Energy balance in rock drilling. SPE Journal 1963; 3: 298-306.

30.   Pessier RC and Fear MJ. Quantifying common drilling problems with mechanical specific energy and a bit-specific coefficient of sliding friction. In: SPE Annual Technical Conference and Exhibition, Washington, D.C., 1992; SPE 24584: 373-388.

31.   Dupriest FE. Comprehensive drill-rate management process to maximize rate of penetration. In: 2006 SPE Annual Technical Conference and Exhibition, San Antonio, Texas, USA, 2006; SPE 102210: 1-10.

32.   Curry D, Fear MJ, and Govzitch A. Technical limit specific energy - an index to facilitate drilling performance evaluation In: SPE/IADC Drilling Conference, Amsterdam, Netherlands, 2005; SPE 92318: 1-8.

33.   Detournay E and Atkinson C. Influence of pore pressure on the drilling response in low-permeability shear-dilatant rocks. International Journal of Rock Mechanics and Mining Sciences 2000; 37: 1091-1101.

34.   Detournay E and Defourny P. A phenomological model for the drilling action of drag bits. International Journal of Rock Mechanics and Mining Sciences & Geomechanics Abstracts 1992; 29: 13-23.

35.   Detournay E and Drescher A. Plastic flow regimes for a tool cutting a cohesive-frictional material. In: 4th International Symposium on Numerical Models in Geomechanics, Numerical Models in Geomechanics, Swansea, UK, 1992; 367-376.

36.   Merchant E. Mechanics of the metal cutting process .1. Orthogonal cutting and a type-2 chip. Journal of Applied Physics 1945; 16: 267-275.

37.   Merchant ME. Basic mechanics of the metal-cutting process. Journal of Applied Mechanics 1944; 11: 168-175.

38.   Zijsling DH. Single cutter testing: A key for pdc bit development. In: Offshore Europe 87, Aberdeen, Scotland, 1987; SPE 16529, 1-12.

39.   Calhoun WM, Caicedo HU, and Ewy RT. Method for predicting rate of penetration using bit-specific coefficient of sliding friction and mechanical efficiency as a function of confined compressive strength. Patent US 7412331 B2, 11/015899, 2008.

40.   Skempton AW. The pore pressure coefficients A and B. Geotechnique 1954; 4: 143-147.

41.   Rice JR and Cleary MP. Some basic stress diffusion solutions for fluid-saturated elastic porous media with compressible constituents. Rev. Geophys. 1976; 14: 227-241.

42.   Detournay E and Cheng AH-D. Fundamentals of poroelasticity. In: Hudson JA, Editor. Comprehensive rock engineering: Principles, practice and projects. Analysis and design method, vol. 2. Oxford: Pergamon; 1993. p. 113-171.

43.   Hamiel Y, Lyakhovsky V, and Agnon A. Rock dilation, nonlinear deformation, and pore pressure change under shear. Earth and Planetary Science Letters 2005; 237: 577-589.

44.   Cowin SC. Bone poroelasticity. Journal of Biomechanics 1999; 32: 217-238.

45.   Cheng AHD, Abousleiman Y, and Roegiers JC. Review of some poroelastic effects in rock mechanics. International Journal of Rock Mechanics and Mining Sciences & Geomechanics Abstracts 1993; 30: 1119-1126.

46.   Han G and Dusseault MB. Description of fluid flow around a wellbore with stress-dependent porosity and permeability. Journal of Petroleum Science and Engineering 2003; 40: 1-16.

47.   Jaeger JC and Cook NGW. Fundamentals of rock mechanics, 3rd ed. New York: Halsted Press; 1979.

48.   Mohr O. Abhandlungen aus dem gebiete der technisrche mechanik [treatise on topics in engineering mechanics], 2nd ed. Berlin: Ernst und Sohn; 1914.

49. Coulomb CA. Application des regles de maxima et minima a quelques problemes de statique relatifs a l'architecture [application of the rules of maxima and minima to some problems of statics related to architecture]. Acad. Roy. Sci. Mem. Math. Phys., 1773; 7: 343-382.

50. Mohr O. Welche umstande bedingen die elastizitasgrenze und den bruch eines materials? [what are the conditions for the elastic limit and the fracturing of a material?]. Z. Ver. dt. Ing. 1900; 44: 1524-1530, 1572-1577.

51. Murrell SAF. The effect of triaxial stress systems on the strength of rocks at atmospheric temperatures. Geophysical Journal of the Royal Astronomical Society 1965; 10: 231-281.

52. Zambrano-Mendoza O. Error-in-variables for failure criteria applied to the near-wellbore region. Ph.D. Dissertation, Texas A&M University, College Station, TX, 2004.

53. Labuz JF, Riedel JJ, and Dai ST. Shear fracture in sandstone under plane-strain compression. Engineering Fracture Mechanics 2006; 73: 820-828.

54. New England Research, Inc (NER). Elastic constants and strength of berea sandtone. [cited May 1, 2011]. Available from: http://ner.com/pdf/NER_tn_berea.pdf.

55. Warren TM, Winters WJ, and Onyia EC. Method of determining rock compressive strength. Patent US 4914591, 173514, 1990.

56. Moore DPL. How to predict pore pressure. Petroleum Engineer International 1982: 144,146,148, 152.

57. Schlumberger. Oilfield glossary. [cited April 28, 2011]. Available from: http://www.glossary.oilfield.slb.com/Display.cfm?Term=true%20vertical%20depth.

58. Combs GD. Prediction of pore pressure from penetration rate. In: Fall Meeting of the Society of Petroleum Engineers of AIME, Houston, Texas, 1968; SPE 2162: 1-16.

59. Cunningham RA and Eenink JG. Laboratory study of effect of overburden, formation and mud column pressures on drilling rate of permeable formations. Transactions of the American Institute of Mining and Metallurgical Engineers 1959; 216: 9-15.

60.   Eckel JR. Effect of pressure on rock drillability. Transactions of the American Institute of Mining and Metallurgical Engineers 1958; 213: 1-6.

61.   Murray AS and Cunningham RA. Effect of mud column pressure on drilling rates. Transactions of the American Institute of Mining and Metallurgical Engineers 1955; 204: 196-204.

62.   Fedorov VV. A thermodynamic theory of the mechanical strength and failure of a solid body. Strength of Materials 1971; 3: 1290-1293.

63.   Rafatian N, Miska SZ, Ledgerwood LW, Yu M, and Ahmed R. Experimental study of MSE of a single PDC cutter under simulated pressurized conditions. In: SPE/IADC Drilling Conference and Exhibition, Amsterdam, The Netherlands, 2009; SPE 119302: 1-12.

64.   Rafatian N, Miska SZ, Ledgerwood LW, Yu M, Ahmed R, et al. Experimental study of MSE of a single PDC cutter interacting with rock under simulated pressurized conditions. SPE Drilling & Completion 2010; 25: 10-18.

65.   Ledgerwood LW. Discrete element modeling of rock cutting under high pressure conditions. Patent PCT/US2007/024596, 60/872,057, 2006.

66.   Ledgerwood LW. Discrete element modeling of rock destruction under high pressure conditions. Patent WO 2008/066895 A2, 2008.

67.   Montgomery DC. Design and analysis of experiments, 5th ed. New York: John Wiley & Sons, Inc.; 2001.

68.   SAS Institute Inc. JMP documentation. Cary, NC, 2009.

VITA

Name: Juan Alberto Rivas Cardona

Address: FMC Technologies, 11220 TC Jester Blvd., Houston, TX 77067

Email Address: albert.rivas10@gmail.com

Education: B.S., Mechanical Engineering, Universidad de Guanajuato, Mexico, 2004

                  M.S., Mechanical Engineering, Texas A&M University, 2006

                  Ph.D., Mechanical Engineering, Texas A&M University, 2011

AWARDS

- B.S. degree awarded with *Laureate* honors, 2004.

- National scholarship from CONACYT (Mexican National Council of Science and Technology) for graduate studies, 2004-2009.

SELECTED PUBLICATIONS

- Rivas-Cardona A, Marotta E, Whitsitt E, Experimental and analytical investigation of the cool-down behavior of an insulated pipe assembly under subsea conditions. SPE Journal, (accepted for publication, 2011).

- Rivas-Cardona A, Banerjee D, Microfluidic device for delivery of multiple inks for Dip Pen Nanolithography. Journal of Micro/Nanolithography MEMS MOEMS 2007; 6(3) SPIE 033004:1-9.

- Khoo NC, Sinha SK, Luzik E, Rivas-Cardona A, Banerjee D, Simple inexpensive technique for the synthesis of single-walled carbon nanotube films by chemical vapor deposition (CVD). 3rd. Int. Conference on Technological Advances of Thin Films and Surfaces, Singapore, December, 2006.

- Rivas-Cardona A, Hernandez-Guerrero A, Romero-Mendez R, Lesso-Arroyo R, Liquid-mixed convection in a closed enclosure with highly-intensive heat fluxes. International Journal of Heat and Mass Transfer 2004; 47: 4089-4099.